Yarn Balloons, Differential Geometry and the Navier-Stokes Equations

Gregory Edward Cave

A thesis submitted in fulfilment of the requirements for the award of Doctor of Philosophy

School of Mathematical and Physical Sciences

Faculty of Science

University of Technology Sydney

Australia

January 2023

Declaration

CERTIFICATE OF ORIGINAL AUTHORSHIP

I, Gregory Edward Cave declare that this thesis, is submitted in fulfilment of the requirements for the award of Doctor of Philosophy, in the Faculty of Science at the University of Technology Sydney.

This thesis is wholly my own work unless otherwise referenced or acknowledged. In addition, I certify that all information sources and literature used are indicated in the thesis.

This document has not been submitted for qualifications at any other academic institution.

This research is supported by the Australian Government Research Training Program.

Signature: Production Note:
Signature removed prior to publication.

Date: 20-1-23

Acknowledgements

It is no exaggeration to say that this thesis was more than twenty years in the making. So first I would like to thank every person in that time who suggested I do a PhD. You were right, you were all right. Second, I would like to thank the people at UTS who made the decision to appoint my supervisor Professor Anthony Dooley to the newly created position of Head of School, because without that decision this thesis would not exist. Most importantly, I would like to thank Tony for everything he has done for me, and I appreciate your wit and wisdom, your supportive and collaborative nature, your patience, your insights and your vast experience as a supervisor, all of which meant my candidature was an enjoyable and challenging experience, which I very much appreciate. Next I would like to thank all my friends and colleagues in the School of Mathematical and Physical Sciences (MaPS), who have always been friendly, supportive and helpful, and my fellow students at the Groups Analysis Geometry (GAG) seminars, who helped make Tony's efforts in creating a beneficial milieu a success. Next I would like to thank my mum and dad for all their support, and all my close friends who have been very understanding over the years it has taken me to complete this thesis.

This conventional thesis is in the format of "Conventional Thesis".

Contents

List of Figures

List of Tables

Abstract

In the textile industry, there are hundreds of millions of ring spindles or equivalent devices in use today around the world converting millions of tonnes of short staple fibers such as cotton or polyester into clothing and other textiles. The aim of this thesis is to improve the mathematical model of yarn spinning devices to potentially lead to an improvement in the efficiency of the production process. Past research in this area, referred to as the *Padfield model*, expressed the yarn balloon equations in cylindrical polar coordinates, in a reference frame rotating with a constant angular velocity. The air drag was assumed to be proportional to the velocity normal to the yarn squared, while the tangential component was neglected, and the drag coefficient C_D was assumed to be equal to 1 for all values of the Reynolds number Re, because the exact functional relationship between C_D and Re is not known. The ultimate objective of this thesis is to improve the accuracy of the mathematical model of this system by representing the yarn balloon equations in intrinsic coordinates, and finding a more accurate representation of the air drag term in these equations along the entire length of the yarn balloon. This is achieved by finding a new exact similarity solution of the 2-D incompressible steady state Navier-Stokes equations which will enable significant progress to be made in finding the functional relationship between C_D and Re for $0 < Re < 47$. The process through which this similarity solution is used to find the correspond-

ing physical solution is described in detail for $0 < Re < 47$. The viscous solution in the boundary layer is matched to the inviscid external solution so that all boundary conditions are satisfied. This is significant progress towards improving the mathematical model of yarn spinning devices through finding the relationship between C_D and Re for low Reynolds numbers. The solution found here also has more applications than just the yarn balloon problem, and thus a greater importance.

Extended Abstract

In the textile industry, there are hundreds of millions of ring spindles or equivalent devices in use today around the world converting millions of tonnes of short staple fibers such as cotton or polyester into clothing and other textiles. Any improvement in the mathematical model of yarn spinning can potentially lead to an improvement in the efficiency of the production process. In ring spinning and over-end unwinding, or using the two-for-one twister device, as the yarn is drawn through the device, it is rotated around a fixed axis creating what is known as a *yarn balloon*. The *yarn element* is a cylinder of length δs used to represent an infinitesimally small section of the yarn at the point P. Newton's laws of motion have been applied to the rotating yarn to describe this yarn balloon shape. The equations governing the dynamics of the yarn balloon will be referred to as the Equations of Motion (EoM), and are also known as the *yarn balloon equations*. The EoM are a system of three time-dependent, coupled second order non-linear differential equations. For typical settings used for the yarn spinning devices mentioned above, the yarn element moving through still air will experience drag proportional to the velocity (v) of the yarn element squared, in the opposite direction to the velocity. However, more generally the exact functional relationship of drag to velocity is not known. The yarn is modelled as a flexible, inextensible cylinder and the yarn element is represented as a long smooth circular cylinder in a two-dimensional

(2-D) fluid flow. The formula for drag [60] is

$$D = \rho a C_D v^2$$

where ρ is the density of air, a is the radius of the yarn and C_D is the drag coefficient. The exact functional relationship between the drag coefficient and the Reynolds number (Re), a dimensionless number used to characterize the air flow around the yarn element, is not known. The Reynolds number corresponding to air flow around the yarn element is a function of arc length s in the yarn balloon. Therefore the air drag at each point along the yarn balloon is a function of C_D and thus Re. That is, the air drag depends both on v^2 and Re, and because Re also depends upon v, as Re changes, thus the functional relationship of air drag to velocity is currently not known. **In this thesis, progress is made in finding the functional relationship between C_D and Re and thus air drag and velocity for fluid flow around a circular cylinder for $0 < Re < 47$.**

Past research in this area will be referred to as the *Padfield model*, as it was Padfield [55] who first used a dimensionless parameter defined in Chapter 3 as p_0 to model air drag. In the Padfield model, the yarn balloon equations were expressed in cylindrical polar coordinates, in a reference frame rotating with a constant angular velocity. The air drag was assumed to be proportional to the velocity normal to the yarn squared, while the tangential component was neglected, and the drag coefficient was assumed to be equal to 1. The 2-D Navier-Stokes equations govern the behavior of an incompressible viscous fluid in a two dimensional domain. According to [33], a *boundary layer* is a thin layer close to a solid boundary within which the effect of *vorticity* is important, however high the Reynolds number of the fluid flow may be. The point at which boundary layer separation occurs depends upon the Reynolds

number, and **significant progress is made in this thesis towards finding the exact functional relationship between the separation point and** Re **for fluid flow around a circular cylinder for** $6.29 < Re < 47$.

The ultimate objective of this thesis is to improve the accuracy of the mathematical model of this system by representing the yarn balloon equations in intrinsic coordinates, and finding a more accurate representation of the air drag term in these equations along the entire length of the yarn balloon. This is achieved by finding a new exact solution of the 2-D Navier-Stokes equations which will enable significant progress to be made in finding the functional relationship between C_D and Re for $0 < Re < 47$. The new method created in this thesis to find this similarity solution can also be applied to the 2-D time dependent Navier-Stokes equations in an attempt to find the corresponding similarity solution for $47 < Re < 190$, and subsequently find the functional relationship between C_D and Re over this range. For $190 < Re < 10^4$, the remaining range of interest for the yarn balloon problem, the solution is three dimensional, so even if the method created here is not amenable to the 3-D Navier-Stokes equations, C_D could be assumed to be 1 over this region only, which would still lead to a better model for the system than currently exists. Our intention is then to use this relationship between C_D and Re to express the air drag in terms of the Reynolds number at each point along the yarn balloon as accurately as possible, although this has not been achieved yet. In this thesis we represent the yarn balloon equations in a new frame of reference in intrinsic coordinates. With this new framework the drag coefficient for multi-strand yarns, and non-smooth hairy yarns can now be incorporated more accurately into our model than the Padfield model.

In Chapter 1, past research in the areas of yarn spinning, differential geometry and fluid dynamics is referenced, and its relevance to the new results that I will present in this thesis is discussed. In Chapter 2, the definitions and equations from the theory that will be used in this thesis are catalogued.

In Chapter 3, we establish a framework to model a yarn balloon in vacuo. We find matrices to transform the basis vectors from cylindrical polar coordinates to the Frenet-Serret frame and the Darboux frame. Some exact solutions are found, and although analytical expressions were obtained for solutions in this case by [68], [14], [16] and [69], the approach that we have used in Chapter 3 is different.

This framework, established for the case with no air drag, is successfully utilised in Chapter 4 to model the effect of air drag. In Chapter 4 we add the Padfield air drag term to the model from Chapter 3 and thus provide a new model accommodating air drag. In the Padfield model, the system was modelled in a reference frame S, which rotated at a constant rate (ω) around a fixed axis (coincident with the spindle of the device), which contained the origin O. In Chapter 4, we assume that the yarn path (the vectors $\mathbf{T}$ and $\mathbf{N}$) always lies in a vertical plane. This plane is able to rotate around a point O', the centre of rotation for a rotating reference frame S', moving relative to the fixed point O in the frame S. The dimensionless EoM are found in this new reference frame, and the Padfield air drag term expressed in terms of the new coordinates in frame S'.

In Chapter 5, a new representation of the Navier-Stokes equations in intrinsic coordinates is found. Also the approach to air drag with the Navier-Stokes equations and conformal mapping is outlined.

In Chapter 6, we develop a new similarity solution to the Navier-Stokes equations in the boundary layer. A similarity transformation is applied to the two-dimensional steady state Navier-Stokes equations for an incompressible fluid, with no body force, in polar coordinates. An extra condition relating the external speed $U(\theta)$, the fluid speed at the edge of the boundary layer, to the width of the boundary layer $g(\theta)$ is required to obtain a fourth order non-linear ordinary differential equation for $f(\eta)$ which represents the velocity gradient normal to the boundary, across the boundary layer. This differential equation is reduced to quadrature, thus obtaining a **new similarity solution to the two-dimensional Navier-Stokes equations, a self-similar solution of the second kind.** The process through which this similarity solution is used to find the corresponding **physical solution** is described in detail for $0 < Re < 47$. From this solution, expressions for the Reynolds number, and the separation point are found, as well as a new constant of the motion, known as the **turbulent viscosity**. Also in Chapter 6, incidentally, as part of the search for similarity solutions, a new solution to a third order non-linear differential equation is found.

Chapter 1

Historical Background

The process of making yarn, string or rope has existed for many thousands of years. During the industrial revolution, this process was mechanised. In 1828 the *ring frame* or *ring spinning* machine was invented, and within a couple of decades was in widespread use due to its simplicity and improved productivity compared to previous systems. The industrial process of manufacturing yarn has many stages. Ring spinning involves the twisting of fibers into yarn, and the winding of this yarn onto a package. As the yarn is drawn through the device, it passes through a fixed point on the axis about which the yarn rotates, called the guide eye. It then passes through a small C-shaped ring called the traveler, which is able to rotate around a horizontal ring. The yarn is then wound onto a bobbin, mounted on a spindle. The ring is part of a ring-rail, a horizontal platform around the bobbin which slowly moves up and down, determining what part of the bobbin the yarn is wound onto. The two-for-one twister is a machine used to insert twist into multi-folded yarn. The yarn is unwound from a coaxial package, drawn through the hollow spindle of the device, and over a circular, coaxial plate called the over-run plate. It then passes through the guide eye, and is wound onto another package. As the

name suggests, over-end unwinding is the process by which yarn is unwound from a large cylindrical package to a guide eye, which is located on the axis of the package. For ring spinning, we are interested in the path the yarn takes from the guide eye to the traveler. For the two-for-one twister, we are concerned with the path the yarn takes from the rim of the over-run plate to the guide eye. For over-end unwinding, it is the path the yarn takes after it lifts off from the surface of the package to the guide eye. In all three cases, as the yarn moves through the air it rotates around the axis of symmetry of the system.

To give some sense of the number of devices in use at present, according to Frederick Abernathy in the foreword of Batra & Fraser [2], quoting figures from the United Nations, the total number of ring spindles in use in the world in 2012 was 244,863,631. In promotional material for Toyota's RX-300 Ring Spinning frame [26][27], they claim to have 22 million of their spindles in use worldwide (based on sales from 1967 to 2015). Each machine now being sold has up to 1824 spindles. According to Rieter [28], a supplier of systems for short-staple fiber spinning, in a document produced for investors, "A total of more than 250 million spindle equivalents are used worldwide to produce yarn from the around 50 million tons of staple fibers...every year, between 11 and 13 million spindle equivalents are installed worldwide: spinning mill owners invest in rationalization, replacement or expansion. In 2019, Rieter delivered 1.32 million spindle equivalents (2018: 2.15 million)."

Attempts to gain a better understanding of this system go back at least as far as 1881 [29], however as the spindle rotational speeds were increased, in an effort to increase throughput, yarn breakages became more frequent, which affected productivity and quality of the finished product (each time the

yarn breaks, the machine must be stopped, and the two ends of the yarns tied together). This situation made a deeper understanding of how the system worked more and more necessary. Some early attempts provided rules of thumb that contemporary practitioners in the industry would have found useful. However, now that the system has been mathematically modelled, with the model showing reasonable agreement with experimental results, the use of current machines can be optimised, and the prospect of designing better machines now exists. As stated in [2], the practical reason why these processes have been mathematically modelled is to "...help practitioners to optimize the process, so as to obtain the highest productivity without sacrificing quality..."

In the yarn textile industry, a multi-stage process is used to transform natural fibres such as cotton into various types of yarn [1]. At various stages in this process the yarn is unwound from a package and is drawn through a device (a ring spinning frame or a two-for-one twister) before it is wound onto another package. As it is drawn through this device, it rotates at high speed around a spindle forming a shape called a yarn balloon (Figure 3.1). It is this shape that many researchers from a number of disciplines have attempted to model, most recently Fraser [2] and his collaborators, who modelled this situation with a set of highly non-linear differential equations, with appropriate boundary conditions. They were able to solve the differential equations numerically, and demonstrated their model had a reasonably good fit with empirical observations of the system, but with scope for improvement in some areas. It is this model that we intend to improve upon; the details of which will form a significant part of this document.

Newton's laws of motion have been applied to the rotating yarn to describe the shape it forms in the processes mentioned above. This shape is referred

to as the yarn balloon, and the equations governing the dynamics of the yarn balloon will be referred to as the Equations of Motion (EoM). The EoM are three time-dependent, coupled second order non-linear differential equations

$$m\Big\{D^2\mathbf{r} + 2\omega\mathbf{k}\wedge D\mathbf{r} + \omega^2\mathbf{k}\wedge(\mathbf{k}\wedge\mathbf{r})\Big\} = \frac{d}{ds}\left(T_e\frac{d\mathbf{r}}{ds}\right) + \mathbf{F}, \tag{1.0.1}$$

where T_e is the tension in the yarn (a scalar) at a point P, whose position vector is given by $\mathbf{r}$. The linear density of the yarn is m, and the differential operator D is given by

$$D = \frac{\partial}{\partial t} - V_0(t)\frac{\partial}{\partial s}$$

following the motion of P relative to the frame rotating with constant angular velocity $\omega\mathbf{k}$ about the z-axis. $V_0(t)$ is the linear speed with which the yarn is drawn through the guide eye of the device. The force per unit length due to air drag is given by $\mathbf{F}$.

Various simplifying assumptions have been made in order to make progress towards a comprehensive set of solutions for the EoM. Neglecting terms that contain a derivative with respect to time simplifies the EoM and leads to what is referred to as the *quasi-stationary* equations. That is, as the yarn is drawn through the device, the yarn balloon appears unchanging to the naked eye. When air drag is also neglected, the system of equations is significantly simplified. Gray [68] presents an exact solution for a "uniform chain revolving with steady angular speed ... about an axis Oz while under the action of no forces" including the special case of a "revolving chain in a plane containing the axis of rotation". Mack [14] presents an exact formula for the balloon curve involving elliptic integrals and states that this solution has been given by previous authors. Crank [15] provides the substitutions used by Baltz [61] to obtain the solution (although this paper is not readily available). Hanna

[16] presents exact solutions for the EoM with only air drag neglected, for general boundary conditions. In fact, he has addressed a broader situation of an inextensible, flexible, twistable inertial string rotating rigidly about a fixed axis. Hanna and Pendar [69] extended the work of these authors by presenting a solution where the yarn is drawn through the yarn balloon with a constant linear speed. That is, the case above is augmented by the addition of yarn tangential motion, which introduces a Coriolis force, and hence the solutions are no longer planar. Hanna [16] also speculates on the effect of the addition of air drag by referencing Aristoff and Stone [17], who numerically modelled the aerodynamics of a skipping rope. In their model, both ends of the rope are on the axis of rotation. With negligible air drag, the rope shape is always coplanar. When air drag is significant in size in comparison to the centrifugal force term, the rope is deflected off the plane, and their results show a discontinuity in the slope at the midpoint of the rope. It is not clear whether or not this is an unphysical numerical result. Regardless of that, this result is very relevant to what will be done in this thesis, in particular the rationale used for the modelling in Chapter 4.

Chakrabarti and Hanna [18] consider strings subjected to a uniform body force and drag forces proportional to velocity. In finding solutions for this system, they represent the string as a curve which is a function of arc length (s) and time (t), with an adapted orthonormal frame (i.e. the Frenet frame). This assumption differs from the widely used assumption of the drag force being proportional to the velocity squared, in the direction normal to the yarn, which has been thought to be more appropriate for yarn rotating at the high angular velocities typical of the modern yarn spinning devices.

Fraser and his colleagues were the first to present a comprehensive analysis of the three processes mentioned above, including realistic formulations of the boundary conditions applicable in each case. These efforts began with Fraser [19] for ring spinning, Fraser, Ghosh and Batra [20] for over-end unwinding, and Fraser [21] for two-for-one twisting. Although the EoM apply to all three processes, the boundary conditions for each are significantly different. The time independent differential equations were expressed in dimensionless form, and were solved using a numerical scheme (Runge Kutta method with shooting technique). Up to seven dimensionless parameters were required for the quasi-stationary solutions of the EoM. That is, each yarn balloon shape found corresponds to a single point on a hyper-surface in seven dimensions. The relationship between these parameters was explored by solving the EoM for a range of values for all seven parameters. For the ring spinning case, there are six parameters for the free balloon, and seven parameters when the traveler is included [19], while for the two-for-one twister case, there are six parameters when yarn elasticity is included [7].

Fraser [2] mentions that Mack & Smart [22] conducted experiments measuring air drag force as a function of Reynolds number (Re) for some typical yarns. Expressing the air drag force in terms of the Reynolds number is one of the main objectives of this thesis. In the Padfiled model, used by recent authors, the yarn is assumed to be cylindrical in shape, and the drag coefficient of the yarn (C_D) is assumed to be 1. This assumption is valid when the balloon shape has a large maximum radius, however for some balloon shapes, the maximum radius is relatively small, and thus the speed of the yarn is also smaller, and therefore the Reynolds number will also be smaller. The functional relationship between C_D and Re has been the subject of much intellectual effort, and many

empirical studies, for example [31], with a plot of this empirical relationship appearing in many textbooks, [60], [33], [30], [8] for example. So clearly C_D changes with arc length along the yarn balloon, and is not a constant, as has been the simplifying assumption used in all previous studies. Finding C_D as a function of Re is addressed in Chapter 6. In the studies of fluid flow around a circular cylinder, the drag coefficient typically refers to a smooth cylinder. Mack & Smart [22] found that for Reynolds numbers in the range of interest for industrial yarn spinning, the deduced value of C_D for monofilament yarns were almost identical to the values for a smooth cylinder, however for many types of yarn, the drag coefficient is higher than this, for example continuous filament yarns, or spun yarns. Thus another objective of this thesis is to make it possible to incorporate the effect of yarn hairiness and multi-plied yarns on C_D more accurately into our model.

In the Padfield model, air drag in the direction tangential to the yarn path is neglected. This assumption, that only the air drag normal to the yarn path is significant originally comes from the experiments of Mack & Smart [22], where they measured the tangential and normal component of air drag on yarn attached to a rectangular frame. Kothari & Leaf [50] deduced from data provided by Popov, Komarov & Sluchanovskaya, in a paper now not readily available that "the tangential air-drag parameter will generally be less than one-tenth of the value of the normal air-drag parameter and will often be nearer to one-twentieth that value". Kim *et al.* [51] derive the transient-state equation of motion that accurately contains all the boundary conditions at the guide eye and lift-off points, in an attempt to understand the effect of neglecting tangential air drag and gravity in this model. They conclude that the effect of this assumption on the maximum balloon radius is within 4 %. I will inves-

tigate if the tangential component of air drag becomes significant for some yarn balloon shapes, where the curvature of the yarn path increases sharply as the yarn changes direction. These yarn balloons have already been identified as exhibiting limit cycle behaviour by Stump & Fraser [23] for ring spinning and the two-for-one twister. Clark *et al.* [24] investigated this experimentally, and did observe this behaviour, however the parameter values corresponding to these solutions predicted by the theoretical model shows some discrepancy with the observed values. Also, for yarn balloon shapes with relatively small maximum radius, as this maximum radius decreases and the tension at the guide eye increases, the agreement of the model with the observed values deteriorates, which is consistent with the point made in the previous paragraph in regards to the Reynolds number.

The relationship between yarn twist and torsion in single and multi-ply yarn has been explored by [52], [53] and [54]. The total torsion τ in an initially straight length of yarn that is twisted and bent into a curved path is the sum of two terms. The material twist obtained by rotating the yarn around the axis or centre line of the yarn, and the *tortuosity* obtained by deforming the axis of the yarn into a curved path. The second quantity is given by the change in the binormal vector $\frac{dB}{ds}$, which corresponds to the usual definition of torsion of a curve, in the differential geometry literature (2.2.4). Fraser & Stump [52] concluded that "in typical textile yarn ring-spinning balloons the yarn path is independent of the twist in the yarn to first order in small terms". Twist in multi-ply yarn has been investigated by [53] and [54]. Multi-ply yarn have a third contribution to the total torsion of a yarn, caused by the approximately helical path of each fiber or strand in the yarn.

The ultimate objective of this thesis is to improve the mathematical model and gain a better understanding of the problem by expressing the EoM in an intrinsic coordinate system, using differential geometry, and representing air drag in a new way, so that either these equations can be solved analytically, or some progress can be made in this direction. Air drag depends upon the Reynolds number, while the Reynolds number changes along the length of a yarn balloon, and in fact even the definition of the Reynolds number changes depending upon the situation. If we were to consider the Reynolds number to be a quantity defined locally instead of globally, then we could simply define $Re = \frac{\alpha'}{\kappa\nu}$, for a curve α with curvature κ, and viscosity of the air ν. In this thesis, I only consider the steady state case, so the curve α represents the path of a particular fluid element or streamline. This idea is explored in Chapter 5, where the concepts of differential geometry are applied to the Navier-Stokes equations.

If a quasi-stationary yarn is rotated 2π radians about its axis of rotation, we have a yarn balloon. We now have a curve (i.e. the yarn path) embedded in surface (the yarn balloon), and this situation is amenable to investigation with some elementary techniques from differential geometry [3], [5], [6], [4]. Lenz et. al.[43], which was published during the time this thesis was being written, represented the yarn balloon equations in terms of the Frenet basis, and used Padfield's air drag term.

Fluid dynamics is a very broad field of study with many modern applications across many discipline areas [13]. There are many different types of fluid, and many different situations in which fluids flow [33], [8]. The Navier-Stokes equations are fundamental to this field. These equations have been studied with two or three spatial dimensions, as time dependent or steady state equations,

and model the flow of an incompressible Newtonian fluid of constant density ρ and constant viscosity μ. Many different techniques are currently used to solve these equations, which are briefly summarized in [42]. Many exact solutions to these equations have been found [35], [25]. Exact solutions have also been found for the so-called boundary layer equations [35], [32], [59]. These equations were derived from the 2-D Navier-Stokes equations by Prandtl, and were applied to the case of a flat plate by Blasius, and an inclined wedge by Falkner & Skan [8]. Symmetry methods have been widely used to find exact solutions of ODE's [9], [37], [38], [39]. Drazin and Riley [25] review the history of the derivation of the Navier-Stokes equations and survey the full range of exact solutions. They assert that "...the maturity of both the theory of the Navier-Stokes equations and the Lie theory of differential equations makes it unlikely that many more exact solutions of the Navier-Stokes equations remain to be discovered. For the same reason, those that do remain are probably of little importance. However, recent developments by Ludlow, Clarkson and Bassom [58] in which non-classical reduction methods are employed, as opposed to the classical Lie group method, may offer an alternative way ahead." Ludlow *et al.* [58] use the Clarkson-Kruskal direct method to find similarity reductions and exact solutions for the two-dimensional incompressible Navier-Stokes equations. Although they claimed many novel exact solutions, they did not claim to have found every possible similarity reduction (due to a number of simplifications that they introduced to "ease slightly the totally overwhelming computational task that we would otherwise have faced"), nor did they claim that any of their new solutions had a physical interpretation although they did say that "It would be amazing if at least some of our new solutions do not have physical interpretation". The solution found in this thesis does appear to be different from what they found although we cannot be certain because

their "reductions contain a number of arbitrary functions and/or constants", which gives "a large degree of flexibility". However, even if it could be shown that the solution found in this thesis was a special case of a more general solution found with the Clarkson-Kruskal direct method used by Ludlow *et al.* [58] or in other papers, the solution found here would still have the significant advantage that the boundary conditions can be satisfied and thus a physical interpretation be found. It appears likely that there will be many applications for the exact solution found here, and therefore it is significant.

Euler's equations of motion model the flow of an *ideal* fluid, that is, an incompressible fluid with constant density and no viscosity. The Navier-Stokes equations can then be viewed as a generalisation of Euler's equations, in which the fluid is now viscous. The linear stress/strain relation (2.4.18), leads to the addition of the extra term in the Navier-Stokes equations. In a similar way, the addition of the air drag term in the yarn balloon equations, leads from the solutions found for these equations in vacuo to the solutions with air drag. Consider the surface mentioned earlier, representing the yarn balloon in vacuo. The air drag is represented as a differential manifold lifting the yarn off the surface at each point. Specifying the precise details of how this actually occurs is explored in Chapters 5 and 6. Kobayashi [48] develops a general formulation for the flow of a Newtonian fluid over manifolds with curvature, including an explicit contribution of the Ricci curvature in the diffusion of momentum.

Dimitriou [46], introduces a "Geometric Potential Theory", a geometrical interpretation to traditional potential theory, combining the kinematics of a two-dimensional incompressible steady flow with its topology. In [47], he goes on to represent the Navier-Stokes equations in the fluid flow's intrinsic coordinate system in what he calls the "velocity-vorticity" formulation.

Energy in a fluid is lost, or dissipated, when an element of the fluid is deformed by the stress tensor acting on it at that point. When a fluid such as air flows past an obstacle (a cylinder or sphere for example), the fluid must adjust to satisfy the boundary condition at the surface of this obstacle. The region in which this adjustment occurs, in the vicinity of the obstacle is called the boundary layer. Outside of this region, the fluid will behave like an inviscid fluid (assuming there is no vorticity upstream of the obstacle) and no energy is lost, while in other circumstances, the fluid can have a shear force acting on it, such as in a boundary layer. An exact solution to the Navier-Stokes equations for steady state, incompressible flow in a boundary layer around a circular cylinder in two dimensions will provide an expression for the Reynolds number and the shear force at the surface of the cylinder, as well as the separation point, all of which is required to calculate a theoretical expression for the air drag. Many experimental studies have been carried out to investigate boundary layers, to measure skin friction, separation points and thus estimate total drag [44], [40]. Numerical simulations have also been carried out to find a formula for the relationship between the separation point and the Reynolds number, over a range of values for Re [49].

A fluid flowing past an obstacle where the Reynolds number is much less than one is known as *Stokes flow* (or creeping flow or slow flow) [33], [8]. The Stokes equations (or slow flow equations) are derived from the Navier-Stokes equations by taking the limit as the Reynolds number approaches zero, leading to the inertia term, $(\mathbf{u} \cdot \nabla)\mathbf{u}$, being neglected entirely. This simplifies the equations, but leads to a difficulty for 2-D flow past a circular cylinder, known as *Stokes' Paradox*. That is, Stokes' equations do not admit a steady-state solution for 2-D flow past a circular cylinder. Any solution to these

equations that satisfy the boundary condition at the surface of the cylinder is unbounded at infinity, and thus cannot satisfy the boundary condition there. Oseen [33] addressed this problem by replacing the inertia term in the Navier-Stokes equations with the term $-\mathbf{U} \cdot \nabla \mathbf{u}$, where $\mathbf{U}$ is the steady flow velocity of the object moving through the fluid, which is at rest at infinity. This term can be considered as a correction term to Stokes' equations. Proudman and Pearson [62] obtained higher order approximations to the solutions of Stokes and Oseen. The essential fact underpinning all of the work referenced in this paragraph is that a solution (to the Navier-Stokes equations) satisfying the no-slip condition on the surface of the cylinder must be matched to another solution (to the Navier-Stokes equations), that satisfies the uniform-stream condition (i.e. the boundary condition at infinity), for any solution of the 2-D Navier-Stokes equations for fluid flow past a circular cylinder to be considered physically realizable.

For a fluid flowing past a circular cylinder with a higher Reynolds number than that for Stokes flow, the boundary layer will separate from the surface of the cylinder before the flow reaches the rear separation point. That is there will be a separation point θ_{sp} where the skin friction becomes zero for the first time, the pressure gradient becomes positive, and after this point, the direction of flow at the surface is reversed [63]. Ahead of the separation point, the structure of the flow has three regions. There are two "layers" in the boundary layer, the inner region near the wall, whose thickness decreases to zero at the separation point, and the outer "main" part of the boundary layer. The third region is the inviscid external potential flow, which satisfies Euler's equations. The region just after the separation point is called the interaction region and also has three layers, referred to as a triple-deck structure. The main deck is the

continuation of the main part of the boundary layer from before the separation point. The lower deck or viscous sublayer next to the surface of the cylinder allows the no-slip condition to be satisfied, and according to [63], is "responsible for the displacement effect of the boundary layer upon the external potential flow", the outer deck. "The velocity profile remains unchanged" in the main deck "throughout the entire region of interaction." The main deck "is merely displaced by the lower deck next to the wall," leaving the interaction of the sublayer with the external potential flow. The triple deck theory overcomes the difficulty in classical boundary layer theory that the separation point is a singularity. The boundary layer equations are parabolic whereas the triple deck equations are elliptical.

According to Sen *et al.* [64], for "steady two-dimensional laminar flow around a stationary circular cylinder" Re_s is the value of the Reynolds number that marks "the onset of the flow separation". "To this day, there is no agreement on the exact value of the laminar separation Reynolds number, Re_s, for the steady unbounded flow". They surveyed a range of studies, experimental, numerical or semi-analytical in nature, and the 12 studies cited give estimates for Re_s in the range $3.2 \leq Re_s \leq 9.6$. Their estimate for Re_s was 6.29, obtained via numerical simulation, and for this value, the flow separates at the rear of the cylinder, that is $\theta_{sp} = \pi$. Wu *et al.* [65] showed that the separation angle decreases from this value with increasing Re, however the discrepancy between experimental studies increases as Re increases, throughout the laminar flow regime up to around $Re \sim 270$, when the transition to turbulence in the wake occurs. The flow is steady and laminar for Re in the range between Re_s and the onset of the unsteady flow regime for $Re \gtrsim 47$. The flow is 2-D up to $Re \sim 190$, with onset of 3-D flow at this value. The transition to turbu-

lence in the separating shear layer occurs at $Re \sim 1200$, while the transition to turbulence in the boundary layer occurs at $Re \sim 2 \times 10^5$. It is only when the flow transitions from a steady 2-D flow to an unsteady 2-D flow at $Re \sim 47$ that the Strouhal number becomes relevant [66].

The surface roughness of the yarn, and the effect this has on air drag needs to be considered. The effect that this roughness has on the fluid on the micro and nano scale is now being considered [45]. Yarn hairiness is the concept of fibre loops or ends protruding from the main bulk of a yarn or fabric. Mack & Smart [22] "estimate the air-drag on a yarn by assuming that it is the same as for a smooth cylinder of the same observed radius" and represent the effect of yarn hairiness of staple yarns in wind tunnels by the change in effective diameter of the yarn. They state that "over the practical range of air-speeds from 40-120 ft/sec (and in fact up to 400 ft/sec), at the balloon's maximum radius ...the projecting fibres are bent round by the air-flow and do not increase the diameter appreciably,... at speeds below 20 ft/sec these fibres are not bent so much and thus the effective diameter of the yarn is greater than its optically observed diameter." They also conclude that "At inclined angles there are tangential and normal components of air-drag and our results show that for smooth yarns the tangential component is quite small and, though greater in the case of hairy yarns, is not big enough to make the resultant of tangential and normal components combined act in a direction opposite to the air velocity." Also that "It is difficult to measure air-drag directly on actual spinning systems, partly owing to the fluctuation of the balloon and partly because there is usually no property of the balloon critically dependent on air-drag." This suggests that yarn hairiness will increase the effective diameter (and thus the air drag) at some sections of the yarn balloon, as the yarn is

drawn through the balloon. Such as near the guide eye where the balloon radius is smallest, where the normal and tangential components of air drag are similar in size, and where the normal component of the air drag changes direction relative to the yarn due to torsion of the yarn path. Yarn hairiness won't be explicitly dealt with in this thesis, however the framework developed in Chapter 4 can potentially be adapted for this purpose.

In Chapter 2, the definitions and equations from the theory that will be used in this thesis are catalogued. In Chapter 3, the EoM are represented in intrinsic coordinates for the *in vacuo* case and some exact solutions are found. The method used here is different to the methods used in [14], [15] and [16]. In Chapter 4, the EoM are represented in a new frame of reference, with intrinsic coordinates and with Padfield's air drag term. This framework was established with the intent of using it to represent the EoM with a new more accurate term for air drag. The final two chapters detail the progress we have made towards finding this new air drag term. In Chapter 5 the 2-D Navier-Stokes equations are represented in intrinsic coordinates, and the connection between the fluid flow around a circular cylinder and the air drag on the yarn element moving in a yarn balloon is considered. The 2-D Navier-Stokes equations have been represented in intrinsic coordinates before [46], [47] however the formulation developed here is in terms of energy, rather than vorticity. In Chapter 6 a new similarity solution of the 2-D steady state Navier-Stokes equations for incompressible fluid is found for flow in the boundary layer. It is a self-similar solution of the second kind. Exact solutions have been found to the boundary layer equations [32], [59], which are an approximation to the 2-D Navier-Stokes equations. Exact solutions to the 2-D Navier-Stokes equations have been found [35], [25] and [58], but not a solution for fluid flow in the boundary layer.

Chapter 2

Mathematical Background

2.1 Introduction

In this chapter we will catalogue and reference the theorems and definitions that form the foundation from which we will work from in preparation for the new work presented in subsequent chapters. Section 2.2 covers the Frenet-Serret-Darboux theory of differential geometry applied to curves and surfaces. Section 2.3 consists of a brief description of the standard model used for the yarn balloon equations. Section 2.4 consists of some basic definitions from fluid dynamics. The final section, Section 2.5 contains some further definitions necessary for the new work done in Chapter 6.

2.2 Elementary differential geometry

Consider a unit speed curve $\alpha(s) : I \to \mathbb{R}^3$ where

$$I = \{s \in \mathbb{R} | 0 \leq s < \infty\}$$

and s is the arc length. The speed function of this curve is

$$\left\| \frac{d\alpha}{ds} \right\| = 1$$

for each s in I. The unit tangent vector field on $\alpha(s)$ is

$$\mathbf{T} = \frac{d\alpha}{ds} \tag{2.2.1}$$

while the principal normal vector field of $\alpha(s)$ is

$$\mathbf{N} = \frac{d\mathbf{T}}{ds}/\kappa = \frac{d^2\alpha}{ds^2}/\kappa \tag{2.2.2}$$

where κ is the curvature function of $\alpha(s)$

$$\kappa(s) = \left\| \frac{d\mathbf{T}}{ds} \right\| = \left\| \frac{d^2\alpha}{ds^2} \right\|.$$

The binormal vector field of $\alpha(s)$ is

$$\mathbf{B} = \mathbf{T} \times \mathbf{N} \tag{2.2.3}$$

where the torsion $\tau(s)$ is defined by the derivative of $\mathbf{B}$

$$\frac{d\mathbf{B}}{ds} = -\tau\mathbf{N}. \tag{2.2.4}$$

The Frenet frame field is defined by (2.2.1), (2.2.2) and (2.2.3) which satisfy the following equations (O'Neill [3] Chapter 2.3)

$$\begin{aligned} &\mathbf{T}\cdot\mathbf{T} = 1, \qquad \mathbf{N}\cdot\mathbf{N} = 1, \qquad \mathbf{B}\cdot\mathbf{B} = 1, \\ &\mathbf{T}\cdot\mathbf{N} = 0, \qquad \mathbf{N}\cdot\mathbf{B} = 0, \qquad \mathbf{B}\cdot\mathbf{T} = 0, \end{aligned} \tag{2.2.5}$$

and

Theorem 1 (O'Neill [3]) *If α is a unit-speed curve with curvature $\kappa > 0$ and torsion τ then*

$$\begin{aligned} \mathbf{T}' &= \quad \kappa\mathbf{N}, \\ \mathbf{N}' &= -\kappa\mathbf{T} \quad + \tau\mathbf{B}, \\ \mathbf{B}' &= \quad -\tau\mathbf{N}. \end{aligned} \tag{2.2.6}$$

Taking the appropriate dot products with the equations in (2.2.6) gives

$$\mathbf{T}' \cdot \mathbf{N} = \kappa, \qquad \mathbf{N}' \cdot \mathbf{T} = -\kappa, \qquad \mathbf{N}' \cdot \mathbf{B} = \tau, \qquad \mathbf{B}' \cdot \mathbf{N} = -\tau, \qquad (2.2.7)$$

where the other five possible dot products are zero

$$\mathbf{T}' \cdot \mathbf{T} = 0, \qquad \mathbf{T}' \cdot \mathbf{B} = 0, \qquad \mathbf{N}' \cdot \mathbf{N} = 0,$$
$$\mathbf{B}' \cdot \mathbf{T} = 0, \qquad \mathbf{B}' \cdot \mathbf{B} = 0.$$

Lemma 1 *If* $\mathbf{v}$ *and* $\mathbf{w}$ *are any tangent vectors to* $\mathbb{R}^3$ *at a point* $\mathbf{p}$ *then the cross product* $\mathbf{v} \times \mathbf{w}$ *is orthogonal to both* $\mathbf{v}$ *and* $\mathbf{w}$*. That is*

$$\mathbf{v} \cdot (\mathbf{v} \times \mathbf{w}) = 0 \qquad \textit{and} \qquad \mathbf{w} \cdot (\mathbf{v} \times \mathbf{w}) = 0. \qquad (2.2.8)$$

Definition 1 *Let* α *be a unit speed curve in* $\mathbb{R}^3$*, with* $\kappa > 0$*. Then* α *is a plane curve if and only if* $\tau = 0$*.*

The plane in which a plane curve lies is called the osculating plane.

Definition 2 *Let* W *be a vector field on* $\mathbb{R}^3$*, and* $\mathbf{v}$ *be a tangent vector field to* $\mathbb{R}^3$ *at the point* $\mathbf{p}$*. The covariant derivative of* W *with respect to* $\mathbf{v}$ *is the tangent vector*

$$\nabla_{\mathbf{v}} W = W(\mathbf{p} + t\mathbf{v})'(0)$$

at the point $\mathbf{p}$*.*

The covariant derivative measures the initial rate of change of $W(\mathbf{p})$ as $\mathbf{p}$ moves in the direction of $\mathbf{v}$.

Definition 3 *If* $\mathbf{p}$ *is a point of the surface* M*, then for each tangent vector* $\mathbf{v}$ *to* M *at* $\mathbf{p}$*, the shape operator of* M *at* $\mathbf{p}$ *is*

$$\mathbf{S}_{\mathbf{p}}(\mathbf{v}) = -\nabla_{\mathbf{v}} \mathbf{U}$$

where $\mathbf{U}$ *is a unit normal vector field on a neighbourhood of* $\mathbf{p}$ *in* M*.*

Definition 4 *Let* $\mathbf{u}$ *be a unit tangent vector to a surface* $M \subset \mathbb{R}^3$ *at a point* $\mathbf{p}$. *The number* $k(\mathbf{u}) = \mathbf{S}(\mathbf{u}) \cdot \mathbf{u}$ *is the normal curvature of* M *in the direction of* $\mathbf{u}$.

The subscript $\mathbf{p}$ will be neglected when there is no ambiguity as to the point at which the shape operator is applied.
The Darboux frame field for the unit speed curve α consists of the three unit vectors $\mathbf{T}, \mathbf{U}$ and $\mathbf{V}$, where $\mathbf{U}$ is the surface normal restricted to α and

$$\mathbf{V} = \mathbf{U} \times \mathbf{T}\,.$$

Theorem 2 (O'Neill [3]) *If* α *is a unit-speed curve in a surface* $M \subset \mathbb{R}^3$ *then*

$$\begin{aligned} \mathbf{T}' &= \quad g\mathbf{V} \quad + k\mathbf{U}, \\ \mathbf{V}' &= -g\mathbf{T} \quad\quad + t\mathbf{U}, \\ \mathbf{U}' &= -k\mathbf{T} - t\mathbf{V}, \end{aligned} \tag{2.2.9}$$

where $k = \mathbf{S}(\mathbf{T}) \cdot \mathbf{T}$ is the normal curvature of M in the direction of $\mathbf{T}$, $t = \mathbf{S}(\mathbf{T}) \cdot \mathbf{V}$ is the normal curvature of M in the direction of $\mathbf{V}$ and g is the geodesic curvature of α.

Definition 5 *If* P *is a square matrix whose columns and rows are orthonormal, then*

$$PP^T = P^T P = I$$

where I *is the identity matrix. Thus* $P^T = P^{-1}$.

2.3 The Padfield model

The time independent or quasi-stationary equations of motion (EoM) for the yarn path in ring spinning or two-for-one twisting (in cylindrical polar coordinates) are

$$\mathbf{k} \wedge (\mathbf{k} \wedge \mathbf{r}) = \frac{d}{ds}\left(T_e \frac{d\mathbf{r}}{ds}\right) + \mathbf{F},$$

where T_e is the tension in the yarn (a scalar) at the point P.

The air drag is given by

$$\mathbf{F} = -\frac{p_0}{16}|\mathbf{v_n}|\mathbf{v_n}, \tag{2.3.10}$$

where p_0 is the dimensionless air drag parameter, first defined by Padfield [55],

$$p_0 = \frac{16 D_n a}{m}\,.$$

Where a is the yarn radius, m is the mass per unit length of the yarn, and

$$D_n = \frac{1}{2}\rho d C_D\,,$$

where ρ is the density of air, d is the yarn diameter and C_D is the drag coefficient for fluid flow past a smooth circular cylinder [22].

$\mathbf{v}$ is the velocity of P relative to the inertial frame of reference

$$\mathbf{v} = \omega \mathbf{k} \wedge \mathbf{r}. \tag{2.3.11}$$

and

$$\mathbf{v_n} = \frac{d\mathbf{r}}{ds} \wedge \left(\mathbf{v} \wedge \frac{d\mathbf{r}}{ds}\right), \tag{2.3.12}$$

Details of how the EoM were derived can be found in [2] and [7] for example. In recent research in this area, such as [19] and [21], and in fact in all research that we are aware of that have adopted the Padfield model, it has been assumed that $C_D = 1$. So for the purposes of this thesis, the assumption that $C_D = 1$ along the entire length of the yarn balloon is considered an integral part of the Padfield model.

2.4 Elementary fluid dynamics

Definition 6 *A fluid is incompressible if*

$$\nabla \cdot \mathbf{u} = 0,$$

where $\mathbf{u}$ *is the velocity following an element of fluid.*

Theorem 3 (Acheson [8]) *Steady state equations of motion for an ideal fluid (incompressible, inviscid and with constant density* ρ*), Euler's equations are*

$$(\mathbf{u} \cdot \nabla)\mathbf{u} = -\frac{1}{\rho}\nabla p + \mathbf{g}, \tag{2.4.13}$$

where p *is pressure and* $\mathbf{g}$ *is the gravitational body force per unit mass, given by*

$$\mathbf{g} = -\nabla\chi.$$

Definition 7 *Using the vector identity*

$$(\mathbf{u} \cdot \nabla)\mathbf{u} = (\nabla \wedge \mathbf{u}) \wedge \mathbf{u} + \nabla\Big(\frac{1}{2}|\mathbf{u}|^2\Big),$$

(2.4.13) *can we written as*

$$(\nabla \wedge \mathbf{u}) \wedge \mathbf{u} = -\nabla H, \tag{2.4.14}$$

where

$$H = \frac{p}{\rho} + \frac{1}{2}|\mathbf{u}|^2 + \chi. \tag{2.4.15}$$

Definition 8 *Vorticity* ω *is defined by*

$$\omega = \nabla \wedge \mathbf{u},$$

and a flow is irrotational when $\nabla \wedge \mathbf{u} = 0$.

Definition 9 *In steady fluid flow, a streamline is the path that an element of fluid will take as the fluid flows.* $\mathbf{u}$ *is always tangential to a streamline. Taking the dot product of* $\mathbf{u}$ *with* (2.4.14)*,*

$$(\mathbf{u}\cdot\nabla)H = 0$$

demonstrates that H *is constant along a streamline. Also, for an ideal fluid, the vorticity* ω *is constant along any streamline.*

Definition 10 (Acheson[8]) *If an ideal fluid is in steady irrotational flow, then* H *is constant throughout the whole flow field. This is because* (2.4.14) *reduces to* $\nabla H = 0$ *because the flow is irrotational.*

Definition 11 (Acheson[8]) *A 2D irrotational flow, uniform with speed* U *at infinity, past a fixed circular cylinder with radius* a *has velocity potential and stream function*

$$\phi = U\left(r + \frac{a^2}{r}\right)\cos\theta \qquad \textit{and} \qquad \psi = U\left(r - \frac{a^2}{r}\right)\sin\theta\,. \tag{2.4.16}$$

and so the components of the fluid velocity in polar coordinates are

$$u_r = U\left(1 - \frac{a^2}{r^2}\right)\cos\theta \qquad \textit{and} \qquad u_\theta = -U\left(1 + \frac{a^2}{r^2}\right)\sin\theta\,. \tag{2.4.17}$$

Definition 12 *At any point in a fluid, the stress* $\mathbf{t}$ *on a surface element* δS*, with normal* $\mathbf{n}$ *is given by* $t_i = T_{ij}n_j$*. A Newtonian fluid is a viscous fluid such that the shear stress tensor is given by*

$$T_{ij} = -p\delta_{ij} + \mu\Big(\frac{\partial u_j}{\partial x_i} + \frac{\partial u_i}{\partial x_j}\Big) \tag{2.4.18}$$

in Cartesian coordinates.

Theorem 4 (Batchelor [33]) *Two-dimensional steady state equations of motion for an incompressible fluid, with no body force, in polar coordinates, the*

Navier-Stokes equations are

$$\left(u_r\frac{\partial}{\partial r}+\frac{u_\theta}{r}\frac{\partial}{\partial\theta}\right)u_r-\frac{u_\theta^2}{r}=-\frac{1}{\rho}\frac{\partial p}{\partial r}+\nu\left(\nabla^2 u_r-\frac{u_r}{r^2}-\frac{2}{r^2}\frac{\partial u_\theta}{\partial\theta}\right),$$
$$\left(u_r\frac{\partial}{\partial r}+\frac{u_\theta}{r}\frac{\partial}{\partial\theta}\right)u_\theta+\frac{u_r u_\theta}{r}=-\frac{1}{\rho r}\frac{\partial p}{\partial\theta}+\nu\left(\nabla^2 u_\theta+\frac{2}{r^2}\frac{\partial u_r}{\partial\theta}-\frac{u_\theta}{r^2}\right),$$
$$\frac{1}{r}\frac{\partial}{\partial r}(ru_r)+\frac{1}{r}\frac{\partial u_\theta}{\partial\theta}=0\,, \tag{2.4.19}$$

where kinematic viscosity $\nu=\frac{\mu}{\rho}$*, and the components of velocity are* u_r *and* u_θ*.*

Definition 13 (Rosenhead [40]) *Skin friction is defined as the shear stress exerted by the fluid on the surface over which it flows*

$$\tau_w=\mu\frac{\partial u}{\partial n}\Big|_{n=0}\,, \tag{2.4.20}$$

where u *is the speed of the fluid parallel to the surface, and* n *is the coordinate measured along a line perpendicular to the surface.*

Definition 14 (Waleffe [67]) Eddy *or* turbulent *viscosity is defined as*

$$\nu_T=L_T U_T \tag{2.4.21}$$

where L_T *is the characteristic length or "mixing length" and* U_T *is the characteristic velocity.*

Definition 15 (Batchelor [33]) *The Reynolds number is a dimensionless parameter defined as*

$$Re=\frac{UL}{\nu}\,,$$

where U *is a representative speed and* L *is a representative length, both of which depend upon the particular problem being studied.*

Definition 16 (Batchelor [33]) *The Strouhal number is a dimensionless parameter defined as*

$$St = \frac{nL}{U},$$

where U is a representative speed, and L is a representative length and n is a frequency of oscillation associated with the flow.

2.5 Sundry definitions

Definition 17 *The Pochhammer symbol is defined as*

$$(a)_0 = 1,$$

$$(a)_n = a(a+1)(a+2)(a+3)\cdots(a+n-1), \quad n = 1, 2, 3, \ldots \ .$$

Definition 18 (Seaborn [11]) *The Hypergeometric function is defined by the series*

$$ {}_2F_1(a, b; c; z) = \sum_{n=0}^{\infty} \frac{(a)_n (b)_n}{n!(c)_n} z^n. \tag{2.5.22}$$

Definition 19 (Euler) *The incomplete Beta function is defined by*

$$B_x(p, q) = \int_0^x t^{p-1}(1-t)^{q-1} dt = \frac{x^p}{p} {}_2F_1(p, 1-q; p+1; x)\,, \tag{2.5.23}$$

where $\Re(p) > 0$ *and* $\Re(q) > 0$.

Definition 20 (Polyanin & Zaitsev [12]) *The Emden-Fowler equation is*

$$\frac{d^2y}{dx^2} = Ax^n y^m\,, \tag{2.5.24}$$

when $n = 0$*, the solution to this equation is*

$$x = \pm \int \Big(\frac{2A}{m+1} y^{m+1} + C_1 \Big)^{-\frac{1}{2}} dy\,.$$

Concluding Remarks This thesis brings together three distinct branches of mathematics. With regards to the nomenclature of the many quantities, variables and constants used, priority is given to the most widely used and accepted symbol in the context of the original discipline. For any repeated symbols, I hope that the context makes it clear to the reader what my intention is. Any constant of the form C_i, where i is an integer, represents a constant of integration. This is not to be confused with C_D, which represents the drag coefficient. In Chapters 3 and 6, where I integrate differential equations on many occasions, my intention is for the constants of integration C_i to be regarded as different for each separate solution that is found.

Chapter 3

The yarn balloon equations in a vacuum in intrinsic coordinates

3.1 Introduction

The objective of this chapter is to represent the EoM in intrinsic coordinates, and to investigate the solutions of the EoM for the yarn balloon in vacuo.

In Section 3.2, the 3×3 matrix that represents the transformation from the Frenet frame to cylindrical polar coordinates is found. In Section 3.3, the curve α, representing the yarn path is rotated around the axis of symmetry to create a surface M. An expression for the angle ϕ between the principal normal N to the curve α and the unit normal U to the surface M is found. This angle determines the relationship between the Darboux frame and the Frenet frame. Thus in Section 3.4, the matrix that represents the transformation from the Darboux frame to cylindrical polar coordinates is found. Finally in Section 3.5, the solutions of the EoM for the yarn balloon in vacuo can now be found using the framework developed in the previous three sections.

3.2 The transformation between cylindrical polar coordinates and the Frenet frame

Consider a unit speed curve $\mathbf{R}(s) : I \to \mathbb{R}^3$ which will be used to represent the position of the yarn (with arc length s) in three dimensions, where

$$I = \{s \in \mathbb{R} | 0 \leq s < \infty\}.$$

We assume that the yarn is inextensible and thus

$$\frac{d\mathbf{R}}{ds} \cdot \frac{d\mathbf{R}}{ds} = 1. \tag{3.2.1}$$

This is consistent with the speed function of the curve

$$\left\| \frac{d\mathbf{R}}{ds} \right\| = 1.$$

In cylindrical polar coordinates

$$\mathbf{R}(s) = (r(s), 0, z(s)).$$

The unit tangent vector field on $\mathbf{R}(s)$ is

$$\mathbf{T} = \frac{d\mathbf{R}}{ds} = (r', r\theta', z'). \tag{3.2.2}$$

and its derivative is

$$\frac{d\mathbf{T}}{ds} = \frac{d^2\mathbf{R}}{ds^2} = ((r'' - r\theta'^2), (2r'\theta' + r\theta''), z''). \tag{3.2.3}$$

The principal normal vector field of $\mathbf{R}(s)$ is

$$\mathbf{N} = \frac{d\mathbf{T}}{ds} \Big/ \kappa = \frac{1}{\kappa} \left\{ ((r'' - r\theta'^2), (2r'\theta' + r\theta''), z'') \right\}, \tag{3.2.4}$$

where κ is the curvature function of $\mathbf{R}(s)$

$$\kappa(s) = \left\| \frac{d^2\mathbf{R}}{ds^2} \right\| = \sqrt{(r'' - r\theta'^2)^2 + (2r'\theta' + r\theta'')^2 + z''^2}, \tag{3.2.5}$$

and their derivatives are

$$\frac{d\mathbf{N}}{ds} = \frac{1}{\kappa^2}\Big\{\Big(-\kappa'(r'' - r\theta'^2) + \kappa(r''' - 3r'\theta'^2 - 3r\theta'\theta'')\Big),$$
$$\Big(-\kappa'(2r'\theta' + r\theta'') + \kappa(3r''\theta' - r\theta'^3 + 3r'\theta'' + r\theta''')\Big),$$
$$\Big(-\kappa' z'' + \kappa z'''\Big)\Big\}$$

and

$$\frac{d\kappa}{ds} = \frac{1}{\kappa}\Big(r''r''' - rr'''\theta'^2 + rr'\theta'^4 + 2r^2\theta'^3\theta'' + 3r'r''\theta'^2$$
$$+ 6r'^2\theta'\theta'' + 2rr'\theta'\theta''' + 3rr'\theta''^2 + r^2\theta''\theta''' + z''z'''\Big).$$

The binormal vector field of $\mathbf{R}(s)$ is

$$\mathbf{B} = \mathbf{T} \times \mathbf{N} = \frac{1}{\kappa}\Big\{((r\theta'z'' - (2r'\theta' + r\theta'')z'), -(r'z'' - (r'' - r\theta'^2)z'),$$
$$(r'(2r'\theta' + r\theta'') - r\theta'(r'' - r\theta'^2)))\Big\} \tag{3.2.6}$$

and

$$\frac{d\mathbf{B}}{ds} = -\tau\mathbf{N} = -\frac{\tau}{\kappa}\Big\{((r'' - r\theta'^2), (2r'\theta' + r\theta''), z'')\Big\}. \tag{3.2.7}$$

Three equivalent expressions for τ can be obtained by differentiating the right hand side of equation (3.2.6) and equating each component to the corresponding component of equation (3.2.7),

$$\tau = \frac{1}{u}\Big\{\Big(\theta'z'u + z'v' - r\theta'w'\Big) + (-z'v + r\theta'w)\frac{(uu' + vv' + ww')}{(u^2 + v^2 + w^2)}\Big\}, \tag{3.2.8a}$$

$$\tau = \frac{1}{v}\Big\{\Big(\theta'z'v - z'u' + r'w'\Big) + (z'u - r'w)\frac{(uu' + vv' + ww')}{(u^2 + v^2 + w^2)}\Big\}, \tag{3.2.8b}$$

$$\tau = \frac{1}{w}\Big\{\Big(-r'\theta'u - r'v' + r\theta'u' - r\theta'^2v\Big) + (r'v - r\theta'u)\frac{(uu' + vv' + ww')}{(u^2 + v^2 + w^2)}\Big\}, \tag{3.2.8c}$$

where

$$u = (r'' - r\theta'^2), \quad v = (2r'\theta' + r\theta''), \quad w = z''$$

and

$$u' = r''' - r'\theta'^2 - 2r\theta'\theta'' \,, \quad v' = 2r''\theta' + 3r'\theta'' + r\theta''' \,, \quad w' = z''' \,.$$

So (3.2.8a) (3.2.8b) and (3.2.8c) are consistent with

Proposition 1

$$\tau = \frac{[\mathbf{N}' \times \mathbf{T}]_i}{[\mathbf{N}]_i}$$

where $[\,]_i$ denotes the i^{th} vector component.

Requiring (3.2.2), (3.2.4) and (3.2.6) to satisfy all the equations in (2.2.5) gives the following relations:

$$r'^2 + (r\theta')^2 + z'^2 = 1 \tag{3.2.9}$$

which is equivalent to (3.2.1). The second equation in (2.2.5) gives (3.2.5). The third equation leads to

$$\begin{aligned}\kappa^2 = {} & (r\theta' z'' - 2r'\theta' z' - r\theta'' z')^2 + (r' z'' - r'' z' + r\theta'^2 z')^2 \\ & + (2r'^2\theta' + rr'\theta'' - rr''\theta' + r^2\theta'^3)^2 \,.\end{aligned} \tag{3.2.10}$$

The fourth equation leads to

$$\frac{1}{\kappa}(r'r'' + rr'\theta'^2 + r^2\theta'\theta'' + z'z'') = 0, \tag{3.2.11}$$

while the last two equations give the scalar triple products in (2.2.8). The second equation in (2.2.7) yields

$$\kappa^2 = -r'r''' + 3r'^2\theta'^2 - 3rr''\theta'^2 + r^2\theta'^4 - r^2\theta'\theta''' - z'z''',$$

while the fourth equation gives

Proposition 2

$$\begin{aligned}\tau = -\frac{1}{\kappa^2}\Big(& rr''\theta' z''' - 3r''^2\theta' z' - 3r'r''\theta'' z' - rr''\theta''' z' + 4rr''\theta'^3 z' - r^2\theta'^3 z''' \\ & + r^2\theta'^2\theta''' z' - r^2\theta'^5 z' - 2r'^2\theta' z''' + 2r'r'''\theta' z' - 6r'^2\theta'^3 z' \\ & - 6rr'\theta'^2\theta'' z' - rr'\theta'' z''' + rr'''\theta'' z' - 3r^2\theta'\theta''^2 z' + 3r'r''\theta' z'' \\ & + 3r'^2\theta'' z'' + rr'\theta''' z'' - rr'''\theta' z'' + 2rr'\theta'^3 z'' + 3r^2\theta'^2\theta'' z''\Big).\end{aligned}$$

Taken together, equations (3.2.2), (3.2.4) and (3.2.6) constitute a transformation from a reference frame in cylindrical polar coordinates to the Frenet reference frame, and can be represented in matrix form

$$\begin{pmatrix} \mathbf{T} \\ \mathbf{N} \\ \mathbf{B} \end{pmatrix} = P \begin{pmatrix} \mathbf{e_r} \\ \mathbf{e}_\theta \\ \mathbf{k} \end{pmatrix},$$

where

$$P = \begin{pmatrix} r' & r\theta' & z' \\ \frac{(r''-r\theta'^2)}{\kappa} & \frac{(2r'\theta'+r\theta'')}{\kappa} & \frac{z''}{\kappa} \\ \frac{(r\theta' z''-(2r'\theta'+r\theta'')z')}{\kappa} & \frac{-(r'z''-(r''-r\theta'^2)z')}{\kappa} & \frac{(r'(2r'\theta'+r\theta'')-r\theta'(r''-r\theta'^2))}{\kappa} \end{pmatrix}.$$

To express the transformation from the Frenet frame to a frame in cylindrical polar coordinates, the inverse of P must be found, and thus

$$\begin{pmatrix} \mathbf{e_r} \\ \mathbf{e}_\theta \\ \mathbf{k} \end{pmatrix} = P^{-1} \begin{pmatrix} \mathbf{T} \\ \mathbf{N} \\ \mathbf{B} \end{pmatrix} \tag{3.2.12}$$

where

$$P^{-1} = \begin{pmatrix} \frac{-(r''-r\theta'^2)(2rr'\theta'^2+r^2\theta'\theta''+z'z'')+r'((2r'\theta'+r\theta'')^2+z''^2)}{\kappa^2} & \\ \frac{-(r''-r\theta'^2)(2r'^2\theta'-r\theta'(r''-r\theta'^2)+rr'\theta'')-(2r'\theta'+r\theta'')z'z''+r\theta'z''^2}{\kappa^2} & \cdots \\ \frac{(4r'^2\theta'^2+(r''-r\theta'^2)^2+4rr'\theta'\theta''+r^2\theta''^2)z'-(r'(r''+r\theta'^2)+r^2\theta'\theta'')z''}{\kappa^2} & \end{pmatrix}$$

$$\begin{pmatrix} \frac{-\kappa(r''-r\theta'^2)(r'^2+r^2\theta'^2+z'^2)}{\kappa^2} & \frac{\kappa(-2r'\theta'z'-r\theta''z'+r\theta'z'')}{\kappa^2} \\ \frac{\kappa(2r'^3\theta'+rr'^2\theta''+r'\theta'(-rr''+r^2\theta'^2+2z'^2)+rz'(\theta''z'-\theta'z''))}{\kappa^2} & \frac{\kappa(r''z'-r\theta'^2z'-r'z'')}{\kappa^2} \\ \frac{-\kappa(r'(r''+r\theta'^2)z'-r'^2z''+r^2\theta'(\theta''z'-\theta'z''))}{\kappa^2} & \frac{\kappa(2r'^2\theta'+rr'\theta''-rr''\theta'+r^2\theta'^3)}{\kappa^2} \end{pmatrix}.$$

The entries in the first column can be simplified by using (3.2.11), and then (3.2.5), while the entries in the second column require the use of (3.2.11) then (3.2.9). Once this has been done, the transformation matrix $P^{-1} = P^T$ as expected from Definition (5)

Proposition 3

$$P^{-1} = \begin{pmatrix} r' & \frac{(r''-r\theta'^2)}{\kappa} & \frac{(r\theta'z''-(2r'\theta'+r\theta'')z')}{\kappa} \\ r\theta' & \frac{(2r'\theta'+r\theta'')}{\kappa} & \frac{-(r'z''-(r''-r\theta'^2)z')}{\kappa} \\ z' & \frac{z''}{\kappa} & \frac{(r'(2r'\theta'+r\theta'')-r\theta'(r''-r\theta'^2))}{\kappa} \end{pmatrix}. \tag{3.2.13}$$

3.3 Surface of revolution for a general curve rotating around a fixed axis

The objective of this section is to consider the path that the yarn takes as it is drawn through the device and envisage a surface that contains this path for every point on the path. The yarn path is represented by a curve, and it is rotated around the axis of symmetry of the device (the spindle about which the device rotates) to create the surface (essentially the yarn balloon mentioned in the introduction). The curve is in a frame of reference S which is rotating at a constant rate around the spindle of the device (which is taken to be the z-axis). The Frenet and Darboux frames will then be calculated at a general point P^* (Figure 3.1) which both lies on the curve and in the surface.

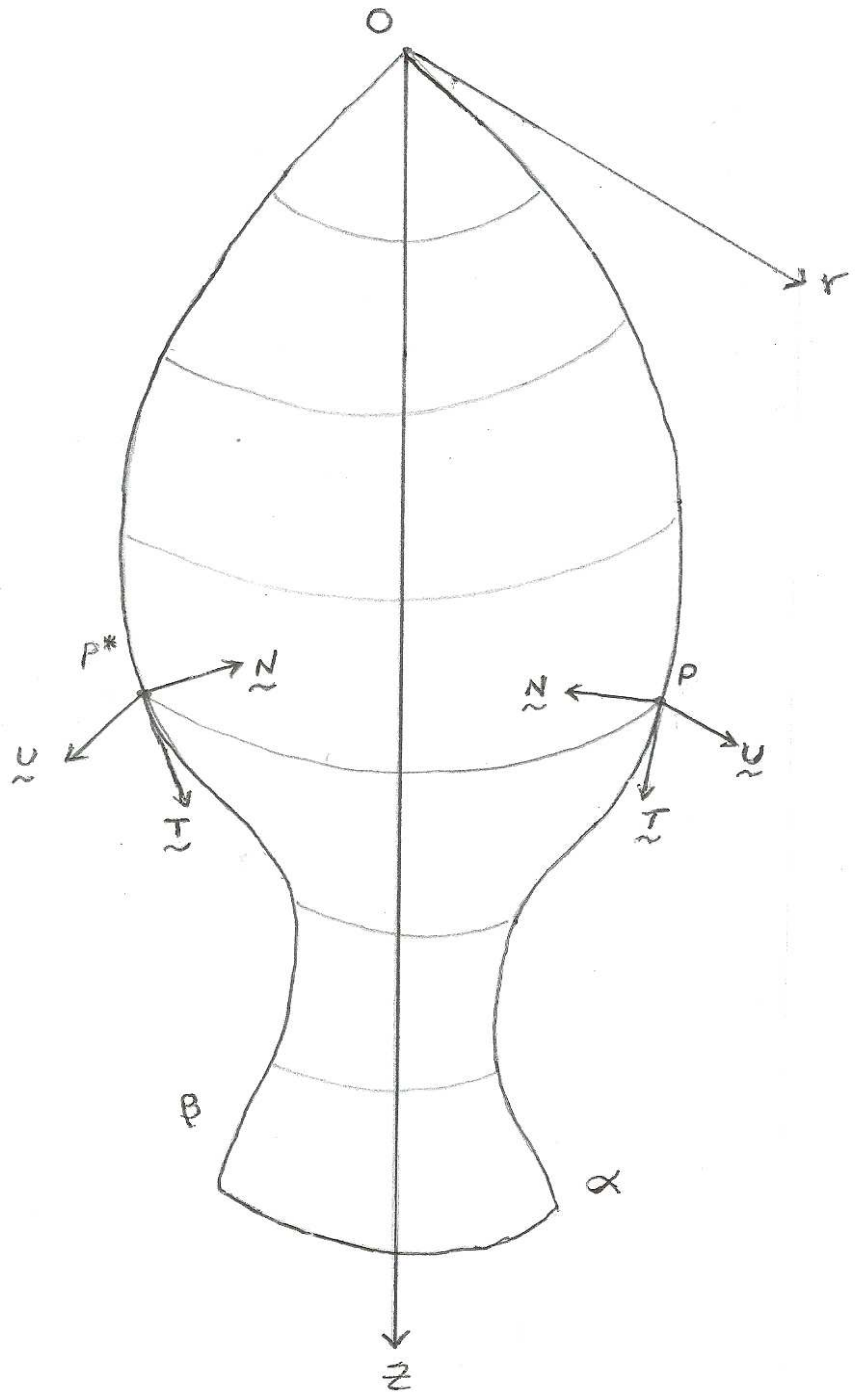

Figure 3.1: The surface of revolution for curves α and β with vectors $\mathbf{T}$, $\mathbf{N}$ and $\mathbf{U}$ at points P and P^*.

Consider a unit speed curve $\alpha(s)$ in $\mathbb{R}^3$. A point P on this curve in cylindrical coordinates $(r(s), \theta(s), z(s))$ is represented in Cartesian coordinates as

$$(r(s)\cos\theta(s), r(s)\sin\theta(s), z(s)).$$

When the arc length $s = 0$, let $r = 0$ and $z = 0$, and define $\theta = 0$ in the direction of $\alpha'(0)$. We define the surface of revolution M of the curve α around the z-axis in Cartesian coordinates. Let D be an open set in $\mathbb{R}^2$ such that $0 \leq s < \infty$, $0 \leq \phi \leq 2\pi$ and define

$$X : D \to \mathbb{R}^3$$

by

$$X(s, \phi) = (r(s)\cos(\phi + \theta(s)), r(s)\sin(\phi + \theta(s)), z(s)).$$

Thus

$$\begin{aligned} X_s = \Bigg(& \frac{dr}{ds}\cos(\phi + \theta(s)) - r(s)\frac{d\theta}{ds}\sin(\phi + \theta(s)), \\ & \frac{dr}{ds}\sin(\phi + \theta(s)) + r(s)\frac{d\theta}{ds}\cos(\phi + \theta(s)), \frac{dz}{ds}\Bigg), \\ X_\phi = & (-r(s)\sin(\phi + \theta(s)), r(s)\cos(\phi + \theta(s)), 0), \end{aligned}$$

and

$$X_s \times X_\phi = (-rz'\cos(\phi + \theta), -rz'\sin(\phi + \theta), rr').$$

Thus the unit normal vector to the surface M at $X(s, \phi)$ is

Proposition 4

$$\begin{aligned} \mathbf{U} &= \frac{X_s \times X_\phi}{\|X_s \times X_\phi\|} \\ &= \frac{1}{\sqrt{r'^2 + z'^2}}(-z'\cos(\phi + \theta), -z'\sin(\phi + \theta), r'). \end{aligned} \tag{3.3.14}$$

The second partial derivatives give the following expressions

$$X_{ss} = \Big((r'' - r\theta'^2)\cos(\phi+\theta) - (2r'\theta' + r\theta'')\sin(\phi+\theta),$$
$$(r'' - r\theta'^2)\sin(\phi+\theta) + (2r'\theta' + r\theta'')\cos(\phi+\theta), z''\Big),$$

$$X_{\phi\phi} = (-r\cos(\phi+\theta), -r\sin(\phi+\theta), 0),$$

$$X_{s\phi} = (-r'\sin(\phi+\theta) - r\theta'\cos(\phi+\theta), r'\cos(\phi+\theta) - r\theta'\sin(\phi+\theta), 0).$$

We now calculate the Gaussian curvature using the recipe outlined in O'Neill [3]. First determine the following real valued functions

$$\mathrm{E} = X_s \cdot X_s = r'^2 + r^2\theta'^2 + z'^2,$$

$$\mathrm{F} = X_s \cdot X_\phi = r^2\theta',$$

$$\mathrm{G} = X_\phi \cdot X_\phi = r^2,$$

$$\mathrm{L} = S(X_s)\cdot X_s = \mathbf{U}\cdot X_{ss} = \frac{1}{\sqrt{r'^2+z'^2}}(r'z'' - r''z' + r\theta'^2 z'),$$

$$\mathrm{M} = S(X_s)\cdot X_\phi = \mathbf{U}\cdot X_{s\phi} = \frac{r\theta' z'}{\sqrt{r'^2+z'^2}},$$

$$\mathrm{N} = S(X_\phi)\cdot X_\phi = \mathbf{U}\cdot X_{\phi\phi} = \frac{rz'}{\sqrt{r'^2+z'^2}}.$$

The Gaussian curvature is

$$K(X) = \frac{\mathrm{LN} - \mathrm{M}^2}{\mathrm{EG} - \mathrm{F}^2} = \frac{rz'(r'z'' - r''z')}{r^2(r'^2+z'^2)^2}$$

and the mean curvature is

$$H(X) = \frac{\mathrm{GL} + \mathrm{EN} - 2\mathrm{FM}}{2(\mathrm{EG} - \mathrm{F}^2)} = \frac{r^2(r'z'' - r''z') + rz'(r'^2+z'^2)}{2r^2(r'^2+z'^2)^{3/2}}.$$

The principal curvature functions are given by

$$k_1, k_2 = H \pm \sqrt{H^2 - K}$$

so

$$k_1 = \frac{(r'z'' - r''z')}{(r'^2+z'^2)^{3/2}}$$

and

$$k_2 = \frac{z'}{r\sqrt{r'^2 + z'^2}}$$

and hence the shape operator is

Proposition 5

$$S = \frac{1}{\sqrt{r'^2 + z'^2}} \begin{pmatrix} \frac{(r'z'' - r''z')}{(r'^2 + z'^2)} & 0 \\ 0 & \frac{z'}{r} \end{pmatrix}.$$

From earlier calculations ((3.2.2), here in Cartesian coordinates) the unit tangent vector field at the point P, which lies both on the curve α and on the surface M is

$$\mathbf{T} = \frac{d\mathbf{R}}{ds} = ((r'\cos\theta - r\theta'\sin\theta), (r'\sin\theta + r\theta'\cos\theta), z'). \tag{3.3.15}$$

The principal normal vector field of α at P is

$$\mathbf{N} = \frac{d\mathbf{T}}{ds}\Big/\kappa = \frac{1}{\kappa}\Big\{(((r'' - r\theta'^2)\cos\theta - (2r'\theta' + r\theta'')\sin\theta),$$
$$((r'' - r\theta'^2)\sin\theta + (2r'\theta' + r\theta'')\cos\theta), z'')\Big\},$$

where κ is the curvature function of α

$$\kappa = \sqrt{(r'' - r\theta'^2)^2 + (2r'\theta' + r\theta'')^2 + z''^2}\,.$$

Consider the curve α rotated by an angle ϕ around the z-axis. The point P mentioned above is rotated to a new point P^*, and there is a new curve β that is congruent to α because this rotation is an isometry. Hence the vectors $\mathbf{T}$ and $\mathbf{N}$ at P^* on β are

$$\mathbf{T} = ((r'\cos(\phi+\theta) - r\theta'\sin(\phi+\theta)), (r'\sin(\phi+\theta) + r\theta'\cos(\phi+\theta)), z')$$

and

$$\mathbf{N} = \frac{1}{\kappa}\Big\{(((r'' - r\theta'^2)\cos(\phi+\theta) - (2r'\theta' + r\theta'')\sin(\phi+\theta)),$$
$$((r'' - r\theta'^2)\sin(\phi+\theta) + (2r'\theta' + r\theta'')\cos(\phi+\theta)), z'')\Big\}. \tag{3.3.16}$$

Let the angle between $\mathbf{N}$ and $\mathbf{U}$ at P^* be ψ, which can be calculated by taking the dot product between (3.3.16) and (3.3.14)

Proposition 6

$$\mathbf{N}\cdot\mathbf{U} = \cos\psi = \frac{1}{\kappa\sqrt{r'^2+z'^2}}(r'z'' - r''z' + r\theta'^2 z'). \tag{3.3.17}$$

Note that this expression is independent of ϕ, so this result applies anywhere on the surface M.

3.4 The transformation between cylindrical polar coordinates and the Darboux frame

The Darboux frame field for the unit speed curve α consists of the three unit vectors $\mathbf{T}(3.3.15), \mathbf{U}(3.3.14)$ and $\mathbf{V}$, where $\mathbf{U}$ is the surface normal, now restricted to the curve α and

$$\begin{aligned}\mathbf{V} &= \mathbf{U}\times\mathbf{T}\\ &= \frac{1}{\sqrt{r'^2+z'^2}}\Big\{(-\sin(\phi+\theta)(r'^2+z'^2) - rr'\theta'\cos(\phi+\theta)),\\ &\quad (\cos(\phi+\theta)(r'^2+z'^2) - rr'\theta'\sin(\phi+\theta)), -r\theta' z')\Big\}.\end{aligned}$$

The transformation between the Frenet frame and the Darboux frame depends only upon ψ, the angle between $\mathbf{N}$ and $\mathbf{U}$, shown in Figure 3.2,

$$\begin{pmatrix}\mathbf{T}\\ \mathbf{N}\\ \mathbf{B}\end{pmatrix} = Q\begin{pmatrix}\mathbf{T}\\ \mathbf{U}\\ \mathbf{V}\end{pmatrix} \tag{3.4.18}$$

where

$$Q = \begin{pmatrix}1 & 0 & 0\\ 0 & \cos\psi & -\sin\psi\\ 0 & -\sin\psi & -\cos\psi\end{pmatrix} \tag{3.4.19}$$

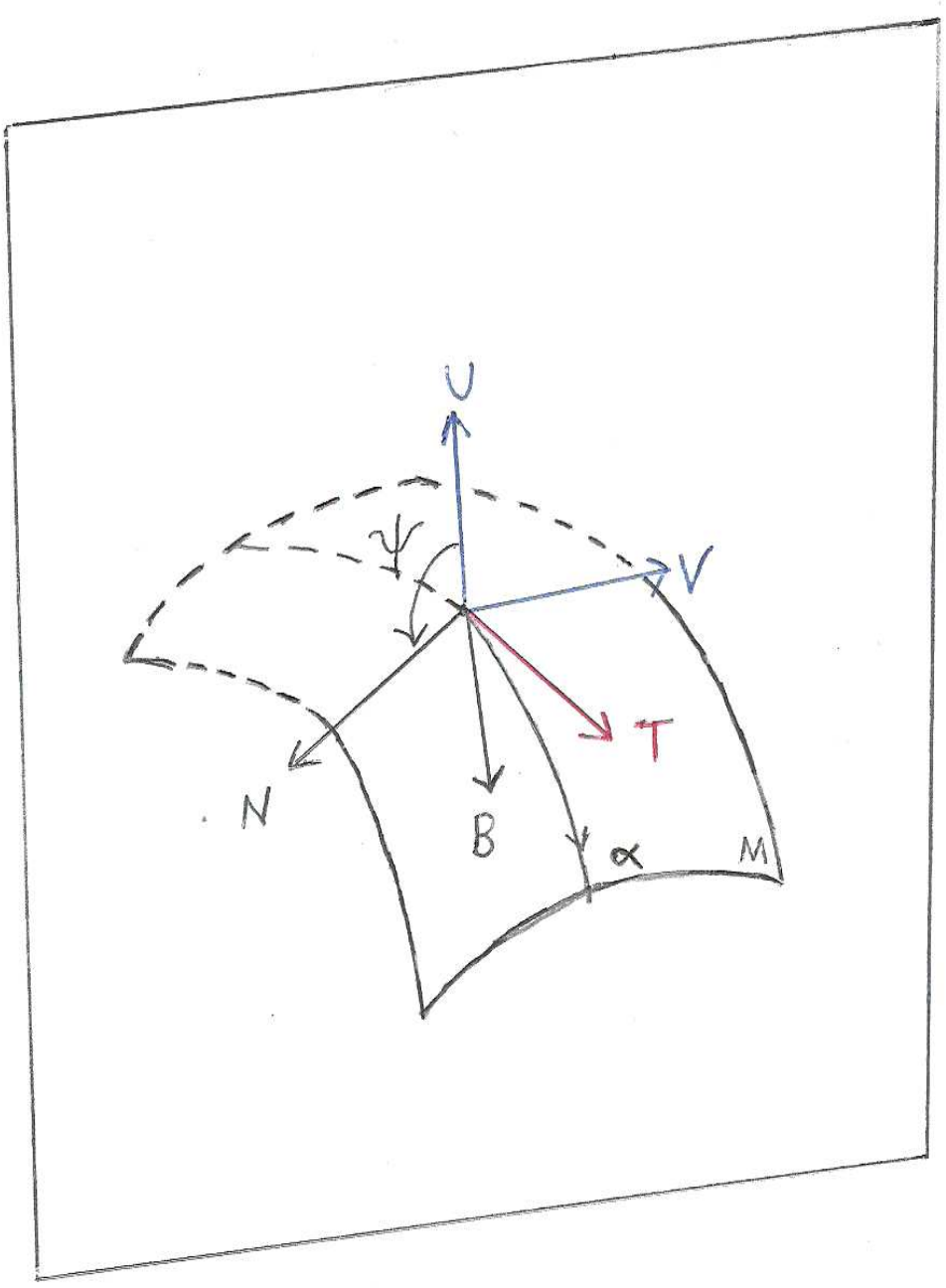

Figure 3.2: The Frenet and Darboux frames at a point on the curve α in the surface M showing the angle ψ between $\mathbf{N}$ and $\mathbf{U}$.

and

$$\sin\psi = \frac{\sqrt{(r'(r''-r\theta'^2)+z'z'')^2+(r'^2+z'^2)(2r'\theta'+r\theta'')^2}}{\kappa\sqrt{r'^2+z'^2}}. \tag{3.4.20}$$

The transformation from cylindrical polar coordinates to the Darboux frame can now be calculated from (3.2.12), (3.2.13) and (3.4.18), (3.4.19) by substituting for $\cos\psi$ from (3.3.17) and for $\sin\psi$ from (3.4.20)

$$\begin{pmatrix} \mathbf{e}_r \\ \mathbf{e}_\theta \\ \mathbf{k} \end{pmatrix} = P^{-1}Q \begin{pmatrix} \mathbf{T} \\ \mathbf{U} \\ \mathbf{V} \end{pmatrix} \tag{3.4.21}$$

where

Proposition 7

$$P^{-1}Q = \begin{pmatrix} r' & \\ r\theta' & \dots \\ z' & \end{pmatrix}$$

$$\begin{pmatrix} \frac{(r''-r\theta'^2)(r'z''-(r''-r\theta'^2)z')-(r\theta'z''-(2r'\theta'+r\theta'')z')\sqrt{(r'(r''-r\theta'^2)+z'z'')^2+(r'^2+z'^2)(2r'\theta'+r\theta'')^2}}{\kappa^2\sqrt{r'^2+z'^2}} \\ \frac{(2r'\theta'+r\theta'')(r'z''-(r''-r\theta'^2)z')-(-rz''+(r''-r\theta'^2)z')\sqrt{(r'(r''-r\theta'^2)+z'z'')^2+(r'^2+z'^2)(2r'\theta'+r\theta'')^2}}{\kappa^2\sqrt{r'^2+z'^2}} \\ \frac{z''(r'z''-(r''-r\theta'^2)z')-(r'(2r'\theta'+r\theta'')-r\theta'(r''-r\theta'^2))\sqrt{(r'(r''-r\theta'^2)+z'z'')^2+(r'^2+z'^2)(2r'\theta'+r\theta'')^2}}{\kappa^2\sqrt{r'^2+z'^2}} \end{pmatrix} \dots$$

$$\begin{pmatrix} -\frac{(r''-r\theta'^2)\sqrt{(r'(r''-r\theta'^2)+z'z'')^2+(r'^2+z'^2)(2r'\theta'+r\theta'')^2}+(r\theta'z''-(2r'\theta'+r\theta'')z')(r'z''-(r''-r\theta'^2)z')}{\kappa^2\sqrt{r'^2+z'^2}} \\ -\frac{(2r'\theta'+r\theta'')\sqrt{(r'(r''-r\theta'^2)+z'z'')^2+(r'^2+z'^2)(2r'\theta'+r\theta'')^2}+(-r'z''+(r''-r\theta'^2)z')(r'z''-(r''-r\theta'^2)z')}{\kappa^2\sqrt{r'^2+z'^2}} \\ -\frac{z''\sqrt{(r'(r''-r\theta'^2)+z'z'')^2+(r'^2+z'^2)(2r'\theta'+r\theta'')^2}+(r'(2r'\theta'+r\theta'')-r\theta'(r''-r\theta'^2))(r'z''-(r''-r\theta'^2)z')}{\kappa^2\sqrt{r'^2+z'^2}} \end{pmatrix}.$$

3.5 No air drag case

As a first step towards solving these equations, it is useful to consider the case where there is no air drag ($p_0 = 0$). The EoM then reduce to

$$-r\mathbf{e_r} = \frac{dT_e}{ds}\frac{d\mathbf{r}}{ds} + T_e\frac{d^2\mathbf{r}}{ds^2}. \tag{3.5.22}$$

Representing this equation in the Frenet frame by substituting for $\mathbf{e_r}$ from (3.2.12), and using (3.2.2) for $\frac{d\mathbf{r}}{ds}$ and using (3.2.3) and (3.2.4) for $\frac{d^2\mathbf{r}}{ds^2}$

$$-rr'\mathbf{T} - \frac{r(r'' - r\theta'^2)}{\kappa}\mathbf{N} - \frac{r(r\theta' z'' - (2r'\theta' + r\theta'')z')}{\kappa}\mathbf{B} = \frac{dT_e}{ds}\mathbf{T} + T_e\kappa\mathbf{N}.$$

Equating the coefficients of $\mathbf{T}, \mathbf{N}$ and $\mathbf{B}$ yields

Proposition 8

$$\frac{dT_e}{ds} + rr' = 0, \tag{3.5.23a}$$

$$T_e\kappa + \frac{r(r'' - r\theta'^2)}{\kappa} = 0, \tag{3.5.23b}$$

$$\frac{r(r\theta' z'' - (2r'\theta' + r\theta'')z')}{\kappa} = 0. \tag{3.5.23c}$$

Similarly, representing (3.5.22) in the Darboux frame by using (3.4.21) and (3.4.18) yields

Proposition 9

$$0 = \frac{dT_e}{ds} + rr', \tag{3.5.24a}$$

$$\begin{aligned} 0 = &\frac{1}{\kappa^2\sqrt{r'^2 + z'^2}}\Big\{ - (T_e\kappa^2 + r(r'' - r\theta'^2))(r'z'' - (r'' - r\theta'^2)z') \\ &+ r(r\theta' z'' - (2r'\theta' + r\theta'')z') \\ &\sqrt{(r'(r'' - r\theta'^2) + z'z'')^2 + (r'^2 + z'^2)(2r'\theta' + r\theta'')^2}\Big\}, \end{aligned} \tag{3.5.24b}$$

$$\begin{aligned} 0 = &\frac{1}{\kappa^2\sqrt{r'^2 + z'^2}}\Big\{r(r\theta' z'' - (2r'\theta' + r\theta'')z')(r'z'' - (r'' - r\theta'^2)z') \\ &+ (T_e\kappa^2 + r(r'' - r\theta'^2))\sqrt{(r'(r'' - r\theta'^2) + z'z'')^2 + (r'^2 + z'^2)(2r'\theta' + r\theta'')^2}\Big\}. \end{aligned} \tag{3.5.24c}$$

Equation (3.5.23a) gives

$$T_e = C_1 - \frac{r^2}{2} \quad \text{where} \quad T_e \geqslant 0. \tag{3.5.25}$$

3.5.1 An integral form for s

Multiplying the numerator of (3.5.23c) by $\frac{1}{r^4\theta'^2}$ yields

$$\frac{z'}{r^2\theta'} = C_2 \tag{3.5.26}$$

assuming $r \neq 0$ and $\theta' \neq 0$. Substituting for T_e from (3.5.25) and for κ from (3.2.5) and using (3.5.26) to eliminate z'' in (3.5.23b) yields

$$(C_1 - \frac{r^2}{2})((r'' - r\theta'^2)^2 + (1 + C_2^2 r^2)(2r'\theta' + r\theta'')^2) + r(r'' - r\theta'^2) = 0\,.$$

At this stage there are three cases where progress can be made with elementary techniques. Further progress requires more advanced techniques.

Firstly, if the tension in the yarn, $T_e = 0$, then $r'' - r\theta'^2 = 0$. This case is not immediately relevant to this investigation.

Secondly, if $r'' - r\theta'^2 = 0$ and $2r'\theta' + r\theta'' = 0$, then multiplying the second equation by $\frac{1}{2\sqrt{\theta'}}$ gives

$$r\sqrt{\theta'} = C_3$$

and then substituting into the first equation gives

$$r^3 r'' = C_3^4.$$

after some further work, the solution is

Proposition 10

$$\begin{aligned} r &= \sqrt{2C_4(s + C_5)^2 + \frac{C_3^4}{2C_4}}, \\ \theta &= \arctan\left(\frac{2C_4(s + C_5)}{C_3^2}\right) + C_7, \\ z &= C_2 C_3^2 s + C_6. \end{aligned}$$

Thirdly, if $2r'\theta' + r\theta'' = 0$ (assuming $r'' - r\theta'^2 \neq 0$) then

$$(C_1 - \frac{r^2}{2})(r'' - \frac{C_3^4}{r^3}) + r = 0.$$

After multiplying both sides by r' and integrating, this leads to

Proposition 11

$$s = \pm \int \frac{r\,\mathrm{d}r}{\sqrt{2r^2(C_4 + \ln(C_1 - \frac{r^2}{2})) - C_3^4}}\,.$$

3.5.2 Planar solutions

Another solution to equations (3.5.23a), (3.5.23b), (3.5.23c), (3.5.24a), (3.5.24b) and (3.5.24c) occurs when the yarn path lies on the vertical plane containing the z-axis, which also rotates around the z-axis. In this case the angle between $\mathbf{U}$ and $\mathbf{N}$ is $\psi = \pi$, and so $\cos\psi = -1$ and $\sin\psi = 0$ yield

$$\begin{aligned}(r'z'' - (r'' - r\theta'^2)z') &= -\kappa\sqrt{r'^2 + z'^2},\\ (r'(r'' - r\theta'^2) + z'z'')^2 + (r'^2 + z'^2)(2r'\theta' + r\theta'')^2 &= 0 \qquad (3.5.27)\end{aligned}$$

and (3.5.23b) yields

$$T_e\kappa^2 + r(r'' - r\theta'^2) = 0 \qquad (3.5.28)$$

where T_e is again given by equation (3.5.25). Equation (3.5.27) implies that

$$r'(r'' - r\theta'^2) + z'z'' = 0 \quad \text{and} \qquad (3.5.29)$$

$$2r'\theta' + r\theta'' = 0. \qquad (3.5.30)$$

Multiplying (3.5.30) by r leads to

$$r^2\theta' = C_2. \qquad (3.5.31)$$

Using this expression to substitute for θ' in (3.5.29), then integrating gives

$$\frac{1}{2}\Big(r'^2 - \frac{C_2^2}{r^2} + z'^2\Big) = C_3\,. \qquad (3.5.32)$$

Similarly substituting (3.5.25) and (3.5.31) into (3.5.28) gives

$$-r\Big(r'' - \frac{C_2^2}{r^3}\Big) = \Big(C_1 - \frac{r^2}{2}\Big)\Big(\Big(r'' - \frac{C_2^2}{r^3}\Big)^2 + z''^2\Big). \tag{3.5.33}$$

The boundary condition for ring spinning and the two-for-one twister at the guide eye is that

$$r = 0\,, z = 0 \quad \text{at} \quad s = 0$$

and so

$$C_2 = 0 \quad \text{and} \quad \theta = C_4$$

that is, the solution lies in the $r - z$ plane as expected, for yarn spinning applications. For an inextensible yarn, (3.5.32) becomes

$$r'^2 + z'^2 = 1$$

and equation (3.5.33) then becomes

$$-rr'' = \Big(C_1 - \frac{r^2}{2}\Big)\Big(r''^2 + z''^2\Big).$$

Concluding Remarks The results derived in this chapter are in agreement with previous authors [68], [15], [14], [16], that solutions to the yarn balloon equations in a vacuum are planar in the reference frame S with constant angular rotation. Some more work is required here to obtain a complete set of analytical solutions, although it is likely that it will only replicate the results of [68], [14] and [16]. The solutions found by [69] with the extension of constant tangential motion V_0 are not planar, due to the inclusion of Coriolis forces. However, if V_0 is very small compared to the linear velocity of the yarn element, and we only consider quasi-stationary solutions, the Coriolis term can be neglected and thus the solutions are planar.

In the next chapter we will now consider the case where Padfield's dimensionless air drag parameter p_0 is non-zero, rewriting the yarn balloon equations,

including Padfield's air drag term, in intrinsic coordinates. The fact that the solutions found in this chapter are planar provides the basis for the new frame of reference used in the next chapter.

Chapter 4

The yarn balloon equations with Padfield's air drag term in intrinsic coordinates

4.1 Introduction

In this section, the objective is to set up the framework that will be used to model the yarn balloon with air drag, using the Padfield model. The yarn balloon equations were recast in an intrinsic coordinate system in the previous chapter for the yarn balloon in vacuo. The effect of air drag in this system is significant, in fact it is essential to the proper functioning of devices such as the two-for-one twister, in that it is through air drag that the boundary condition at the rim of the over-run plate can be achieved. In Section 4.2, the justification for the assumption that $\mathbf{B}$ remains horizontal is presented. In Section 4.3 a new reference frame S' is defined. It is assumed that $\mathbf{B}$ remains horizontal along the entire yarn balloon, and so the yarn path lies in a vertical osculating plane. In Section 4.4, the EoM are expressed in the new reference

frame S' with the intrinsic coordinates. In Section 4.5, Padfield's air drag term is used in the expression of the EoM found in Section 4.4. The task of determining a new, more accurate air drag term for the EoM in this new framework is addressed in Chapters 5 and 6.

4.2 The justification for modelling B as remaining horizontal

Consider a yarn element of length δs at point P in the yarn balloon, at an angle β to the vertical (Figure 4.1), and an angle $(\phi - \Phi)$ with the ray OP on the horizontal plane. With air drag proportional to v^2, and $v^2 = r^2 e_\theta$ in the quasi-stationary case, then air drag is proportional to r^2. The change in r along the yarn element is

$$\delta r = \cos(\phi - \Phi) \sin\beta \, \delta s \, . \tag{4.2.1}$$

If there is a change in magnitude of the air drag force across the yarn element then a rotation will occur. Consider the two extreme cases for a single loop balloon. If the yarn element is horizontal, with $\mathbf{T}$ pointing radially outwards, $\delta r = \delta s$ in (4.2.1) and the yarn element rotates such that $\mathbf{T}$ and $\mathbf{B}$ move in the horizontal plane. If the yarn element is vertical, there is a slight differential across the width of the yarn which will act to rotate the yarn element around the yarn axis. In this case, $\mathbf{T}$ is unchanged while $\mathbf{B}$ moves horizontally.

Now consider the case somewhere in between these two extremes,

$$0 < (\phi - \Phi) < \frac{\pi}{2} \quad \text{and} \quad 0 < \beta < \frac{\pi}{2} \, .$$

As $(\phi - \Phi)$ increases, δr gets smaller, and so the amount of rotation caused by the air drag is reduced. As β increases from zero, the plane in which $\mathbf{B}$

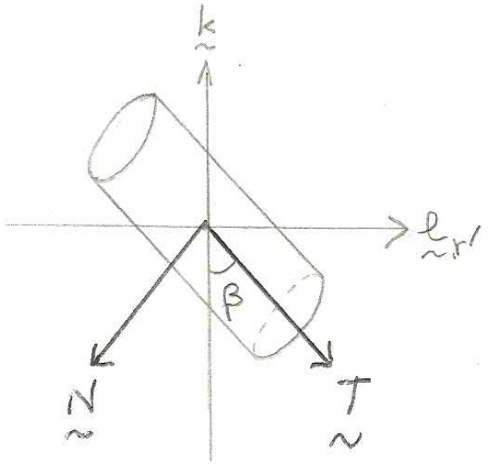

Figure 4.1: The yarn element in reference frame S', with $\mathbf{T}$ making an angle β with the vertical axis.

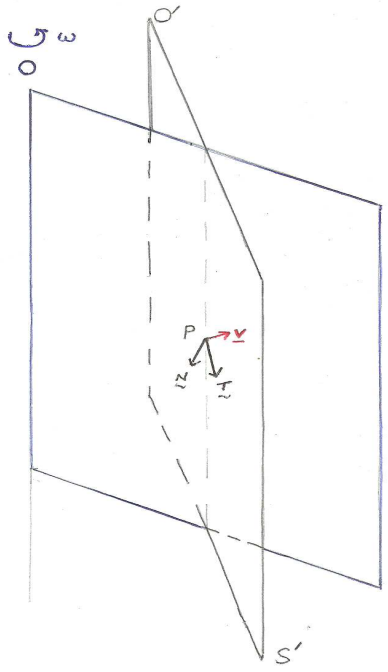

Figure 4.2: The yarn element at P is planar in reference frame S', which moves relative to the rotating reference frame S.

is rotated is at an angle β to the horizontal, however the amount of rotation around the yarn axis gets smaller.

Therefore, as a first attempt to model this situation, I will assume that **B** is always horizontal and thus **T** and **N** lie in a vertical plane.

4.3 The new non-inertial reference frame S'

The yarn spinning device rotates at an angular velocity of ω about the spindle, or axis of rotation, which contains the point O fixed in an inertial reference frame coincident with the guide eye. With no air drag, the yarn path remains on a vertical plane through O, rotating with angular velocity ω. Considering a reference frame, S, rotating with angular velocity ω about the axis of rotation containing O, to an observer in this frame, the in vacuo quasi-stationary yarn path appears fixed on a vertical plane. We can imagine that for a yarn element at a point P on this yarn path that any air drag would lift the yarn element off this plane. In fact, as s increases along the yarn path, air drag moves the yarn element further away from the original plane. That is, θ is always an increasing function of s for yarn balloons in the presence of air drag. Therefore we model the yarn path being in a vertical plane, containing **T** and **N**, rotating around a point O', the centre of rotation for a rotating reference frame S', as shown in Figure 4.2. The yarn element is represented as an inclined cylinder. The point O' moves relative to the fixed point O, as s increases as we move along the yarn. The assumption that the plane is vertical means that **B** is horizontal.
To put this another way, the yarn element at P always lies in a plane containing **T** and **N** (by definition), and our objective is to model the effect air drag has on the yarn element and thus this plane. We have assumed that this plane remains vertical, but it is allowed to rotate around a vertical axis containing

the point O'. As s increases as we move along the yarn, O' is allowed to move relative to O.

The position vector of the yarn element in S is $\mathbf{r} = r\mathbf{e}_r + 0\mathbf{e}_\theta + z\mathbf{k}$, while the coordinates in S are $(r(s,t), \theta(s,t), z(s,t))$, in S' they are $(r'(s,t), \theta'(s,t), z'(s,t))$ relative to O' and the coordinates of O' are $(R(s,t), \Theta(s,t), z(s,t))$. So

$$\mathbf{r} = \mathbf{R} + \mathbf{r}' \quad \text{where} \quad \mathbf{R} = R\,\mathbf{e}_R + 0\,\mathbf{e}_\Theta \quad \text{and} \quad \frac{d\mathbf{R}}{ds} = \frac{dR}{ds}\mathbf{e}_R + R\frac{d}{ds}\Big(\mathbf{e}_R\Big), \tag{4.3.2}$$

and

$$\frac{d}{ds}\Big(\mathbf{e}_R\Big) = -R\frac{d\Theta}{ds}\mathbf{e}_\Theta.$$

The position vector of P relative to O' is

$$\mathbf{r}' = r'\mathbf{e}_{r'} + 0\mathbf{e}_{\theta'} + z'\mathbf{k}$$

where $\theta' = 0$ and $z' = z$.

Using the Cosine rule in $\triangle OO'P$ (Figure 4.3),

$$r^2 = R^2 + r'^2 + 2r'R\cos\phi.$$

Using the Sine rule in $\triangle OO'P$,

$$\frac{r'}{\sin\Phi} = \frac{r}{\sin\phi} = \frac{R}{\sin(\phi - \Phi)}.$$

The relationship between the unit vectors is given by rotation matrices

$$\begin{pmatrix} \mathbf{e}_r \\ \mathbf{e}_\theta \\ \mathbf{k} \end{pmatrix} = \begin{pmatrix} \cos(\phi-\Phi) & \sin(\phi-\Phi) & 0 \\ -\sin(\phi-\Phi) & \cos(\phi-\Phi) & 0 \\ 0 & 0 & 1 \end{pmatrix} \begin{pmatrix} \mathbf{e}_{r'} \\ \mathbf{e}_{\theta'} \\ \mathbf{k} \end{pmatrix} \tag{4.3.3}$$

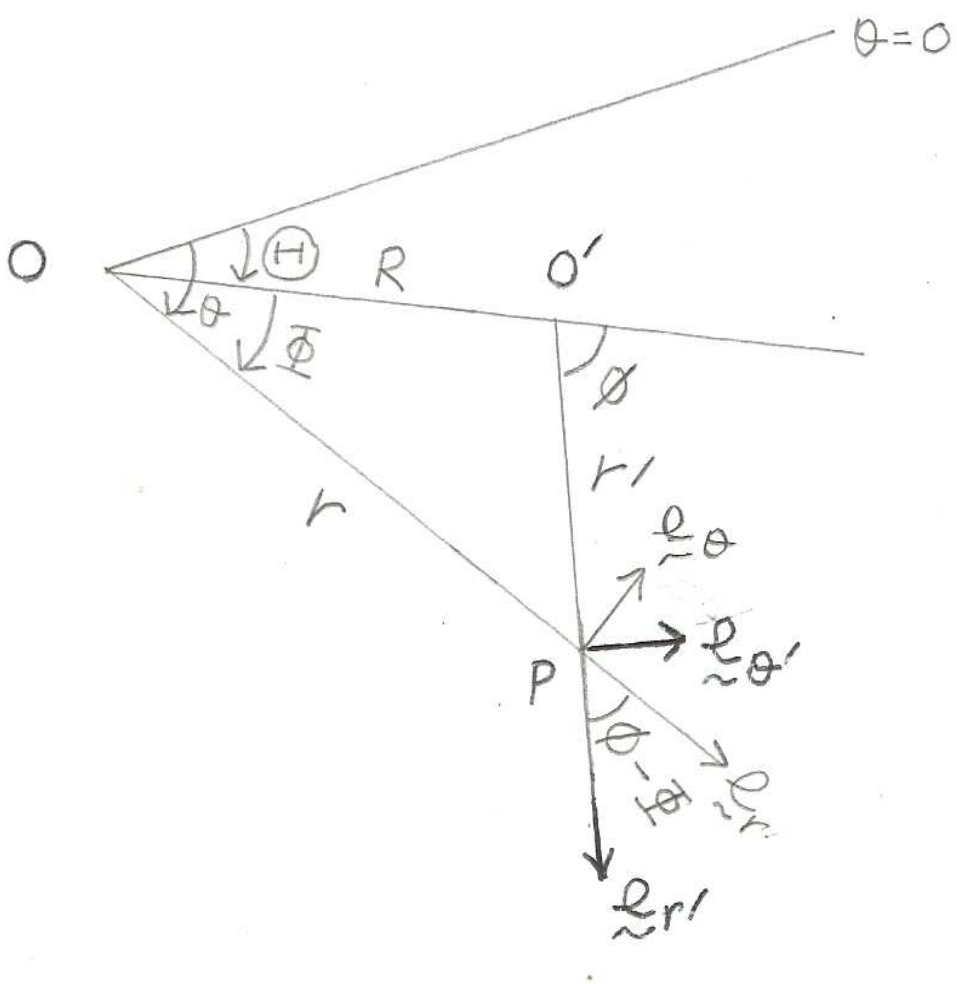

Figure 4.3: A horizontal cross-section showing the distances and angles between the points O, O' and P.

and

$$\begin{pmatrix} \mathbf{e}_R \\ \mathbf{e}_\Theta \\ \mathbf{k} \end{pmatrix} = \begin{pmatrix} \cos\phi & \sin\phi & 0 \\ -\sin\phi & \cos\phi & 0 \\ 0 & 0 & 1 \end{pmatrix} \begin{pmatrix} \mathbf{e}_{r'} \\ \mathbf{e}_{\theta'} \\ \mathbf{k} \end{pmatrix}$$

and

$$\begin{pmatrix} \mathbf{e}_R \\ \mathbf{e}_\Theta \\ \mathbf{k} \end{pmatrix} = \begin{pmatrix} \cos\Phi & \sin\Phi & 0 \\ -\sin\Phi & \cos\Phi & 0 \\ 0 & 0 & 1 \end{pmatrix} \begin{pmatrix} \mathbf{e}_r \\ \mathbf{e}_\theta \\ \mathbf{k} \end{pmatrix} . \tag{4.3.4}$$

Using (3.2.12) and (3.2.13) for the primed coordinates, with $\theta' = 0$,

$$\begin{pmatrix} \mathbf{e}_{r'} \\ \mathbf{e}_{\theta'} \\ \mathbf{k} \end{pmatrix} = \begin{pmatrix} \frac{dr'}{ds} & \frac{\frac{d^2r'}{ds^2}}{\kappa'} & 0 \\ 0 & 0 & 1 \\ \frac{dz'}{ds} & \frac{\frac{d^2z'}{ds^2}}{\kappa'} & 0 \end{pmatrix} \begin{pmatrix} \mathbf{T} \\ \mathbf{N} \\ \mathbf{B} \end{pmatrix} . \tag{4.3.5}$$

From (4.3.3) and (4.3.5)

$$\begin{pmatrix} \mathbf{e}_r \\ \mathbf{e}_\theta \\ \mathbf{k} \end{pmatrix} = \begin{pmatrix} \frac{dr'}{ds}\cos(\phi-\Phi) & \frac{\frac{d^2r'}{ds^2}}{\kappa'}\cos(\phi-\Phi) & \sin(\phi-\Phi) \\ -\frac{dr'}{ds}\sin(\phi-\Phi) & -\frac{\frac{d^2r'}{ds^2}}{\kappa'}\sin(\phi-\Phi) & \cos(\phi-\Phi) \\ \frac{dz'}{ds} & \frac{\frac{d^2z'}{ds^2}}{\kappa'} & 0 \end{pmatrix} \begin{pmatrix} \mathbf{T} \\ \mathbf{N} \\ \mathbf{B} \end{pmatrix} . \tag{4.3.6}$$

From (3.2.10), with $\theta' = 0$,

$$\kappa' = \frac{d^2r'}{ds^2}\frac{dz'}{ds} - \frac{dr'}{ds}\frac{d^2z'}{ds^2} .$$

Next equate the 3 by 3 matrix in (4.3.6) with the corresponding matrix in (3.2.13). Thus all nine corresponding entries are equal

$$\begin{aligned}
\frac{dr}{ds} &= \frac{dr'}{ds}\cos(\phi-\Phi),\\
r\frac{d\theta}{ds} &= -\frac{dr'}{ds}\sin(\phi-\Phi),\\
\frac{dz}{ds} &= \frac{dz'}{ds},\\
\frac{(\frac{d^2r}{ds^2}-r(\frac{d\theta}{ds})^2)}{\kappa} &= \frac{\frac{d^2r'}{ds^2}\cos(\phi-\Phi)}{\kappa'},\\
\frac{(2\frac{dr}{ds}\frac{d\theta}{ds}+r\frac{d^2\theta}{ds^2})}{\kappa} &= -\frac{\frac{d^2r'}{ds^2}\sin(\phi-\Phi)}{\kappa'},\\
\frac{\frac{d^2z}{ds^2}}{\kappa} &= \frac{\frac{d^2z'}{ds^2}}{\kappa'},\\
\frac{(r\frac{d\theta}{ds}\frac{d^2z}{ds^2}-(2\frac{dr}{ds}\frac{d\theta}{ds}+r\frac{d^2\theta}{ds^2})\frac{dz}{ds})}{\kappa} &= \sin(\phi-\Phi),\\
\frac{-(\frac{dr}{ds}\frac{d^2z}{ds^2}-(\frac{d^2r}{ds^2}-r(\frac{d\theta}{ds})^2)\frac{dz}{ds})}{\kappa} &= \cos(\phi-\Phi),\\
\frac{(\frac{dr}{ds}(2\frac{dr}{ds}\frac{d\theta}{ds}+r\frac{d^2\theta}{ds^2})-r\frac{d\theta}{ds}(\frac{d^2r}{ds^2}-r(\frac{d\theta}{ds})^2))}{\kappa} &= 0.
\end{aligned}$$

Considering the yarn element on the osculating plane, because we assume that **B** remains horizontal, the orientation of **T** and **N** can be described by three angles. The angles Θ and ϕ that determine the orientation of the osculating plane, and the angle β that **T** makes with $-k$. It is clear from the diagram using trigonometry that the relationship between the unit vectors is given by

$$\begin{pmatrix} \mathbf{e}_{r'} \\ \mathbf{e}_{\theta'} \\ \mathbf{k} \end{pmatrix} = \begin{pmatrix} \sin\beta(s) & -\cos\beta(s) & 0 \\ 0 & 0 & 1 \\ -\cos\beta(s) & -\sin\beta(s) & 0 \end{pmatrix} \begin{pmatrix} \mathbf{T} \\ \mathbf{N} \\ \mathbf{B} \end{pmatrix}. \tag{4.3.7}$$

Comparing this with (4.3.5) we have

$$\frac{dr'}{ds} = \sin\beta(s), \quad \frac{dz'}{ds} = -\cos\beta(s) \quad \text{and} \quad \kappa' = -\frac{d\beta}{ds}$$

and thus

$$r'(s) = \int_0^s \sin\beta(\tilde{s})d\tilde{s}.$$

The objective of this chapter is to express the EoM in the new reference frame S' with intrinsic coordinates. The first step will be to express the EoM in frame S' for an unspecified air drag term $\mathbf{F}$, then the second step is to use Padfield's air drag term. So in the next section I will present the results for this first step.

4.4 EoM expressed in the non-inertial reference frame S'

In the reference frame S, which rotates with a constant angular velocity ω, a general point P in the yarn balloon is represented by the position vector $\mathbf{r}$ defined above. The velocity of the point P in the inertial reference frame, using the position vector $\mathbf{r}$ from the frame S is given by

$$\mathbf{v} = D\mathbf{r} + \omega k \wedge \mathbf{r} \quad \text{where} \quad D = \frac{\partial}{\partial t} - V_0(t)\frac{\partial}{\partial s}\,, \tag{4.4.8}$$

and $V_0(t)$ is the linear speed with which the yarn is drawn through the guide eye of the device. This velocity $\mathbf{v}$ remains unchanged no matter which non-inertial reference frame we choose. So to represent (4.4.8) in the frame S', we need to substitute (4.3.2) into (4.4.8) and express every term resulting from $\mathbf{v}$ in terms of $\mathbf{r}'$ and the unit vectors $\mathbf{e}_{r'}$ and $\mathbf{e}_{\theta'}$. Thus

$$D\mathbf{r} = D\mathbf{r}' + \Big(\frac{\partial R}{\partial t} - V_0(t)\frac{\partial R}{\partial s}\Big)\mathbf{e}_R + R\Big(\frac{\partial \Theta}{\partial t} - V_0(t)\frac{\partial \Theta}{\partial s}\Big)\mathbf{e}_\Theta$$

and

$$\omega k \wedge \mathbf{r} = \omega R\mathbf{e}_\Theta + \omega r'\mathbf{e}_{\theta'}. \tag{4.4.9}$$

So

$$\begin{aligned}\mathbf{v} = {} & D\mathbf{r}' + R\cos\phi(\omega\mathbf{k}\wedge\mathbf{e}_{r'}) + R\sin\phi(\mathbf{k}\wedge(\omega\mathbf{k}\wedge\mathbf{e}_{r'})) + \omega r'\mathbf{e}_{\theta'} \\ & + \left\{\Big(\frac{\partial R}{\partial t} - V_0(t)\frac{\partial R}{\partial s}\Big)\cos\phi - R\Big(\frac{\partial\Theta}{\partial t} - V_0(t)\frac{\partial\Theta}{\partial s}\Big)\sin\phi\right\}\mathbf{e}_{r'} \\ & + \left\{\Big(\frac{\partial R}{\partial t} - V_0(t)\frac{\partial R}{\partial s}\Big)\sin\phi + R\Big(\frac{\partial\Theta}{\partial t} - V_0(t)\frac{\partial\Theta}{\partial s}\Big)\cos\phi\right\}\mathbf{e}_{\theta'}\,.\end{aligned}$$

If we think of this expression for $\mathbf{v}$ as an operator acting on a vector in the S' frame, we can apply this operator to $\mathbf{r}$ twice and express every resultant term in terms of $\mathbf{r}'$ and the unit vectors $\mathbf{e}_{r'}$ and $\mathbf{e}_{\theta'}$ to obtain an expression for the acceleration in the inertial reference frame

$$\begin{aligned}\mathbf{a} = {} & D^2\mathbf{r}' + 2(\omega\mathbf{k}\wedge(D\mathbf{r}')) \\ & + \Big\{\omega R(\sin\phi D\theta' - \cos\phi D(\Theta+\phi)) - 2\omega\sin\phi DR - \omega^2(r' + R\cos\phi) \\ & + (D^2R - R(D\Theta)^2)\cos\phi - (RD^2\Theta + 2DRD\Theta)\sin\phi\Big\}\mathbf{e}_{r'} \\ & + \Big\{ - \omega R(\cos\phi D\theta' + \sin\phi D(\Theta+\phi)) + 2\omega\cos\phi DR - \omega^2(R\sin\phi) \\ & + (D^2R - R(D\Theta)^2)\sin\phi + (RD^2\Theta + 2DRD\Theta)\cos\phi\Big\}\mathbf{e}_{\theta'}\,.\end{aligned}$$

The EoM expressed in reference frame S is given by (1.0.1). Using the calculations in this section the EoM in S' are given by

$$
\begin{aligned}
m\Big\{ & D^2\mathbf{r}' + 2\omega\mathbf{k}\wedge D\mathbf{r}' + \\
& + \Big\{\omega R(\sin\phi D\theta' - \cos\phi D(\Theta+\phi)) - 2\omega\sin\phi DR - \omega^2(r' + R\cos\phi) \\
& + (D^2R - R(D\Theta)^2)\cos\phi - (RD^2\Theta + 2DRD\Theta)\sin\phi\Big\}\mathbf{e}_{r'} \\
& + \Big\{ -\omega R(\cos\phi D\theta' + \sin\phi D(\Theta+\phi)) + 2\omega\cos\phi DR - \omega^2(R\sin\phi) \\
& + (D^2R - R(D\Theta)^2)\sin\phi + (RD^2\Theta + 2DRD\Theta)\cos\phi\Big\}\mathbf{e}_{\theta'}\Big\} \\
& = \frac{\partial}{\partial s}\Big(T_e\frac{\partial\mathbf{r}'}{\partial s}\Big) + \frac{\partial}{\partial s}\Big(T_e\frac{\partial\mathbf{R}}{\partial s}\Big) + \mathbf{F}.
\end{aligned}
$$

To make the EoM dimensionless, first introduce dimensionless variables, defined in terms of the dimensional variables, as follows

$$
\begin{aligned}
& t = \bar{t}\omega,\ \mathbf{r} = \bar{\mathbf{r}}/a = \bar{r}e_r/a + \bar{z}k/a = re_r + zk, \\
& \mathbf{r}' = \bar{\mathbf{r}}'/a = \bar{r}'e_{r'}/a + \bar{z}'k/a = r'e_{r'} + z'k, \\
& \mathbf{R} = \bar{\mathbf{R}}/a = \bar{R}e_R/a + \bar{z}k/a = Re_R + zk, \\
& s = \bar{s}/a,\ \mathbf{v} = \bar{\mathbf{v}}/\omega a,\ T_e = \bar{T}_e/m\omega^2a^2,\ \mathbf{F} = \bar{\mathbf{F}}/m\omega^2a, \\
& D = \frac{\bar{D}}{\omega} = \frac{\partial}{\partial t} - \Omega^{-1}\frac{\partial}{\partial s}.
\end{aligned}
$$

Each symbol with a bar above it, is a variable which has the dimensions of the physical quantity it represents. All the second derivative terms have the same form, with regards to Ω^{-1} and Ω^{-2}. For example,

$$
D^2 = \frac{\partial^2}{\partial t^2} - 2\Omega^{-1}\frac{\partial}{\partial t}\frac{\partial}{\partial s} + \Omega^{-2}\frac{\partial^2}{\partial s^2},
$$

and so only the time derivatives remain when the small terms are neglected in all the terms involving D and D^2.

Therefore the dimensionless EoM in reference frame S' is

$$\begin{aligned}
&\frac{\partial^2\mathbf{r}'}{\partial t^2} + 2(\mathbf{k} \wedge \Big(\frac{\partial \mathbf{r}'}{\partial t}\Big)) \\
&+ \Bigg\{ R(\sin\phi\frac{\partial\theta'}{\partial t} - \cos\phi\frac{\partial(\Theta+\phi)}{\partial t}) - 2\sin\phi\frac{\partial R}{\partial t} - (r' + R\cos\phi) \\
&+ \Big(\frac{\partial^2 R}{\partial t^2} - R\Big(\Big(\frac{\partial\Theta}{\partial t}\Big)^2\Big)\cos\phi - \Big(R\frac{\partial^2\Theta}{\partial t^2} + 2\frac{\partial R}{\partial t}\frac{\partial\Theta}{\partial t}\Big)\sin\phi \Bigg\}\mathbf{e}_{r'} \\
&+ \Bigg\{ - R\Big(\cos\phi\frac{\partial\theta'}{\partial t} + \sin\phi\frac{\partial(\Theta+\phi)}{\partial t}\Big) + 2\cos\phi\frac{\partial R}{\partial t} - R\sin\phi \\
&+ \Big(\frac{\partial^2 R}{\partial t^2} - R\Big(\Big(\frac{\partial\Theta}{\partial t}\Big)^2\Big)\sin\phi + \Big(R\frac{\partial^2\Theta}{\partial t^2} + 2\frac{\partial R}{\partial t}\frac{\partial\Theta}{\partial t}\Big)\cos\phi \Bigg\}\mathbf{e}_{\theta'} \\
&= \frac{\partial}{\partial s}\Big(T_e\frac{\partial\mathbf{r}'}{\partial s}\Big) + \frac{\partial}{\partial s}\Big(T_e\frac{\partial\mathbf{R}}{\partial s}\Big) + \mathbf{F}, \qquad (4.4.10)
\end{aligned}$$

where $\Omega^{-1} = V_0/\omega a \ll 1$, and so the terms multiplied by Ω^{-1} are neglected.

4.5 Quasi-stationary EoM with the Padfield air drag term

When we assume that the yarn balloon is unchanging in the reference frame S, we say that the yarn balloon is quasi-stationary. In this section, we will use Padfield's air drag term (characterized by the assumption that $C_D = 1$ for any shape yarn balloon, and at any point on the entire yarn balloon) expressing it in intrinsic coordinates, in the new formulation of the EoM in the frame of reference S'.

Neglecting all the time dependent terms in (4.4.10), gives the quasi-stationary EoM in frame S'. To evaluate the air drag term in this case, take the dimensionless form of (4.4.9), using (4.3.4) then (4.3.7), then deleting the $\mathbf{T}$ component to get

$$\mathbf{v}_n = R\cos\beta\sin\phi\mathbf{N} + (r' + R\cos\phi)\mathbf{B} \qquad (4.5.11)$$

and

$$|\mathbf{v}_n| = \sqrt{R^2\cos^2\beta\sin^2\phi + (r' + R\cos\phi)^2}\,. \tag{4.5.12}$$

Finally substituting (4.5.11) and (4.5.12) into (2.3.10) we obtain

$$\begin{aligned}\mathbf{F} = &-\frac{p_0}{16}\sqrt{R^2\cos^2\beta\sin^2\phi + (r' + R\cos\phi)^2}\\ &\Big(-R\cos\beta\sin\phi\mathbf{N} + (r' + R\cos\phi)\mathbf{B}\Big).\end{aligned}$$

Thus the $\mathbf{T}$, $\mathbf{N}$ and $\mathbf{B}$ components of the quasi-stationary EoM are

$$\begin{aligned}&\frac{dT_e}{ds} + \sin\beta\Bigg(\cos\phi\Big\{\frac{d}{ds}\Big(T_e\frac{dR}{ds}\Big) - T_eR\Big(\frac{d\Theta}{ds}\Big)^2 + R\Big\} -\\ &\qquad\sin\phi\Big\{\frac{d}{ds}\Big(T_eR\frac{d\Theta}{ds}\Big) + T_e\frac{dR}{ds}\frac{d\Theta}{ds}\Big\} + r'\Bigg) = 0,\\ &\qquad -T_e\frac{d\beta}{ds} \quad +\\ &\cos\beta\Bigg(\cos\phi\Big\{-\frac{dT_e}{ds}\frac{dR}{ds} + T_e\Big(\frac{d^2R}{ds^2} - R\Big(\frac{d\Theta}{ds}\Big)^2\Big) - R\Big\} +\\ &\qquad\sin\phi\Big\{R\frac{dT_e}{ds}\frac{d\Theta}{ds} - T_e\Big(2\frac{dR}{ds}\frac{d\Theta}{ds} + R\frac{d^2\Theta}{ds^2}\Big) -\\ &\qquad\frac{p_0R}{16}\sqrt{R^2\cos^2\beta\sin^2\phi + (r' + R\cos\phi)^2}\Big\} - r'\Bigg) = 0,\\ &\qquad\cos\phi\Big\{R\frac{dT_e}{ds}\frac{d\Theta}{ds} + T_e\Big(2\frac{dR}{ds}\frac{d\Theta}{ds} + R\frac{d^2\Theta}{ds^2}\Big) -\\ &\qquad\frac{p_0R}{16}\sqrt{R^2\cos^2\beta\sin^2\phi + (r' + R\cos\phi)^2}\Big\} \quad +\\ &\qquad\sin\phi\Big\{R + \frac{dT_e}{ds}\frac{dR}{ds} + T_e\Big(\frac{d^2R}{ds^2} - R\Big(\frac{d\Theta}{ds}\Big)^2\Big)\Big\} \quad -\\ &\qquad\frac{p_0r'}{16}\sqrt{R^2\cos^2\beta\sin^2\phi + (r' + R\cos\phi)^2} = 0\,.\end{aligned}$$

Future Work The restriction of $\mathbf{T}$ and $\mathbf{N}$ always being in a vertical plane, and thus $\mathbf{B}$ always being horizontal could be removed, regardless of whether the current model turns out to be accurate enough when the new air drag term has been found, and this new model has been compared to experimental data. However the accuracy will determine how necessary this change would be.

The framework defined in Chapter 4, of the Frenet frame in a rotating reference frame potentially could be applied to many other situations, particularly where more than one rotation is evident.

Concluding Remarks In this chapter, a new reference frame S' is derived and is then utilized in conjunction with the insights from Chapter 3, that the solutions in vacuo are planar, to model the effect of air drag on the yarn element at every point along the yarn balloon. Specifically this is achieved by expressing the EoM in S' with intrinsic coordinates. In the final section, Padfield's air drag term is expressed in intrinsic coordinates. A secondary goal in this chapter, to determine if this new formulation would lead to an analytical expression for the yarn path with the Padfiled air drag term has not been achieved yet. So exact solutions for the EoM were not found, and the EoM were not solved numerically for any of the relevant boundary conditions, because this has been done extensively in the past [2]. However with this new framework the drag coefficient for the yarn represented by a smooth flexible cylinder, for multi-strand yarns, and non-smooth hairy yarns can now be incorporated more accurately into our model than the Padfield model.

In the next chapter, we will represent the Navier-Stokes equations in intrinsic coordinates, and explore how to use these equations to derive a more accurate air drag term for the yarn balloon equations.

Chapter 5

The Navier-Stokes equations in intrinsic coordinates

5.1 Introduction

In this Chapter, I will be using the framework established by Dimitriou [46], [47], to explore boundary layer solutions of the Navier-Stokes equations in intrinsic coordinates for 2-D fluid flow around a circular cylinder.

Dimitiou's novel approach leads to a new formulation of the Navier-Stokes equation.

Theorem 5 (Dimitriou [47]) *The velocity-vorticity formulation of the planar Navier-Stokes equation is*

$$(\mathbf{u} \cdot \nabla)\omega = \nu \triangle \omega \tag{5.1.1}$$

and in intrinsic coordinates it is

$$u \frac{\partial \omega}{\partial s} = \nu \triangle \omega \,. \tag{5.1.2}$$

He also defined a new quantity called the Geometric Vorticity $\mathbf{\Gamma}$, which is the curl of the global curvature vector κ_G (5.2.6). He also was able to express the flow velocity as a function of geometric parameters. This idea complements the idea expressed in this thesis of a local Reynolds number (5.3.13), which combines two physical properties of the fluid with a geometric property of the fluid. Dimitriou also introduced the idea of the *geometric-vorticity diagram* in which pairs of values for $\frac{\partial \kappa_s}{\partial s}$ and $-\frac{\partial \kappa_n}{\partial n}$ are computed and plotted along a streamline, thereby being able to clearly visualize which flow areas have vorticity, and which do not. This idea could potentially be used in the future to model what happens to the air flow in the vicinity of the yarn balloon, given that devices such as the two-for-one twister are always operated in rows, adjacent to each other, divided by a metal panel or separator, and with a yarn guide and pot in close proximity to the yarn balloon. Thus turbulent air created by the yarn balloon, reflecting off these adjacent hard surfaces, and affecting the drag experienced by the yarn balloon is a distinct possibility.

In Section 5.2, using Dimitriou's framework, I will represent the 2-D Navier-Stokes equations in a new way: the change in head (H) in the direction parallel to the fluid flow, and normal to the fluid flow. In Section 5.3, I will represent this equation in vector form in 2-D, and attempt to do so in 3-D in Appendix C. In Section 5.4, I apply the boundary layer assumptions to the equation found in Section 5.2, and investigate what this says about how H changes along a streamline, or along a potential line in the boundary layer. In Section 5.5 I will consider how the connection between the fluid flow around a circular cylinder and the air drag on the yarn element moving in a yarn balloon can best be established. In Section 5.6, I make a first attempt to find the complex potential and stream function for a 2-D flow around a cylinder with a separation point

by using conformal mapping.

5.2 A representation of the Navier-Stokes equations in intrinsic coordinates

Consider representing the fluid flow by streamlines, that is the paths along which individual fluid elements move when the fluid flows. Each streamline is a curve, and the distance along the curve from some fixed point is s. Potential lines are lines of constant s, and each potential line is also a curve, with parameter n.

So for a 2-D flow we have the streamline coordinate system (s, n), with unit tangent vector $\mathbf{T} = \frac{\mathbf{u}}{u}$, and a unit vector $\mathbf{N}$ normal to it. the curvature of a streamline is κ_s, while the curvature of the orthogonal potential line is κ_n. Therefore the global curvature vector can be defined as

$$\kappa_{\mathbf{G}} = -\kappa_n \mathbf{T} + \kappa_s \mathbf{N} \quad \text{where} \quad \kappa_{\mathbf{s}} = |\nabla \times \mathbf{T}|\mathbf{k} \quad \text{and} \quad \kappa_{\mathbf{n}} = (\nabla \cdot \mathbf{T})\mathbf{k} \quad (5.2.3)$$

with the initial assumption that the fluid is incompressible and the flow is irrotational,

$$\nabla \cdot (u\mathbf{T}) = u\nabla \cdot \mathbf{T} + \nabla u \cdot \mathbf{T} = 0$$

and so

$$u\kappa_n = -\frac{\partial u}{\partial s}\,. \quad (5.2.4)$$

Also

$$\nabla \times (u\mathbf{T}) = u\nabla \times \mathbf{T} + \nabla u \times \mathbf{T} = 0$$

and so

$$u\kappa_s = \frac{\partial u}{\partial n}\,. \quad (5.2.5)$$

Combining (5.2.4) and (5.2.5), the modulus of $\kappa_{\mathbf{G}}$ from (5.2.3) is

$$\kappa_G^2 = \kappa_s^2 + \kappa_n^2 = \frac{1}{u^2}\Big(\Big(\frac{\partial u}{\partial s}\Big)^2 + \Big(\frac{\partial u}{\partial n}\Big)^2\Big)$$

or

$$\kappa_{\mathbf{G}} = \frac{\nabla u}{u}\,. \tag{5.2.6}$$

Now allowing vorticity to be non-zero, taking (2.4.14) and adding a term that represents the effect of viscosity, the Navier-Stokes equation can be written as

$$\nabla H = \mathbf{u} \times \omega + \nu \nabla^2 \mathbf{u} \tag{5.2.7}$$

where $\omega = \nabla \times \mathbf{u} = \omega \mathbf{k}$ for a 2-D flow.

Equation (5.2.4) is unchanged, but (5.2.5) now becomes

$$-\frac{\partial u}{\partial n} + u\kappa_s = \omega \tag{5.2.8}$$

and so

$$\kappa_s = \frac{1}{u}\frac{\partial u}{\partial n} + \frac{\omega}{u}$$

and hence (5.2.6) becomes

$$\kappa_{\mathbf{G}} = \frac{\nabla u}{u} + \frac{\omega}{u}\mathbf{N}\,.$$

In intrinsic coordinates,

$$\nabla \equiv \mathbf{T}\frac{\partial}{\partial s} + \mathbf{N}\frac{\partial}{\partial n}$$

and so the Laplacian becomes

$$\begin{aligned}\Delta \equiv \nabla \cdot \nabla = \mathbf{T} \cdot \Big(\frac{\partial \mathbf{T}}{\partial s}\Big)\frac{\partial}{\partial s} + \mathbf{T} \cdot \Big(\frac{\partial \mathbf{N}}{\partial s}\Big)\frac{\partial}{\partial n} + \mathbf{N} \cdot \Big(\frac{\partial \mathbf{T}}{\partial n}\Big)\frac{\partial}{\partial s} + \mathbf{N} \cdot \Big(\frac{\partial \mathbf{N}}{\partial n}\Big)\frac{\partial}{\partial n} \\ + \frac{\partial^2}{\partial s^2} + \frac{\partial^2}{\partial n^2}\,.\end{aligned} \tag{5.2.9}$$

The Frenet-Serret equations can be expressed in terms of the streamline curvature κ_s, and the streamline torsion τ_s as follows

$$\frac{\partial \mathbf{T}}{\partial s} = \kappa_s \mathbf{N}\,, \quad \frac{\partial \mathbf{N}}{\partial s} = -\kappa_s \mathbf{T} + \tau_s \mathbf{B}\,, \quad \frac{\partial \mathbf{B}}{\partial s} = -\tau_s \mathbf{N}\,.$$

For a planar flow, $\tau_s = 0$ and $\mathbf{B} \equiv \mathbf{k}$ and so

$$\begin{aligned}
&\frac{\partial \mathbf{T}}{\partial s} = \kappa_s \mathbf{N}\,, && \frac{\partial \mathbf{N}}{\partial s} = -\kappa_s \mathbf{T},\\
&\frac{\partial \mathbf{T}}{\partial n} = \kappa_n \mathbf{N}\,, && \frac{\partial \mathbf{N}}{\partial n} = -\kappa_n \mathbf{T},\\
&\frac{\partial^2 \mathbf{T}}{\partial s^2} = -\kappa_s^2 \mathbf{T} + \frac{\partial \kappa_s}{\partial s}\mathbf{N}\,, && \frac{\partial^2 \mathbf{N}}{\partial s^2} = -\frac{\partial \kappa_s}{\partial s}\mathbf{T} - \kappa_s^2 \mathbf{N},\\
&\frac{\partial^2 \mathbf{T}}{\partial n^2} = -\kappa_n^2 \mathbf{T} + \frac{\partial \kappa_n}{\partial n}\mathbf{N}\,, && \frac{\partial^2 \mathbf{N}}{\partial n^2} = -\frac{\partial \kappa_n}{\partial n}\mathbf{T} - \kappa_n^2 \mathbf{N}\,.
\end{aligned}$$

Substituting into (5.2.9),

$$\Delta = -\kappa_s \frac{\partial}{\partial n} + \kappa_n \frac{\partial}{\partial s} + \frac{\partial^2}{\partial s^2} + \frac{\partial^2}{\partial n^2}\,.$$

Evaluating the two terms on the right hand side of (5.2.7),

$$\mathbf{u} \times (\nabla \times \mathbf{u}) = \Big(-\kappa_s u^2 + u\frac{\partial u}{\partial n}\Big)\mathbf{N},$$

$$\nabla^2 \mathbf{u} = \mathbf{T}(\Delta u) + 2(\nabla u \cdot \nabla)\mathbf{T} + u\Delta \mathbf{T}\,.$$

Now substituting these two terms into (5.2.7)

$$\begin{aligned}
\nabla H = \nu \Big\{ \kappa_n \frac{\partial u}{\partial s} - \kappa_s \frac{\partial u}{\partial n} + \frac{\partial^2 u}{\partial s^2} + \frac{\partial^2 u}{\partial n^2} - u\kappa_s^2 - u\kappa_n^2 \Big\}\mathbf{T} \qquad (5.2.10)\\
+ \Big\{ \Big(-\kappa_s u^2 + u\frac{\partial u}{\partial n}\Big) + \nu\Big(2\kappa_s \frac{\partial u}{\partial s} + 2\kappa_n \frac{\partial u}{\partial n} + u\frac{\partial \kappa_s}{\partial s} + u\frac{\partial \kappa_n}{\partial n}\Big)\Big\}\mathbf{N}\,.
\end{aligned}$$

Using

$$u^2 \kappa_G^2 = \Big(\frac{\partial u}{\partial s}\Big)^2 + \Big(\frac{\partial u}{\partial n} + \omega\Big)^2$$

and

$$\frac{1}{u}\frac{\partial}{\partial s}(u\omega) = \frac{2\omega}{u}\frac{\partial u}{\partial s} + u\frac{\partial}{\partial s}\Big(\frac{\omega}{u}\Big)$$

in (5.2.10), we have

$$\begin{aligned}\nabla H = \nu\Big(&- 2u\kappa_G^2 + \omega\kappa_s + \frac{\partial^2 u}{\partial s^2} + \frac{\partial^2 u}{\partial n^2}\Big)\mathbf{T} \\ &+ \Big(- u\omega + \frac{\nu}{u}\frac{\partial}{\partial s}(u\omega)\Big)\mathbf{N}\,. \end{aligned} \tag{5.2.11}$$

5.3 An alternative representation of (5.2.7)

Considering (5.2.7), we can represent the intrinsic coordinates in vector form

$$\mathbf{T} = \frac{\mathbf{u}}{u}, \quad \mathbf{N} = \frac{\omega \times \mathbf{u}}{u\omega}, \quad \mathbf{B} = \frac{\nabla \times \mathbf{u}}{\omega}$$

and take the dot product of (5.2.7) with each of these vectors. For a 2-D planar flow,

$$(\mathbf{u} \times \omega) \cdot (\nabla \times \omega) = -\mathbf{u} \cdot \nabla\Big(\frac{1}{2}\omega^2\Big),$$

this expression is evaluated in 3-D Cartesian coordinates in appendix (C). Therefore (5.2.7) can be written as

$$\nabla H = (\nu\frac{\mathbf{u}}{u} \cdot \nabla^2\mathbf{u})\frac{\mathbf{u}}{u} - \Big(u\omega - \frac{\nu\mathbf{u}}{u\omega} \cdot \nabla\Big(\frac{1}{2}\omega^2\Big)\Big)\frac{\omega \times \mathbf{u}}{u\omega}$$

or equivalently,

$$\nabla H = (\nu\mathbf{T} \cdot \nabla^2\mathbf{u})\mathbf{T} - \Big(u\omega - \frac{\nu}{\omega}\mathbf{T} \cdot \nabla\Big(\frac{1}{2}\omega^2\Big)\Big)\mathbf{N}\,. \tag{5.3.12}$$

The equation (5.3.12) is an alternative representation of (5.2.7), and in fact there are many equivalent representations of the Navier-Stokes equations, such as (5.1.1) and (5.1.2), and many examples in [8]. The objective of this exercise apart from a purely academic interest is to find a representation that is

amenable to the problem that you wish to solve, or on the other hand, if a new formulation is found, find a problem that it can be useful in solving. Unfortunately, at this stage we have been unable to achieve either of these objectives with the representation found here. Similarly, we can define the local Reynolds number as

$$Re = \frac{u}{\nu\kappa_G} = \frac{u^2}{\nu\sqrt{\frac{\partial u}{\partial s}^2 + (\frac{\partial u}{\partial n} + \omega)^2}}\,. \tag{5.3.13}$$

It is not clear to me at this stage how this can be used to recast the Navier-Stokes equations in general, as I have attempted to do in this thesis. However, it may be possible in specific circumstances, that is, depending upon the domain and the boundary conditions. There are many situations where the Reynolds number is determined by the geometry of the domain, and so Re will be fixed over some local neighbourhood, however in general Re will vary over an entire domain.

5.4 Boundary layer equations in intrinsic coordinates

In this section, the standard boundary layer assumptions [8], [33] are applied to the Navier-Stokes equations in intrinsic coordinates. The boundary layer of a fluid flow is the region in which the velocity of the fluid adjusts from the external inviscid flow to zero velocity on the solid boundary. The hypothesis is that the viscous term is of the same order of magnitude as the inertia term in the Navier-Stokes equations in a thin layer close to the boundary.

Assume that the boundary layer has thickness δ, and streamline curvature $\kappa_s \sim O(\frac{1}{a})$, for a 2-D laminar flow around a circular cylinder of radius a. The

key assumption is that

$$\left|\frac{\partial u}{\partial n}\right| \gg \left|\frac{\partial u}{\partial s}\right|$$

in the boundary layer. That is

$$\frac{U_0}{\delta} \gg \frac{U_0}{a} \quad \text{because} \quad \delta \ll a\,,$$

where U_0 denotes some typical value of u. Next

$$u\kappa_s \sim O\Big(\frac{U_0}{a}\Big) \quad \text{and} \quad \frac{\partial u}{\partial n} \sim O\Big(\frac{U_0}{\delta}\Big)$$

and so from (5.2.8)

$$\omega \sim O\Big(\frac{U_0}{\delta}\Big)\,. \tag{5.4.14}$$

We require the largest term with viscosity on the right hand side of (5.2.11) to be of the same order of magnitude as the corresponding term on the left hand side. That is

$$\frac{\partial H}{\partial s} = \nu\frac{\partial^2 u}{\partial n^2}$$

or in terms of magnitudes,

$$\frac{U_0^2}{\delta a} \sim \frac{\nu U_0}{\delta^3}\,.$$

The order of magnitude of each term in (5.2.11) from largest to smallest is then

$$\begin{aligned}
\frac{\partial H}{\partial n} &\sim u\omega \sim O\Big(\frac{U_0^2}{\delta}\Big),\\
\frac{\partial H}{\partial s} &\sim \nu\frac{\partial^2 u}{\partial n^2} \sim O\Big(\frac{U_0^2}{a}\Big),\\
\frac{\nu}{u}\frac{\partial}{\partial s}(u\omega) &\sim \nu\omega\kappa_s \sim O\Big(\frac{U_0^2\delta}{a^2}\Big),\\
\nu u\kappa_G^2 &\sim \nu\frac{\partial^2 u}{\partial s^2} \sim O\Big(\frac{U_0^2\delta^2}{a^3}\Big).
\end{aligned}$$

Dimitriou [47] expressed the Navier-Stokes equations in intrinsic coordinates in what he calls the velocity-vorticity formulation

$$u\frac{\partial\omega}{\partial s} = \nu\Big(\kappa_n\frac{\partial\omega}{\partial s} - \kappa_s\frac{\partial\omega}{\partial n} + \frac{\partial^2\omega}{\partial s^2} + \frac{\partial^2\omega}{\partial n^2}\Big)\,.$$

With the boundary layer assumptions, this equation becomes

$$u\frac{\partial\omega}{\partial s} = \nu\frac{\partial^2\omega}{\partial n^2}.$$

Alternatively, using the same assumptions, (5.2.11) yields two equations. In the **T** direction,

$$\frac{\partial H}{\partial s} = \nu\frac{\partial^2 u}{\partial n^2}\,,$$

while in the **N** direction,

$$\frac{\partial H}{\partial n} = -u\omega\,. \tag{5.4.15}$$

From (5.4.14), $\omega = -\frac{\partial u}{\partial n}$ and so (5.4.15) becomes

$$\frac{\partial H}{\partial n} = \frac{\partial}{\partial n}\Big(\frac{1}{2}u^2\Big)\,. \tag{5.4.16}$$

Integrating along a potential line, across the entire width of the boundary layer,

$$\Big[H\Big]_{n=0}^{n=g(s)} = \frac{1}{2}U(s)^2$$

where the width of the boundary layer is $g(s)$, at the boundary $u = 0$, and at the edge of the boundary layer, the external speed is $U(s)$. At the boundary,

$$H = \frac{p(s)}{\rho} + \chi$$

while at the edge of the boundary layer

$$H = \frac{p(s)}{\rho} + \frac{1}{2}U^2 + \chi\,.$$

This implies that the pressure in the boundary layer is equal to the pressure in the external inviscid mainstream flow, for any given value of s, and is consistent with Prandtl's remark in his famous 1905 paper that "the pressure distribution of the free fluid will be impressed on the transition layer". Acheson [8] states on page 268 that the boundary layer equations are also valid for a curved boundary (as well as a straight boundary), because although $\frac{\partial p}{\partial y}$ is comparable

in magnitude with $\frac{\partial p}{\partial x}$ for a curved boundary, due to the substantial pressure gradient in the y-direction that is required to balance the centrifugal effect of the flow around the curved surface, although the two pressure gradients are comparable in magnitude, changes in p across the boundary layer are still much smaller than changes in p along the boundary. Equation (5.4.16) is consistent with this analysis, because it is saying that the change in H across the boundary layer is predominantly due to the change in the magnitude of u, and any change in p across the boundary layer is an order of magnitude smaller.

In the **T** direction, (5.2.11) yields the equation

$$\frac{\partial H}{\partial s} = \nu \frac{\partial^2 u}{\partial n^2}\,, \tag{5.4.17}$$

where these terms are much smaller than those in (5.4.15). Hence the change in H along a potential line is much greater that the change in H along a streamline. It is well known [33] that pressure p is maximum at the front stagnation point, and decreases as s increases, moving away from this point. So $\frac{dp}{ds} < 0$ implies that $\frac{\partial^2 u}{\partial n^2} < 0$ and thus $\frac{\partial H}{\partial s} < 0$, and it is reasonable to infer that H is decreasing due to the viscous dissipation of energy. An estimate for this dissipation of energy over the entire boundary layer is calculated by integrating along each streamline in the boundary layer from the front stagnation point to the separation point, and then integrating that across the width of the boundary layer. Thus for flow around a circular cylinder, by symmetry, it is

$$2\int_0^{s_{sp}} \int_0^{g(s)} \nu \frac{\partial^2 u}{\partial n^2} dn ds = -2\int_0^{s_{sp}} \nu \frac{\partial u}{\partial n}\Big|_{n=0} ds$$

where s_{sp} is the distance along the streamline of the separation point from the stagnation point. Noting that $\frac{\partial u}{\partial n}\Big|_{n=g(s)} = 0$ at the edge of the boundary layer, and so even though the width of the boundary layer depends on s, this term

is always zero. I am unsure as to the accuracy of my calculation here for a couple of reasons. First is the approximations made to obtain the boundary layer equations. Second, is that around both stagnation points, as n increases, moving away from the boundary, the boundary layer assumptions break down. The assumptions that are necessary in the derivation of the boundary layer equations stem from the hypothesis that the boundary layer is attached to the wall. Thus the boundary layer equations are not suitable to model what occurs when the boudary layer separates from the wall.

Even with these caveats, it is clear that an exact expression for $\frac{\partial u}{\partial n}\Big|_{n=0}$ must be found in order to estimate air drag as accurately as possible. This expression is proportional skin friction (2.4.20).

Equation (5.4.17) also describes what is happening between the separation point and the rear stagnation point. There will be another boundary layer, and as s decreases from the rear stagnation point, $\frac{dp}{ds} > 0$, and so the pressure is decreasing as we move towards the separation point. Also, $\frac{\partial^2 u}{\partial n^2} > 0$ and thus $\frac{\partial H}{\partial s} > 0$, and hence H decreases as we move towards the stagnation point.

5.5 The approach to air drag with conformal mapping

The model developed in Chapter 4 uses the intrinsic coordinates $\mathbf{T}$, $\mathbf{N}$ and $\mathbf{B}$. In the Padfield model, it is assumed that the air drag force lies in the $\mathbf{N}-\mathbf{B}$ plane. A fluid flow with only the $\mathbf{N}$ and $\mathbf{B}$ components relative to the yarn element corresponds to fluid flow around a circular cylinder, with radius equal to the radius of the yarn (because the initial assumption was to model the yarn as a circular cylinder). This leaves the remaining air flow in the $\mathbf{T}$ direction, tangential to the yarn element, moving along the surface of the yarn element,

parallel to the axis of the yarn. In most situations, the curvature of this path will be small, and thus the drag generated would be more like that from flow across a smooth flat plate, which is typically much smaller than for flow around a circular cylinder, and thus air drag in the tangential direction is neglected. It is known [33], [30], [8] that C_D versus Re is not a linear relationship, so even considering the component of air drag in the $\mathbf{N}-\mathbf{B}$ plane separately from the component of air drag in the $\mathbf{T}$ direction introduces an error.

A better way of modelling this situation is to consider the orientation of the yarn element in relation to the direction of air flow. The shape of the yarn balloon determines this orientation and thus the shape of the horizontal cross-section in relation to the direction of air flow (see Figure 5.1). The entire yarn balloon can then be considered as many horizontal cross-sections, with a yarn element embedded in each one, and the air drag on each element is obtained by considering the 2-D fluid flow around the cross-section of the yarn element. If the direction of air flow lies in the $\mathbf{N}-\mathbf{B}$ plane, then we have 2-D flow past a circular cylinder as described above. If the $\mathbf{N}-\mathbf{B}$ plane relative to the yarn element is not horizontal, that is, $\mathbf{T}$ is not vertical, then the cross-section of the yarn element will be an ellipse instead of a circle. Conformal maps are a useful technique because they preserve streamlines, and so the streamlines for the flow past the circular cylinder will be mapped to streamlines for flow past an elliptical cylinder. If the drag coefficient C_D for fluid flow past a circular cylinder as a function of Reynolds number (Re) can be found, then a conformal mapping from a circle to an ellipse can be used to find the drag coefficient C_D for flow around an ellipse. For each horizontal cross-section, the velocity of the yarn element determines the corresponding Re and thus the C_D of the yarn element.

This model will work best when $\mathbf{T}$ changes slowly. For sections of the yarn

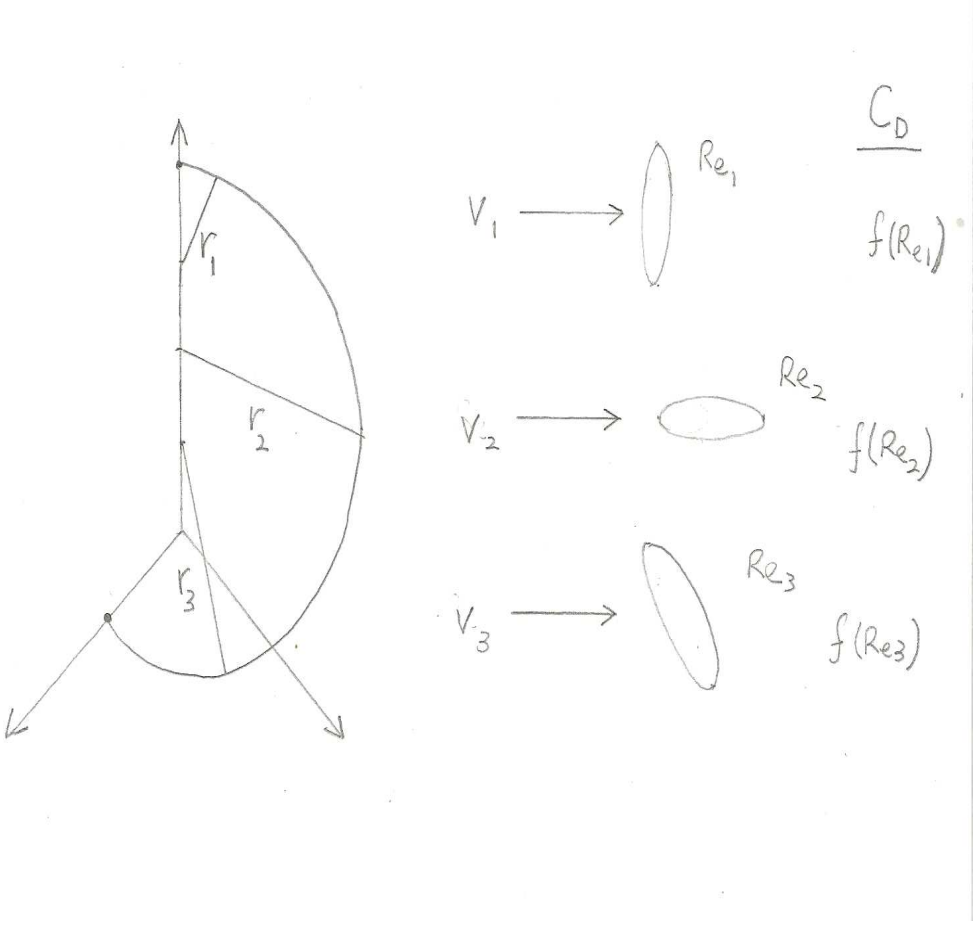

Figure 5.1: The orientation of the yarn element in a typical yarn balloon (left), leading to three horizontal cross-sections (middle) and the corresponding drag coefficient C_D as a function of Reynolds number Re for each one (right).

balloon where **T** changes more quickly, that is the curvature of the yarn is larger, it is plausible that this model may not capture the full dynamics of what is happening with the fluid flow around the yarn in this region. That is, the air flow is three-dimensional (3-D), and the 3-D Navier-Stokes equations are required to more accurately model what is happening. For example, moving down from the guide eye of the yarn balloon, the Reynolds number increases as the radius of the yarn balloon increases. Attached vortices will form, and may detach from the yarn if Re reaches a critical value. However, as we move along the yarn in the yarn balloon, the yarn will rotate and change its orientation, so that the part of the yarn element that could be described as the front of the cylinder, pushing into the air will change, thus changing the position of the attached vortices, which may then be detached from the yarn balloon even if the critical Reynolds number has not been reached.

An alternative approach is to consider the yarn element as a small cylinder moving along the real axis, and using a Schwarz-Christoffel transformation, map the upper half plane to the exterior of a larger circle on the complex plane. In this way, the force acting on the yarn element as it moves along the real axis, determined from the fluid flow around a circular cylinder can be transformed to a force acting on the yarn element moving in a circle in the yarn balloon as it rotates around the spindle.

The Cayley transform

$$w = f(z) = \frac{z+i}{z-i}$$

maps the upper half plane to the exterior of the unit disk. So in Cartesian coordinates, this is a conformal mapping

$$(x, y) \mapsto \left(\frac{x^2+y^2-1}{x^2+y^2+1-2y}, \frac{2x}{x^2+y^2+1-2y} \right).$$

5.6 Conformal mapping of a laminar flow in the upper half plane to a flow around a semicircle with a separation point

Consider the well known [8] example of a uniform irrotational flow past a circular cylinder of radius a, with speed U at infinity. The complex potential is

$$w(z) = U\Big(z + \frac{a^2}{z}\Big)$$

and letting $z = re^{i\theta}$ the velocity potential is

$$\phi = U\Big(r + \frac{a^2}{r}\Big)\cos\theta$$

and the stream function is

$$\psi = U\Big(r - \frac{a^2}{r}\Big)\sin\theta\,.$$

It has been observed experimentally that for the flow of a uniform incompressible viscous fluid past a circular cylinder [33], the flow will detach from the surface of the cylinder at some point, as the flow moves around the surface of the cylinder from the front stagnation point. The point where this occurs is called the separation point, and it depends upon the Reynolds number. For the irrotational flow described above, it could be said that there is no separation point in this case, however another way to think about this is to say that the separation point is at angle $\pm\pi$ radians from the front stagnation point, at the rear stagnation point. Thus we can compose a conformal mapping of a uniform flow in the upper half plane to a flow around a circle of radius a, with a separation point at an angle $\frac{\pi}{m}$ from the front stagnation point. This is done by mapping the upper half plane to the upper half plane with a semi-circle of radius a removed. Then this domain is mapped to an infinite sector of angle

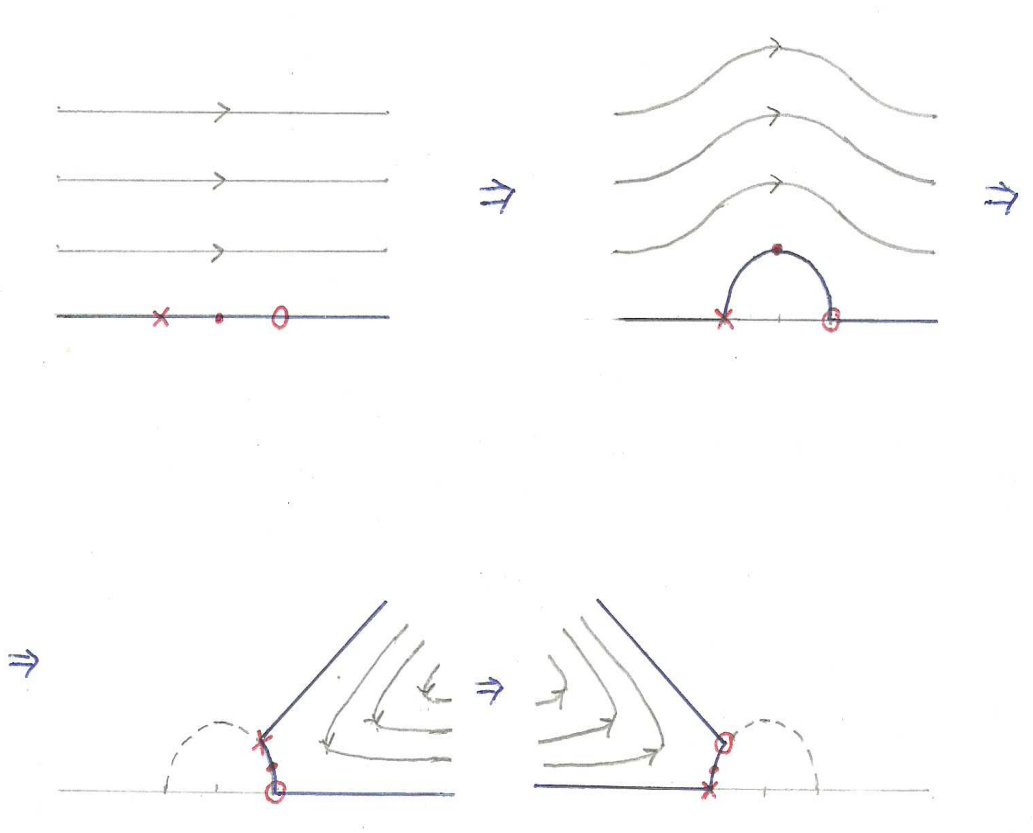

Figure 5.2: A conformal mapping from the upper half plane to an infinite sector of angle $\frac{\pi}{m}$ from the front stagnation point, of the upper half plane with a circle of radius a removed.

$\frac{\pi}{m}$, and finally a rotation by an angle $(\pi - \frac{\pi}{m})$, as shown in Figure 5.2. So an irrotational flow in this domain has complex potential

$$\Omega(z) = U\left(\left(e^{\frac{i(m-1)\pi}{m}}z\right)^m + \frac{a^2}{\left(e^{\frac{i(m-1)\pi}{m}}z\right)^m}\right),$$

or

$$\Omega(z) = U\left(\left(e^{i(m-1)\pi}z^m\right) + \frac{a^2}{\left(e^{i(m-1)\pi}z^m\right)}\right).$$

Let $z = re^{i\theta}$ then

$$\Omega(r,\theta) = U\left(\left(r^m e^{i(m\theta+(m-1)\pi)}\right) + \frac{a^2}{\left(r^m e^{i(m\theta+(m-1)\pi)}\right)}\right),$$

and so the velocity potential is

$$\phi = U\left(r^m + \frac{a^2}{r^m}\right)\cos(m\theta + (m-1)\pi)$$

and the stream function is

$$\psi = U\left(r^m - \frac{a^2}{r^m}\right)\sin(m\theta + (m-1)\pi)\,. \tag{5.6.18}$$

The stream function (5.6.18) is neither a solution to Euler's equation, nor is it a solution to the Navier-Stokes equations, however its form, being a product of velocity U, a function of r^m, and a sinusoidal function of θ suggests a way forward that is explored further in the next chapter.

Discussion Drag tangential to the yarn has always been neglected in the Padfield model, due to empirical results which showed that it is much smaller than the normal component of drag when the radius of the yarn balloon is large.

Skin friction occurs in a laminar flow due to the velocity gradient across the boundary layer, which causes shear stresses between the fluid flowing in adjacent streamlines. Therefore skin friction will always be present for flow around a circular cylinder, for example, because for all Reynolds numbers there will be a boundary layer in which the speed of the fluid adjusts from zero at the surface to the external speed at the edge of the boundary layer. Pressure drag occurs when the boundary layer separates, and a turbulent wake is created, and occurs in addition to skin friction.

For regions of the yarn balloon where the radius of the yarn balloon is large, the Reynolds number of the fluid surrounding the yarn (i.e. the air) will be larger, and pressure drag will dominate. Conversely, when the radius is small, the Reynolds number is smaller and thus skin friction must be taken into account.

Concluding Remarks In Chapter 5, a new representation of the Navier-Stokes equations in intrinsic coordinates is found. This result was used to find a rough estimate for the dissipation of energy over the boundary layer for fluid flow around a circular cylinder.

The objective of section 5.5 is to link drag from fluid flow around a circular cylinder to the drag acting on the yarn element moving in the yarn balloon. This has not been completed yet, however the results obtained in Chapter 6 are significant progress towards this goal.

The expression for the stream function in the last section (5.6.18) suggests a possible form for the stream function, and this is taken up in the next chapter, where a new similarity solution of the 2-D Navier-Stokes equations is found. This is the crucial result to link Re and C_D for air flow around the yarn element.

Chapter 6

A new approach to air drag through a similarity solution of the Navier-Stokes equation

6.1 Introduction

In this chapter, the two-dimensional steady state Navier-Stokes equations for an incompressible fluid with no body force (2.4.19) will be investigated in the boundary layer that exists as fluid flows around a circular cylinder. A well known method of modelling fluid flow around an object is to neglect terms in (2.4.19) that are small, leading to what is known as the boundary layer equations. Similarity solutions to these equations have been found [32], [59]. For example, in Chapter 8 of [8] where the author uses a similarity method to reduce the boundary layer equations to an ODE for the situation of fluid flow past a flat plate. In this example, the width of the boundary layer was given by a function $g(x)$, which depends only on x, the coordinate tangential to the plate, and $U(x)$ was the speed of the fluid at the edge of the boundary layer.

The velocity profile was then given by a certain function $f(y/g(x))$, where y was the coordinate normal to the plate. This function f depends only upon $\eta = (y/g(x))$ such that as the width of the boundary layer changes with x, $f(\eta)$ remains qualitatively the same. The key insight was that terms involving $g(x)$ and $U(x)$ and their derivatives in the boundary layer equations are constant, thus leaving a differential equation in $f(\eta)$ that was solved numerically. The constant terms also led to expressions for $g(x)$ and $U(x)$.

The objective of this chapter is to extend this idea to find an exact solution to the Navier-Stokes equations in a boundary layer. Drazin & Riley [25] state that "... the phrase 'exact solution'...often denotes a solution which has a simple explicit form, usually an expression in finite terms of elementary or other well known special functions. Sometimes an exact solution is taken to be one which can be reduced to the solution of an ordinary differential equation or a system of a few ordinary differential equations." In this thesis, we will use the first statement here as our definition of an exact solution.

Ma & Hui [32] state that "Most existing exact solutions in fluid mechanics are similarity solutions in the sense that the number of independent variables is reduced by one or more. They may be derived by dimensional arguments, by the group-theoretic method, or by the ad hoc method of free parameters. Among them the group-theoretic method, which includes the dimensional analysis as a special case, is the most systematic in generating similarity solutions."

Solutions of a PDE system that map into themselves under the action of a local symmetry of the PDE system are invariant. Bluman, Cheviakov & Anco state that "Such solutions are called *invariant solutions (similarity solutions)* and include the well-known *self-similar solutions (automodel solutions)* that result from scaling symmetries. ... Self-similar solutions...that also arise from

reduction through a dimensional analysis argument are called a *self-similar solution of the first kind* whereas one arising strictly as an invariant solution is called a *self-similar solution of the second kind*."
Barenblatt & Zel'dovich [57] state that "Much later it was realized that self-similar solutions do not represent merely specific examples. In actual fact they describe the 'intermediate-asymptotic' behavior of solutions of wider classes of initial, boundary, and mixed problems, i.e., they describe the behavior of these solutions away from the boundaries of the region of independent variables or, alternatively, in the region where in a sense the solution is no longer dependent on the details of the initial and/or boundary conditions but the system is still far from being in a state of equilibrium."

In this chapter we apply a transformation to (2.4.19) such that we can represent a boundary layer in the boundary conditions (6.2.5). We define the stream function (6.2.1) as a product of three variables, $g(\theta), U(\theta)$ and $f(\eta)$. We then look for solutions for g, U and f that satisfy the equations (6.2.6a) and (6.2.6b). We look for solutions such that terms in these equations comprising g, U and their derivatives are independent of θ. A number of solutions for g and U are found, in each case leading to an ODE for f. When the ODE is solved for f, the corresponding expressions for the stream function $\psi(\theta, \eta)$ and the pressure $p(\theta, \eta)$ are then found.

The purpose of finding this exact solution to the Navier-Stokes equations in the boundary layer is to find the functional relationship between the drag coefficient and the Reynolds number in the boundary layer of the air flow around the yarn element. This relationship encapsulates the transition from laminar to turbulent flow, the separation of the boundary layer, the onset of the drag crisis, etc that is, how all the observed phenomena that depend upon

the Reynolds number affect air drag as the Reynolds number changes. The shape, orientation and smoothness of the yarn element will then determine the relationship between the drag coefficient (for a smooth circular cylinder) and the air drag term corresponding to the yarn element. The circular symmetry of the yarn balloon may enable the 2-D solutions found here to be suitable for this task, however it may be that 3-D solutions to the Navier-Stokes equations are required. This question has not yet been answered.

In Section 6.2, a similarity transformation is applied to the 2-D Navier-Stokes equations in polar coordinates. In Section 6.3, the condition that all coefficients in (6.2.6a) and (6.2.6b) are independent of θ is explored. In Section 6.4, the condition that all coefficients of each term involving f and η and the derivatives of f in (6.2.6a) and (6.2.6b) are independent of θ is explored. This leads to thirteen constants, of two different types, denoted Group A and Group B. Solutions for U and g are found for each group, and solutions for U and g that make both Group A and Group B terms constant are sought. In Section 6.5, some solutions to the Navier-Stokes equations are found, in which pressure is constant. In Section 6.6, more constant pressure solutions are found in the first two sub-sections, while in the third sub-section, with a specific relationship between U and g, and an assumption for the relationship between constants, a fourth order non-linear ordinary differential equation is found, which is then reduced to quadrature, yielding a non-trivial boundary layer solution to the 2-D Navier-Stokes equations. From this solution, expressions for the Reynolds number, as well as the Strouhal number in terms of the Reynolds number, and the separation point are found.

6.2 A similarity transformation applied to (2.4.19)

Consider fluid flow around a fixed point, governed by (2.4.19). This could be flow around an object such as a circular cylinder, or flow in a vortex. Let the stream function be

$$\psi = U(\theta)g(\theta)f(\eta), \quad \text{where} \quad \eta = r/g(\theta) \tag{6.2.1}$$

where

$$\mathbf{u} = \nabla \times (\psi \mathbf{k}),$$

and thus

$$u_r = \frac{1}{r}\frac{\partial \psi}{\partial \theta}, \quad \text{and} \quad u_\theta = -\frac{\partial \psi}{\partial r}. \tag{6.2.2}$$

$g(\theta)$ represents the width of the boundary layer, and $f(\eta)$ is the velocity profile of the fluid speed u_r, that is, how the fluid speed tangential to the circular boundary changes as the point of interest moves radially outwards from the boundary. $U(\theta)$ is the corresponding speed of the fluid at the edge of the boundary layer (parallel to the boundary).

Clearly (6.2.2) satisfies the 2-D incompressibility condition in plane polar coordinates, the third equation in (2.4.19). Evaluating (6.2.2) with (6.2.1) yields

$$u_r = \frac{f}{r}(U'g + Ug') - \frac{Uf'g'}{g} \quad \text{and} \quad u_\theta = -Uf' \tag{6.2.3}$$

and

$$\frac{\partial}{\partial r}(f(\eta)) = \frac{f'}{g} \quad \text{and} \quad \frac{\partial}{\partial \theta}(f(\eta)) = \frac{-rf'g'}{g^2}\,, \tag{6.2.4}$$

where the prime indicates differentiation with respect to the relevant independent variable. That is, U and g are differentiated with respect to θ, while f is differentiated with respect to η.

The boundary conditions are

$$f(0) = f'(0) = 0\,, \quad f'(\infty) = 1\,. \tag{6.2.5}$$

The third condition here reflects the fact that u_θ tends to $U(\theta)$, the external speed as we leave the boundary layer.

Theorem 6 *If we substitute the expressions for u_r and u_θ* (6.2.3)*, into* (2.4.19) *with* (6.2.4) *and $r = \eta g$, then we obtain:*

$$\begin{aligned}
\frac{1}{\rho g}\frac{\partial p}{\partial \eta} =& - f'''\left(\frac{\nu U g'}{g^3} + \frac{\nu U g'^3}{g^5}\right) - \frac{f'^2}{\eta}\left(\frac{UU'g'}{g^2} - \frac{U^2 g'^2}{g^3} + \frac{U^2 g''}{g^2} - \frac{U^2}{g}\right) \\
& - \frac{f''}{\eta}\left(- \frac{\nu U'}{g^2} - \frac{3\nu U' g'^2}{g^4} + \frac{2\nu U g'}{g^3} + \frac{3\nu U g'^3}{g^5} - \frac{3\nu U g' g''}{g^4}\right) \\
& + \frac{f f''}{\eta}\left(\frac{UU'g'}{g^2} + \frac{U^2 g'^2}{g^3}\right) - \frac{f'}{\eta^2}\left(\frac{\nu U g'''}{g^3} + \frac{3\nu U' g''}{g^3} + \frac{3\nu U'' g'}{g^3} - \frac{\nu U'}{g^2}\right) \\
& - \frac{f f'}{\eta^2}\left(\frac{U'^2}{g} + \frac{UU'g'}{g^2} + \frac{2U^2 g'^2}{g^3} - \frac{U^2 g''}{g^2} - \frac{UU''}{g}\right) \\
& + \frac{f}{\eta^3}\left(\frac{\nu U'''}{g^2} + \frac{\nu U g'''}{g^3} + \frac{3\nu U' g''}{g^3} + \frac{3\nu U'' g'}{g^3}\right) \\
& + \frac{f^2}{\eta^3}\left(\frac{U'^2}{g} + \frac{2UU'g'}{g^2} + \frac{U^2 g'^2}{g^3}\right),
\end{aligned} \tag{6.2.6a}$$

$$\begin{aligned}
\frac{1}{\rho g \eta}\frac{\partial p}{\partial \theta} =& - f'''\left(\frac{\nu U}{g^2} + \frac{\nu U g'^2}{g^4}\right) - \frac{f'^2}{\eta}\left(\frac{UU'}{g} + \frac{U^2 g'}{g^2}\right) \\
& - \frac{f''}{\eta}\left(\frac{\nu U}{g^2} - \frac{\nu U g''}{g^3} - \frac{2\nu U' g'}{g^3}\right) + \frac{f f''}{\eta}\left(\frac{UU'}{g} + \frac{U^2 g'}{g^2}\right) \\
& - \frac{f'}{\eta^2}\left(- \frac{\nu U}{g^2} + \frac{2\nu U g''}{g^3} + \frac{4\nu U' g'}{g^3} + \frac{\nu U''}{g^2}\right) \\
& + \frac{f f'}{\eta^2}\left(\frac{UU'}{g} + \frac{U^2 g'}{g^2}\right) + \frac{f}{\eta^3}\left(\frac{2\nu U g''}{g^3} + \frac{4\nu U' g'}{g^3} + \frac{2\nu U''}{g^2}\right).
\end{aligned} \tag{6.2.6b}$$

6.3 A condition on U and g

In this section, we consider the requirement that all terms involving U and g and their derivatives in (6.2.6a) and (6.2.6b) are independent of θ, that is,

$$\frac{U^2}{g}, \quad \frac{UU''}{g}, \quad \frac{U'^2}{g}, \quad \frac{UU'g'}{g^2}, \quad \frac{U^2g''}{g^2}, \quad \frac{U^2g'^2}{g^3} \tag{6.3.7}$$

from (6.2.6a) and

$$\frac{UU'}{g}, \quad \frac{U^2g'}{g^2} \tag{6.3.8}$$

from (6.2.6b) are all constant, while

$$\begin{gathered}\frac{\nu U'}{g^2}, \quad \frac{\nu U'''}{g^2}, \quad \frac{\nu Ug'}{g^3}, \quad \frac{\nu Ug'''}{g^3}, \quad \frac{\nu U'g''}{g^3}, \\ \frac{\nu U''g'}{g^3}, \quad \frac{\nu U'g'^2}{g^4}, \quad \frac{\nu Ug'g''}{g^4}, \quad \frac{\nu Ug'^3}{g^5}\end{gathered} \tag{6.3.9}$$

from (6.2.6a) and

$$\frac{\nu U}{g^2}, \quad \frac{\nu U''}{g^2}, \quad \frac{\nu Ug''}{g^3}, \quad \frac{\nu U'g'}{g^3}, \quad \frac{\nu Ug'^2}{g^4} \tag{6.3.10}$$

from (6.2.6b) are all constant.

Theorem 7 *Every term from* (6.3.7) *and* (6.3.8) *is independent of* θ *if and only if*

$$g(\theta) = Ae^{\alpha\theta} \quad \textit{and} \quad U(\theta) = \sqrt{A}ke^{\frac{\alpha\theta}{2}} \tag{6.3.11}$$

where A *is a real constant, and* α *and* k *are complex constants.*

If

$$g(\theta) = Ae^{\alpha\theta} \quad \text{and} \quad U(\theta) = \sqrt{A}ke^{\frac{\alpha\theta}{2}}$$

then the terms in (6.3.7) are

$$k^2, \quad \frac{\alpha^2k^2}{4}, \quad \frac{\alpha^2k^2}{4}, \quad \frac{\alpha^2k^2}{2}, \quad \alpha^2k^2 \quad \text{and} \quad \alpha^2k^2$$

and the terms in (6.3.8) are

$$\frac{\alpha k^2}{2} \quad \text{and} \quad \alpha k^2$$

and all these terms are independent of θ.

If all the terms from (6.3.7) and (6.3.8) are independent of θ, then consider the first term in (6.3.7), $\frac{U^2}{g}$, and the second term in (6.3.8), $\frac{U^2 g'}{g^2}$, and together this implies that $\frac{g'}{g}$ is constant. If we let

$$\frac{g'}{g} = \alpha \quad \text{then} \quad g(\theta) = Ae^{\alpha\theta}\,,$$

then combining this with $\frac{U^2}{g} = k^2$ yields the required expression for U. ■

Theorem 8 *Every term from* (6.3.9) *and* (6.3.10) *is independent of* θ *if and only if*

$$g(\theta) = Ae^{\alpha\theta} \quad \textit{and} \quad U(\theta) = \frac{k}{\nu}A^2 e^{2\alpha\theta} \tag{6.3.12}$$

where A *and* ν *are real constants, and* α *and* k *are complex constants.*

This proof follows a similar path to that for Theorem 7. If

$$g(\theta) = Ae^{\alpha\theta} \quad \text{and} \quad U(\theta) = \frac{k}{\nu}A^2 e^{2\alpha\theta}$$

then the terms in (6.3.9) are

$$2\alpha k, \quad 8\alpha^3 k, \quad \alpha k, \quad \alpha^3 k, \quad 2\alpha^3 k, \quad 4\alpha^3 k, \quad 2\alpha^3 k, \quad \alpha^3 k \quad \text{and} \quad \alpha^3 k$$

and the terms in (6.3.10) are

$$k, \quad 4\alpha^2 k, \quad \alpha^2 k, \quad 2\alpha^2 k \quad \text{and} \quad \alpha^2 k$$

and all these terms are independent of θ.

If all the terms from (6.3.9) and (6.3.10) are independent of θ, then consider the first term in (6.3.10), $\frac{\nu U}{g^2}$, and the third term in (6.3.9), $\frac{\nu U g'}{g^3}$, and together this implies that $\frac{g'}{g}$ is constant. If we let

$$\frac{g'}{g} = \alpha \quad \text{then} \quad g(\theta) = Ae^{\alpha\theta}\,,$$

then combining this with $\frac{\nu U}{g^2} = k$ yields the required expression for U. ■

For a similarity solution, there would need to exist an expression for $g(\theta)$ and $U(\theta)$ such that all terms in (6.3.7), (6.3.8), (6.3.9) and (6.3.10) are constant. Expressing the first equation of (6.3.7) as $U = kg^{1/2}$ and taking the appropriate derivatives for U

$$U' = \frac{kg'}{2g^{1/2}}, \quad U'' = \frac{kg''}{2g^{1/2}} - \frac{kg'^2}{4g^{3/2}} \quad \text{and} \quad U''' = \frac{kg'''}{2g^{1/2}} - \frac{3kg'g''}{4g^{3/2}} + \frac{3kg'^2}{8g^{5/2}}\,, \tag{6.3.13}$$

and then substituting these expressions into the terms from (6.3.9) and (6.3.10), we obtain the following differential equations for $g(\theta)$

$$g' = kg^{5/2}, \quad g'' = kg^{5/2} \quad \text{and} \quad g''' = kg^{5/2}, \tag{6.3.14a}$$

$$g' = kg^{3/2}, \quad g' = kg^{7/4}, \quad g'g'' = kg^{7/2} \quad \text{and} \quad g = k, \tag{6.3.14b}$$

$$\frac{g''}{g^{5/2}} - \frac{g'^2}{2g^{7/2}} = k \quad \text{and} \quad \frac{g'g''}{g^{7/2}} - \frac{g'^3}{2g^{9/2}} = k, \tag{6.3.14c}$$

$$\frac{g'''}{g^{5/2}} - \frac{3g'g''}{2g^{7/2}} + \frac{3g'^3}{4g^{9/2}} = k\,. \tag{6.3.14d}$$

The general solution to the first equation in (6.3.14a) is

$$g = \left(\frac{-2}{3(k\theta + C_1)}\right)^{2/3},$$

while for the second equation in (6.3.14a) it is

$$g^2\,{}_2F_1\left(\frac{2}{7}, \frac{1}{2}; \frac{9}{7}; -\frac{4kg^{7/2}}{7C_1}\right)^2 = C_1(\theta + C_2)^2, \quad C_1 \neq -\frac{8}{7}g^{7/2}$$

where ${}_2F_1(a, b; c; z)$ is the hypergeometric function (2.5.22). Using (2.5.23), this expression can be written as

$$\frac{1}{7}\left(\frac{4}{7C_1}\right)^{3/7}\left(\frac{-1}{k}\right)^{4/7} B_x\left(\frac{2}{7}, \frac{1}{2}\right)^2 = (\theta + C_2)^2, \quad x = -\frac{4kg^{7/2}}{7C_1}.$$

The general solution for the third equation in (6.3.14a) is

$$\frac{1}{3}k\theta^3 g^{5/2} - 2g = -C_1\theta^2 + 2C_2\theta - C_3$$

using the method of integrating factors from Chapter 7 of [9].

Substituting $U = kg^{1/2}$ and (6.3.13) into (6.2.6a) and (6.2.6b)

$$\begin{aligned}\frac{1}{\rho g}\frac{\partial p}{\partial \eta} =& -kf'''\left(\frac{\nu g'}{g^{5/2}} + \frac{\nu g'^3}{g^{9/2}}\right) - \frac{k^2 f'^2}{\eta}\left(-1 - \frac{g'^2}{2g^2} + \frac{g''}{g}\right)\\ &- \frac{kf''}{\eta}\left(\frac{3\nu g'}{2g^{5/2}} + \frac{3\nu g'^3}{g^{9/2}} - \frac{3\nu g' g''}{g^{7/2}}\right)\\ &+ \frac{k^2 ff''}{\eta}\left(\frac{3g'^2}{2g^2}\right) - \frac{kf'}{\eta^2}\left(\frac{\nu g'''}{g^{5/2}} + \frac{3\nu g' g''}{g^{7/2}} - \frac{3\nu g'^3}{4g^{9/2}} - \frac{\nu g'}{2g^{5/2}}\right)\\ &- \frac{k^2 ff'}{\eta^2}\left(\frac{3g'^2}{g^2} - \frac{3g''}{2g}\right)\\ &+ \frac{kf}{\eta^3}\left(\frac{3\nu g'^2}{8g^{9/2}} + \frac{\nu 3g'''}{2g^{5/2}} + \frac{9\nu g' g''}{4g^{7/2}} - \frac{3\nu g'^3}{4g^{9/2}}\right)\\ &+ \frac{k^2 f^2}{\eta^3}\left(\frac{9g'^2}{4g^2}\right), \end{aligned} \tag{6.3.15a}$$

$$\begin{aligned}\frac{1}{\rho g\eta}\frac{\partial p}{\partial \theta} =& -kf'''\left(\frac{\nu}{g^{3/2}} + \frac{\nu g'^2}{g^{7/2}}\right) - \frac{k^2 f'^2}{\eta}\left(\frac{3g'}{2g}\right)\\ &- \frac{kf''}{\eta}\left(\frac{\nu}{g^{3/2}} - \frac{\nu g''}{g^{5/2}} - \frac{\nu g'^2}{g^{7/2}}\right) + \frac{k^2 ff''}{\eta}\left(\frac{3g'}{2g}\right)\\ &- \frac{kf'}{\eta^2}\left(-\frac{\nu}{g^{3/2}} + \frac{5\nu g''}{2g^{5/2}} + \frac{7\nu g'^2}{g^{7/2}}\right)\\ &+ \frac{k^2 ff'}{\eta^2}\left(\frac{3g'}{2g}\right) + \frac{kf}{\eta^3}\left(\frac{3\nu g''}{g^{5/2}} + \frac{3\nu g'^2}{g^{7/2}}\right). \end{aligned} \tag{6.3.15b}$$

Now we look for a similarity solution by investigating the solution (6.3.12), by taking $U = kg^2$ and the appropriate derivatives for U

$$U' = 2kgg', \quad U'' = 2k(g'^2 + gg'') \quad \text{and} \quad U''' = 2k(3g'g'' + gg''')\,. \tag{6.3.16}$$

Substituting these expressions into the terms from (6.3.7) and (6.3.8), the following differential equations for $g(\theta)$ were obtained

$$g'g^2 = k, \quad g''g^2 = k \quad \text{and} \quad gg'^2 = k, \tag{6.3.17}$$

$$g''g^2 + gg'^2 = k \quad \text{and} \quad g = k. \tag{6.3.18}$$

The general solution to the first equation in (6.3.17) is

$$g = \Big(3(k\theta + C_1)\Big)^{1/3},$$

while for the third equation it is

$$g = \left(\frac{3}{2}(\pm\sqrt{k}\theta + C_1)\right)^{2/3}.$$

Substituting $U = kg^2$ and (6.3.16) into (6.2.6a) and (6.2.6b)

$$\begin{aligned}\frac{1}{\rho g}\frac{\partial p}{\partial \eta} =& -k\nu f'''\left(\frac{g'}{g} + \frac{g'^3}{g^3}\right) - \frac{k^2 f'^2}{\eta}\big(-g^3 + gg'^2 + g^2 g''\big)\\ &+ \frac{3k\nu f''}{\eta}\left(\frac{g'^3}{g^3} + \frac{g'g''}{g^2}\right) + \frac{3k^2 ff''}{\eta}\big(gg'^2\big)\\ &- \frac{k\nu f'}{\eta^2}\left(-\frac{2g'}{g} + \frac{6g'^3}{g^3} + \frac{12g'g''}{g^2} + \frac{g'''}{g}\right)\\ &- \frac{3k^2 ff'}{\eta^2}\big(2gg'^2 - g^2 g''\big) + \frac{3k\nu f}{\eta^3}\left(\frac{2g'^3}{g^3} + \frac{6g'g''}{g^2} + \frac{g'''}{g}\right)\\ &+ \frac{9k^2 f^2}{\eta^3}\big(gg'^2\big), \end{aligned} \tag{6.3.19a}$$

$$\begin{aligned}\frac{1}{\rho g\eta}\frac{\partial p}{\partial \theta} =& -k\nu f'''\left(1 + \frac{g'^2}{g^2}\right) - \frac{3k^2 f'^2}{\eta}\big(g^2 g'\big)\\ &- \frac{k\nu f''}{\eta}\left(1 - \frac{g''}{g} - \frac{4g'^2}{g^2}\right) + \frac{3k^2 ff''}{\eta}\big(g^2 g'\big)\\ &- \frac{k\nu f'}{\eta^2}\left(-1 + \frac{4g''}{g} + \frac{10g'^2}{g^2}\right)\\ &+ \frac{3k^2 ff'}{\eta^2}\big(g^2 g'\big) + \frac{6k\nu f}{\eta^3}\left(\frac{g''}{g} + \frac{2g'^2}{g^2}\right). \end{aligned} \tag{6.3.19b}$$

Combining a condition derived from the first term in (6.3.7) with all the terms in (6.3.9) and (6.3.10) gives the differential equations (6.3.14a), (6.3.14b) (6.3.14c) and (6.3.14d) for g. While combining a condition derived from the first term in (6.3.10) with all the terms in (6.3.7) and (6.3.8) gave a different set of differential equations (6.3.17) and (6.3.18). These two conditions

represent two possible relationships between U and g. These relationships are substituted into the differential equation (6.2.6a) and (6.2.6b), giving (6.3.15a) and (6.3.15b) for the first condition, and (6.3.19a) and (6.3.19b) for the second condition. In both cases, it is not clear how any more progress can be made.

Lemma 2 *No solutions for $g(\theta)$ and $U(\theta)$ exist such that all terms from* (6.3.7)*,* (6.3.8)*,* (6.3.9) *and* (6.3.10) *are independent of θ.*

Clearly the solutions (6.3.11) and (6.3.12) are different. If we choose (6.3.11) for U and g, then by Theorem 8, the terms (6.3.9) and (6.3.10) depend on θ. If we choose (6.3.12) for U and g, then by Theorem 7, the terms (6.3.7) and (6.3.8) depend on θ. If we choose other non-trivial functions for U and g, then by both theorems, all terms will depend upon θ. ■

This suggests that a different relationship between U and g is required, in fact one that reconciles the two groups (6.3.7) and (6.3.8) with (6.3.9) and (6.3.10).

6.4 A condition on the coefficients of equations (6.2.6a) and (6.2.6b)

The right hand sides of equations (6.2.6a) and (6.2.6b) are comprised entirely of terms that are the product of a function of η, f and its derivatives, multiplied by a function of g, U and their derivatives with respect to θ. In this section, consider the requirement that every one of these functions of g, U and their derivatives are constant, that is they are in fact independent of θ. If this requirement is met, then the equations (6.2.6a) and (6.2.6b) are functions of terms in f and η with constant coefficients.

This requirement leads to thirteen different conditions upon g, U and their derivatives. Here they are separated into two groups. Group A is

$$\frac{\nu U}{g^2} + \frac{\nu U g'^2}{g^4} = k_1, \tag{6.4.20a}$$

$$\frac{\nu U g'}{g^3} + \frac{\nu U g'^3}{g^5} = k_2, \tag{6.4.20b}$$

$$\frac{\nu U}{g^2} - \frac{\nu U g''}{g^3} - \frac{2\nu U' g'}{g^3} = k_3, \tag{6.4.20c}$$

$$-\frac{\nu U'}{g^2} - \frac{3\nu U' g'^2}{g^4} + \frac{2\nu U g'}{g^3} + \frac{3\nu U g'^3}{g^5} - \frac{3\nu U g' g''}{g^4} = k_4, \tag{6.4.20d}$$

$$-\frac{\nu U}{g^2} + \frac{2\nu U g''}{g^3} + \frac{4\nu U' g'}{g^3} + \frac{\nu U''}{g^2} = k_5, \tag{6.4.20e}$$

$$\frac{\nu U g'''}{g^3} + \frac{3\nu U' g''}{g^3} + \frac{3\nu U'' g'}{g^3} - \frac{\nu U'}{g^2} = k_6, \tag{6.4.20f}$$

$$\frac{2\nu U g''}{g^3} + \frac{4\nu U' g'}{g^3} + \frac{2\nu U''}{g^2} = k_7, \tag{6.4.20g}$$

$$\frac{\nu U'''}{g^2} + \frac{\nu U g'''}{g^3} + \frac{3\nu U' g''}{g^3} + \frac{3\nu U'' g'}{g^3} = k_8\ . \tag{6.4.20h}$$

Group B is

$$\frac{U U'}{g} + \frac{U^2 g'}{g^2} = k_9, \tag{6.4.21a}$$

$$\frac{U U' g'}{g^2} + \frac{U^2 g'^2}{g^3} = k_{10}, \tag{6.4.21b}$$

$$\frac{U U' g'}{g^2} - \frac{U^2 g'^2}{g^3} + \frac{U^2 g''}{g^2} - \frac{U^2}{g} = k_{11}, \tag{6.4.21c}$$

$$\frac{U'^2}{g} + \frac{U U' g'}{g^2} + \frac{2U^2 g'^2}{g^3} - \frac{U^2 g''}{g^2} - \frac{U U''}{g} = k_{12}, \tag{6.4.21d}$$

$$\frac{U'^2}{g} + \frac{2U U' g'}{g^2} + \frac{U^2 g'^2}{g^3} = k_{13}\ . \tag{6.4.21e}$$

It is worth noting here that the expressions in Group A are coefficients of terms f, f', f'' and f''', while the expressions in Group B are coefficients of terms f^2, ff', ff'' and f'^2.

The objective is to find a solution for U and g that satisfied all thirteen equations. Failing that, the objective is to find a solution for U and g that satisfies

some of the thirteen equations, and then eliminate the equations not satisfied as coefficients in (6.2.6a) and (6.2.6b) by requiring that the corresponding terms in f or its derivatives be zero.

The first step is to try to find any solution for U and g that satisfy some of these thirteen conditions. A helpful observation here is that

$$\frac{d^2}{d\theta^2}\Big(Ug\Big) = U''g + 2U'g' + Ug'', \tag{6.4.22a}$$

$$\frac{d^3}{d\theta^3}\Big(Ug\Big) = U'''g + 3U''g' + 3U'g'' + Ug''', \tag{6.4.22b}$$

$$\frac{d}{d\theta}\Big(U^2g^2\Big) = 2(UU'g^2 + U^2gg'), \tag{6.4.22c}$$

$$\frac{d^2}{d\theta^2}\Big(U^2g^2\Big) = 2(U'^2g^2 + UU''g^2 + 4UU'gg' + U^2g'^2 + U^2gg'') \tag{6.4.22d}$$

The first two equations (6.4.22a) and (6.4.22b) are relevant to the equations in Group A, as they are derivatives of the product Ug, while the last two equations (6.4.22c) and (6.4.22d) are relevant to the equations in Group B, as they are derivatives of the product U^2g^2.

At this stage there are many combinations that can be tried, such as the following example, using equations from both Group A and Group B. First combine equations (6.4.21a) and (6.4.21b), which gives the expressions

$$\frac{g'}{g} = \frac{k_{10}}{k_9} \quad \text{and} \quad \frac{d}{d\theta}\Big(U^2g^2\Big) = 2k_9g^3 \ ,$$

using (6.4.20h) then (6.4.20g), the solution obtained is

$$g = C_1e^{\frac{k_{10}}{k_9}\theta} \quad \text{and} \quad U = \pm\sqrt{\frac{k_7k_9C_1}{k_8}e^{\frac{k_{10}}{k_9}\theta} - \frac{2k_9C_2}{C_1^2}e^{-2\left(\frac{k_{10}}{k_9}\theta\right)}} \ .$$

The way forward however, is to find solutions using equations from Group A only and from Group B only.

Using equations from Group A only, combining equations (6.4.20g) and (6.4.20h),

with (6.4.22a) and (6.4.22b) gives the solution

$$g = \left(\frac{2\nu C_3}{k_7}\right)^{1/3} e^{\frac{2k_8}{3k_7}\theta} \quad \text{and}$$
$$U = \left(\frac{C_3^2 k_7^7}{2^7 \nu k_8^6}\right)^{1/3} e^{\frac{4k_8}{3k_7}\theta} + (C_4\theta + C_5)\left(\frac{k_7}{2\nu C_3}\right)^{1/3} e^{-\frac{2k_8}{3k_7}\theta}. \qquad (6.4.23)$$

Using equations from Group B only, combining equations (6.4.21a), (6.4.21b), (6.4.21d) and (6.4.21e), with (6.4.22c) and (6.4.22d) gives the solution

$$g = \left(\frac{C_6}{2k_9}\right)^{1/3} e^{\left(\frac{2k_{13}+k_{10}-k_{12}}{3k_9}\right)\theta} \quad \text{and}$$
$$U = \pm\sqrt{\frac{\left(4C_6k_9^5\right)^{1/3}}{2k_{13}+k_{10}-k_{12}} e^{\left(\frac{2k_{13}+k_{10}-k_{12}}{3k_9}\right)\theta} + C_7\left(\frac{2k_9}{C_6}\right)^{2/3} e^{-2\left(\frac{2k_{13}+k_{10}-k_{12}}{3k_9}\right)\theta}}. \qquad (6.4.24)$$

This is achieved by solving (6.4.21d) for $UU''g^2$ and substituting into (6.4.22d), then further substituting $2g^3$ times (6.4.21e) and g^3 times (6.4.21b) into (6.4.22d),

$$\frac{1}{2}\frac{d^2}{d\theta^2}\left(U^2g^2\right) + k_{12}g^3 = 2U'^2g^2 + 5UU'gg' + 3U^2g'^2 = g^3(2k_{13}+k_{10})$$

then substituting for g^3 from (6.4.21a) to give

$$\frac{1}{2}\frac{d^2}{d\theta^2}\left(U^2g^2\right) = \frac{(2k_{13}+k_{10}-k_{12})}{2k_9}\frac{d}{d\theta}\left(U^2g^2\right).$$

Integrating once gives

$$g^3 = \left(\frac{C_6}{2k_9}\right)e^{\left(\frac{2k_{13}+k_{10}-k_{12}}{3k_9}\right)\theta}$$

then integrating again and rearranging gives the result for U.

Looking past the plethora of constants in these expressions, the important point to note is the relationship between the exponent in g and the exponent in U in each case, and the relationship between the exponents in the two terms in U in each case.

Given the form of the solutions expressed here for g, that is, g will be sinusoidal if the coefficient of the exponent is complex, the sign of the real part will determine whether the amplitude of g increases or decreases as θ increases. Considering equations (6.4.20a) and (6.4.20b), if the expression $1 + \frac{g'^2}{g^2} = 0$ and thus $k_1 = k_2 = 0$ then we have the special case of

$$g = A_1 e^{i\theta} + A_2 e^{-i\theta} = B_1 \cos\theta + B_2 \sin\theta$$

The five terms on the right hand side of (6.4.22d) appear in various combinations in equations (6.4.21b) to (6.4.21e) after they are multiplied by g^3. However, it is not possible to express (6.4.22d) in terms of all five equations in Group B, because the $UU''g^2$ term only appears in (6.4.21d) and thus (6.4.21d) and (6.4.21c) cannot both be used. However, if (6.4.24) and the subsequent derivatives of U and g are substituted into (6.4.21c) then

$$g = \left(\frac{C_6}{2k_9}\right)^{1/3} e^{\pm i\theta} \quad \text{and} \quad U = \pm\sqrt{\mp\frac{\left(4C_6k_9^2\right)^{1/3}}{3}e^{\pm i\theta} + C_7\left(\frac{2k_9}{C_6}\right)^{1/3} e^{\mp 2i\theta}}\,.$$

The solution mentioned above, (6.4.23), is obtained by using only two of the equations from Group A. All eight equations in Group A can be combined to obtain a solution for U and g, along with constraints on the corresponding constants k_i, as follows. Firstly combining (6.4.20f) and (6.4.20h) gives

$$U''' + U' = \frac{(k_8 - k_6)}{\nu} g^2\,. \tag{6.4.25}$$

Secondly combining the equations (6.4.20c), (6.4.20e) and (6.4.20g) with the use of (6.4.22a) gives the constraint

$$k_3 + k_5 = \frac{k_7}{2} \, .$$

Thirdly, using equations (6.4.20a), (6.4.20b) and (6.4.20d), we obtain the differential equation

$$\frac{d}{d\theta}\Big(Ug\Big) = \frac{k_1^2(3k_2 - k_4)}{\nu(k_1^2 + 3k_2^2)} g^3 \, . \tag{6.4.26}$$

This is achieved by first substituting from (6.4.20a) into (6.4.20b) and (6.4.20d), and then substituting for g' into the other equation.

Fourthly, combining the equations (6.4.26) and (6.4.20g) gives

$$\begin{aligned} g &= \left(\frac{\nu C_8(k_1^2 + 3k_2^2)}{k_1^2(3k_2 - k_4)}\right)^{1/3} e^{\frac{k_7(k_1^2+3k_2^2)}{6k_1^2(3k_2-k_4)}\theta} \quad \text{and} \\ U &= \frac{2}{k_7}\left(\frac{C_8^2}{\nu}\right)^{1/3}\left(\frac{k_1^2(3k_2 - k_4)}{(k_1^2 + 3k_2^2)}\right)^{4/3} e^{\frac{k_7(k_1^2+3k_2^2)}{3k_1^2(3k_2-k_4)}\theta} \\ &\quad + C_9\left(\frac{k_1^2(3k_2 - k_4)}{\nu C_8(k_1^2 + 3k_2^2)}\right)^{1/3} e^{-\frac{k_7(k_1^2+3k_2^2)}{6k_1^2(3k_2-k_4)}\theta} \, . \end{aligned} \tag{6.4.27}$$

The solutions for U and g given by (6.4.23) and (6.4.27) are identical if

$$C_4 = 0 \quad \text{and} \quad C_5 = C_9 \quad \text{and} \quad C_3 = \frac{2k_8 C_8}{k_7} \quad \text{and} \quad \frac{k_7^2}{4k_8} = \frac{k_1^2(3k_2 - k_4)}{(k_1^2 + 3k_2^2)}$$

and finally substituting this solution into (6.4.25) gives

$$(k_8 = 0 \quad \text{or} \quad C_5 = 0 \quad \text{or} \quad \frac{2k_8}{3k_7} = \pm i) \quad \text{and} \quad (k_8 - k_6) = \frac{k_7^2}{2k_8}\left(1 + \left(\frac{4k_8}{3k_7}\right)^2\right) . \tag{6.4.28}$$

Each of the first two conditions in (6.4.28) yield an infinite value for U. Considering the last two conditions in (6.4.28), the unique solution of U and g which satisfies all the equations in Group A is

$$g = g_0 e^{\pm i\theta} \quad \text{and} \quad U = -\frac{C_3}{9g_0} e^{\pm 2i\theta} + \frac{C_5}{g_0} e^{\mp i\theta} \, . \tag{6.4.29}$$

where

$$g_0 = \left(\frac{2\nu C_3}{k_7}\right)^{1/3} \quad \text{and} \quad (k_8 - k_6) = \pm k_7 i \quad \text{and} \quad k_3 + k_5 = \frac{k_7}{2}\,.$$

To find the unique solution for U and g that satisfies all equations in Group B, (6.4.24) and the subsequent derivatives are substituted into (6.4.21c). Thus the unique solution of U and g which satisfies all the equations in Group B is

$$g = g_1 e^{\pm i\theta} \quad \text{and} \quad U = \pm\sqrt{\mp\frac{C_6}{3g_1^2}e^{\pm i\theta} + \frac{C_7}{g_1}e^{\mp 2i\theta}} \tag{6.4.30}$$

where

$$g_1 = \left(\frac{C_6}{2k_9}\right)^{1/3}\,.$$

To find the unique solution for U and g that satisfies all equations in Group A and Group B, equate the corresponding expressions in (6.4.29) and (6.4.30). Equating the two expression for g gives

$$C_6 = \frac{4\nu k_9 C_3}{k_7}\,.$$

Squaring both expressions for U and then equating the corresponding terms gives

$$\frac{C_3^2}{81g_0^2} = 0, \quad C_5 = \pm\frac{6\nu k_9}{k_7} \quad \text{and} \quad C_7 = \frac{C_5^2}{g_0}\,. \tag{6.4.31}$$

The first equation in (6.4.31) arises due to the fact that the $e^{4i\theta}$ term appears only when U in (6.4.29) is squared, and not when U in (6.4.30) is squared. This equation can be expressed in terms of C_3, k_7 and ν, and can be satisfied by taking the limit when C_3 or k_7 go to zero, or ν goes to infinity. That is

$$\lim\left(\frac{k_7 C_3^2}{1458\nu}\right)^{2/3} \to 0\,. \tag{6.4.32}$$

So the solution for U, subject to this limit is

$$U = -\frac{1}{9}\Big(\frac{C_3^2 k_7}{2\nu}\Big)^{1/3} e^{\pm 2i\theta} \pm \frac{k_9}{3}\Big(\frac{4\nu^2}{C_3 k_7^2}\Big)^{1/3} e^{\mp i\theta},$$

or factorizing the term $\frac{1}{U_0}$

$$U = \left(\frac{2\nu}{C_3^2 k_7}\right)^{1/3}\left(-\frac{1}{9}\left(\left(\frac{C_3^2 k_7}{2\nu}\right)^{1/3} e^{\pm i\theta}\right)^2 \pm \frac{C_3 k_9}{3}\left(\left(\frac{C_3^2 k_7}{2\nu}\right)^{1/3} e^{\pm i\theta}\right)^{-1}\right). \tag{6.4.33}$$

Considering the dimensions of all the terms in (6.4.33), the characteristic velocity can be taken as $U_0 = \left(\frac{C_3^2 k_7}{2\nu}\right)^{1/3}$. With $g = g_0 e^{\pm i\theta}$, the characteristic length can be taken as $L = g_0 = \left(\frac{2\nu C_3}{k_7}\right)^{1/3}$. Therefore the Reynolds number is

$$Re = \frac{C_3}{\nu} \tag{6.4.34}$$

and the dimensionless solution can be represented as

$$\bar{g} = \frac{g}{g_0} = e^{\pm i\theta} \quad \text{and} \quad \bar{U} = \frac{U}{U_0} = -\frac{1}{9}e^{\pm 2i\theta} \pm \frac{2\nu k_9}{3C_3 k_7} e^{\mp i\theta}. \tag{6.4.35}$$

The ratio $\frac{k_9}{k_7}$ has dimensions $\frac{U_0 L}{\nu}$ and thus $\frac{\nu k_9}{C_3 k_7}$ does not depend upon Re. What happens to g and U when the limit (6.4.32) is evaluated in various possible ways is explored in Table 6.1 below.

Theorem 9 *A physically realizable viscous fluid flow has a finite viscosity and a finite Reynolds number. No such solution to the Navier-Stokes equations, that satisfies* (6.4.32) *and* (6.4.33)*, exists.*

So for a physically realizable viscous fluid flow, $\nu \in (0, \infty)$ and $Re \in (0, \infty)$. A fluid flow is a similarity solution if (6.4.35) is satisfied, subject to the limit (6.4.32). This limit exists if either $\nu \to \infty$ or $C_3 \to 0$ or $k_7 \to 0$. Considering these three possibilities in turn. The first possibility can be ruled out immediately because if the viscosity is infinite, then by definition the solution is not physically realizable. The second possibility can also be ruled out because of (6.4.34), the definition of Re, because if $C_3 \to 0$, then $Re \to 0$. For the remaining possibilities, when the viscosity is finite, C_3 is non-zero and $k_7 \to 0$ so that (6.4.32) is satisfied, if k_9 is non-zero, U is not physically realizable, which

leaves the only remaining possibility, when $k_9 \to 0$ also. To investigate this final case, consider the ratio $\frac{k_9}{k_7}$ from the definition of these constants, (6.4.20g) and (6.4.21a), that is

$$\frac{k_9}{k_7} = \frac{(Ug)\frac{d}{d\theta}(Ug)}{2\nu\frac{d^2}{d\theta^2}(Ug)}\,.$$

The most general solution to this equation in this case is that Ug is constant. However, from (6.4.33),

$$Ug = -\frac{1}{9}C_3 e^{\pm 3i\theta} \pm \frac{2\nu k_9}{3k_7}\,,$$

and given that in this case, C_3 is non-zero, there is a contradiction. Thus in none of these possibilities, is the solution physically realizable. ■

When the amplitude g_0 or U_0 or both approach infinity, for example $U \to -\infty e^{i\theta}$, the functions g and/or U are not finite for all real values, except for a finite, periodic set of real values where they are indeterminate, that is $(\theta = \frac{(2n+1)}{2}\pi)$, where $n \in \mathbb{Z}$. The ninth row of Table 6.1, the case where $k_7 \to 0$ and $k_9 \to 0$ while $C_3 \in (0, \infty)$ and $\nu \in (0, \infty)$, given the analysis in the proof above suggests that Ug equal to a constant is worth further investigation.

The solution for the dimensionless speed $\bar{U}$, subject to the limit (6.4.32), and $\bar{g}$ can be written as

$$\bar{g} = e^{\pm i\theta} \quad \text{and} \quad \bar{U} = \mathbb{F}(e^{\pm i\theta})$$

where

$$\mathbb{F}(X) = -\frac{1}{9}X^2 \pm \frac{2}{3}\frac{\nu k_9}{C_3 k_7}\frac{1}{X}\,. \tag{6.4.36}$$

Comparing this equation to (6.4.23), it is clear that expressions derived from Group A terms have exponential terms of the form $e^{2\alpha\theta}$ and $e^{-\alpha\theta}$, which is

C_3	k_7	ν	k_9	U	g_0	U_0	Re
0	$\neq 0$	$(0,\infty)$	$\neq 0$	$\pm\infty e^{\mp i\theta}$	0	0	0
$(0,\infty)$	0	$(0,\infty)$	$\neq 0$	$\pm\infty e^{\mp i\theta}$	∞	0	$(0,\infty)$
$\neq 0$	$\neq 0$	∞	$\neq 0$	$\pm\infty e^{\mp i\theta}$	∞	0	0
0	0	$(0,\infty)$	$\neq 0$	$\pm\infty e^{\mp i\theta}$	Indeterminate	0	0
0	$\neq 0$	∞	$\neq 0$	$\pm\infty e^{\mp i\theta}$	Indeterminate	0	0
$\neq 0$	0	∞	$\neq 0$	$\pm\infty e^{\mp i\theta}$	∞	0	0
0	0	∞	$\neq 0$	$\pm\infty e^{\mp i\theta}$	Indeterminate	0	0
0	$\neq 0$	$(0,\infty)$	0	Indeterminate $\times e^{\mp i\theta}$	0	0	0
$(0,\infty)$	0	$(0,\infty)$	0	Indeterminate $\times e^{\mp i\theta}$	∞	0	$(0,\infty)$
$\neq 0$	$\neq 0$	∞	0	Indeterminate $\times e^{\mp i\theta}$	∞	0	0
0	0	$(0,\infty)$	0	Indeterminate $\times e^{\mp i\theta}$	Indeterminate	0	0
0	$\neq 0$	∞	0	Indeterminate $\times e^{\mp i\theta}$	Indeterminate	0	0
$\neq 0$	0	∞	0	Indeterminate $\times e^{\mp i\theta}$	∞	0	0
0	0	∞	0	Indeterminate $\times e^{\mp i\theta}$	Indeterminate	0	0

Table 6.1: Values for Re, g_0 and U_0 with limit (6.4.32).

consistent with this function $\mathbb{F}$, in a way that expressions derived from Group B terms are not. This observation naturally leads to the focus of the remainder of this chapter: an attempt to find solutions of equations (6.2.6a) and (6.2.6b).

6.5 A condition on the coefficients of $e^{3\alpha\theta}$ in equations (6.2.6a) and (6.2.6b)

Consider equation (6.4.20h) from Group A, with a guess for g consistent with the results found so far. A solution can then be found

$$g = Ae^{\alpha\theta} \quad \text{and} \quad U = \frac{C_3}{27A\alpha^3}e^{2\alpha\theta} + \frac{1}{A}(C_1\theta^2 + C_4\theta + C_5)e^{-\alpha\theta}\,. \tag{6.5.37}$$

To begin with, for the sake of simplicity, and for U to be consistent with (6.4.36), let $C_1 = C_4 = 0$. When (6.5.37) is substituted into (6.2.6a) and (6.2.6b), the terms involving U, g and their derivatives produce constant terms, $e^{3\alpha\theta}$ terms and $e^{-3\alpha\theta}$ terms. Setting the coefficients of $e^{3\alpha\theta}$ to zero in both equations gives

$$-\frac{ff''}{\eta} + \frac{f'^2}{\eta} - \frac{ff'}{\eta^2} = 0, \tag{6.5.38a}$$

$$-3\alpha^2\frac{ff''}{\eta} + (2\alpha^2 - 1)\frac{f'^2}{\eta} + 3\alpha^2\frac{ff'}{\eta^2} - 9\alpha^2\frac{f^2}{\eta^3} = 0\,. \tag{6.5.38b}$$

Solving for $\frac{f'^2}{\eta}$ in (6.5.38a) and substituting into (6.5.38b), gives an Euler equation. Making the substitution $\eta = e^z$ gives

$$-(1+\alpha^2)\frac{d^2f}{dz^2} + 6\alpha^2\frac{df}{dz} - 9\alpha^2 f = 0\,. \tag{6.5.39}$$

Firstly, $\alpha = \pm i$ makes (6.5.39) into a first order differential equation with solution $f = C_6\eta^{3/2}$. Secondly, $f = C_6\eta^{k_1}$ with $k_1 = \frac{3\alpha}{\alpha \pm i}$ is the solution to the second order differential equation. Both these cases lead to a solution of (6.2.6a) and (6.2.6b) as follows

$$g = Ae^{\pm i\theta}\,, \quad U = \frac{\pm C_3 i}{27A}e^{\pm 2i\theta}\,, \quad f = C_6\eta^{3/2} \quad \text{and} \quad p = C_8$$

and

$$g = Ae^{\alpha\theta}\,, \quad U = \frac{C_3}{27A\alpha^3}e^{2\alpha\theta}\ , \quad f = C_6\eta^{\frac{3\alpha}{\alpha\pm i}} \quad \text{and} \quad p = C_8$$

where $\alpha \in \mathbb{C}$ such that $\frac{\alpha(\alpha\mp i)(\alpha\mp 2i)(2\alpha\mp i)}{\alpha\pm i} \neq 0$ and $\alpha^2 + 1 \neq 0$. However $f = C_6\eta^{3/2}$ does not satisfy the third boundary condition in (6.2.5).

6.6 Reduction to quadrature of equations (6.2.6a) and (6.2.6b)

The form of the various expressions found for g, U and f so far leads to the following hypothesis.

Hypothesis 1 *More solutions to the Navier-Stokes equations,* (6.2.6a) *and* (6.2.6b) *exist of the form*

$$g = Ae^{\alpha\theta}\,, \quad U = \frac{C_3}{27A\alpha^3}e^{2\alpha\theta} + \frac{1}{A}(C_1\theta^2 + C_4\theta + C_5)e^{-\alpha\theta} \quad \textit{and} \quad f = C_6\eta^{k_1} + C_7\eta^{k_2}.$$

To prove this hypothesis, in this section, I will reduce (6.2.6a) and (6.2.6b) to quadrature by first choosing an ansatz for g, U and f, and subsequently finding solutions of the resulting algebraic equations for α, k_1 and k_2.

Substitute $g = Ae^{\alpha\theta}$ and $f = C_6\eta^{k_1} + C_7\eta^{k_2}$ into (6.2.6a) and (6.2.6b) and then integrate with respect to η and θ respectively to obtain two expressions for the pressure p, which of course must be equal. Equation (6.2.6a) then yields terms with $\eta^{k_1-2}, \eta^{k_2-2}, \eta^{k_1+k_2-2}, \eta^{2k_1-2}$ and η^{2k_2-2}, while equation (6.2.6b) only yields terms with the first three expressions. Equating the coefficients of the corresponding terms in η produces the following five equations.

The coefficient of η^{k_1-2} gives

$$(k_1-2)\Bigg((\alpha^2(k_1-1)^2+k_1^2)\int e^{-\alpha\theta}U d\theta \\ -\ 2\alpha(k_1-1)\int e^{-\alpha\theta}U' d\theta\ +\int e^{-\alpha\theta}U'' d\theta\Bigg) = \\ \frac{1}{k_1-2}e^{-\alpha\theta}\Bigg(\alpha(k_1-1)(\alpha^2(k_1-1)^2+k_1^2)U \\ -\ (3\alpha^2(k_1-1)^2+k_1^2)U'+3\alpha(k_1-1)U''-U'''\Bigg).$$

The coefficient of η^{k_2-2} gives

$$(k_2-2)\Bigg((\alpha^2(k_2-1)^2+k_2^2)\int e^{-\alpha\theta}U d\theta \\ -\ 2\alpha(k_2-1)\int e^{-\alpha\theta}U' d\theta\ +\int e^{-\alpha\theta}U'' d\theta\Bigg) = \\ \frac{1}{k_2-2}e^{-\alpha\theta}\Bigg(\alpha(k_2-1)(\alpha^2(k_2-1)^2+k_2^2)U \\ -\ (3\alpha^2(k_2-1)^2+k_2^2)U'+3\alpha(k_2-1)U''-U'''\Bigg).$$

The coefficient of $\eta^{k_1+k_2-2}$ gives

$$(k_1-k_2)^2\int \alpha U^2+UU'd\theta = \frac{1}{k_1+k_2-2}\Bigg((2k_1k_2 \\ +\alpha^2(2+k_1(k_1-2)+k_2(k_2-2)))U^2-(k_1+k_2-2)U'^2 \\ +\alpha(4+k_1^2+k_2(k_2-2)-2k_1(k_2+1))UU'+(k_1+k_2)UU''\Bigg). \quad (6.6.40)$$

The coefficient of η^{2k_1-2} gives

$$\frac{C_6^2}{k_1-1}\Bigg((\alpha^2(k_1-1)^2+k_1^2)U^2-(k_1-1)U'^2-2\alpha(k_1-1)UU'+k_1UU''\Bigg)=0\,. \quad (6.6.41)$$

The coefficient of η^{2k_2-2} gives

$$\frac{C_7^2}{k_2-1}\Bigg((\alpha^2(k_2-1)^2+k_2^2)U^2-(k_2-1)U'^2-2\alpha(k_2-1)UU'+k_2UU''\Bigg)=0\,. \quad (6.6.42)$$

By considering the first and second derivatives of U^2, equations (6.6.40), (6.6.41), (6.6.42) can be represented as a single differential equation for U^2, as follows

$$\int U^2 d\theta = \frac{1}{2\alpha(k_1-k_2)^2(k_1+k_2-2)}$$
$$\Big(-(k_1+k_2)(k_1^2+k_2(-2\alpha^2+k_2-2)+2k_1(k_2-1+\alpha^2(2k_2-1)))U^2$$
$$+\alpha(k_1(k_1+2)-2(k_1-1)k_2+k_2^2)\frac{d}{d\theta}\big(U^2\big)+(k_1+k_2)\frac{d^2}{d\theta^2}\big(U^2\big)\Big)\,.$$

Clearly this yields a cubic polynomial equation for λ when the solution for U is of the form $U^2 = e^{\lambda\theta}$

$$(k_1+k_2)\lambda^3+(2\alpha k_1+\alpha k_1^2+2\alpha k_2-2\alpha k_1k_2+\alpha k_2^2)\lambda^2+$$
$$(2k_1^2+2\alpha^2k_1^2-k_1^3+4k_1k_2+4\alpha^2k_1k_2-3k_1^2k_2-4\alpha^2k_1^2k_2+2k_2^2+2\alpha^2k_2^2$$
$$-3k_1k_2^2-4\alpha^2k_1k_2^2-k_2^3)\lambda$$
$$+4\alpha k_1^2-2\alpha k_1^3-8\alpha k_1k_2+2\alpha k_1^2k_2+4\alpha k_2^2+2\alpha k_1k_2^2-2\alpha k_2^3=0\,.$$

The next sub-sections depend upon the form chosen for U.

6.6.1 A single exponential term for U

Assuming a single exponential term for U, leads to four sets of solutions for (6.2.6a) and (6.2.6b), firstly

$$g = Ae^{\alpha\theta}\,,\quad U = C_5e^{-\alpha\theta}\,,\quad f = C_6\quad\text{and}\quad p = C_8$$

where $\alpha(\alpha^2+1)\neq 0$.
Secondly,

$$g = Ae^{\pm i\theta}\,,\quad U = C_5e^{\mp i\theta}\ ,\quad f = C_6\eta^{k_1}+C_7\eta^{k_2}\quad\text{and}\quad p = C_8 \qquad (6.6.43)$$

where $(k_1-1)(k_1-2)(k_2-1)(k_2-2)(k_1+k_2-2)\neq 0$. Thirdly

$$g = Ae^{\pm i\theta}\,, \quad U = C_5 e^{\pm ni\theta}\,, \quad f = C_6\eta^{\frac{(n+1)}{2}} \quad \text{and} \quad p = C_8$$

where $n+1\neq 0$ and $n(n-1)(n-3)\neq 0$. Fourthly,

$$g = Ae^{\alpha\theta}\,, \quad U = C_5 e^{n\alpha\theta}\,, \quad f = C_6\eta^{\frac{(n+1)\alpha}{\alpha\pm i}} \quad \text{and} \quad p = C_8$$

where $(\alpha^2+1)\neq 0$, $\alpha(n+1)\neq 0$ and $\frac{-n(n-1)(\alpha\mp i)(n\alpha\mp i)((n-1)\alpha\mp 2i)}{\alpha\pm i}\neq 0$.

6.6.2 Two exponential terms for U

The next step is to try an ansatz for U with two exponential terms.

Firstly assume derivatives of Ug are proportional to g^3, which leads to an ansatz for U of the form $U = C_3e^{2\alpha\theta} + C_5e^{-\alpha\theta}$.
This yields a solution

$$g = Ae^{\pm i\theta}\,, \quad U = C_5 e^{\mp i\theta}\,, \quad f = C_6\left(\eta^k + \frac{1}{\eta^k}\right) \quad \text{and} \quad p = C_8\,. \qquad (6.6.44)$$

However this solution does not satisfy the first boundary condition in (6.2.5) for all non-zero real k. The trivial case of $k=0$ does not satisfy the third boundary condition in (6.2.5).

Secondly assume derivatives of Ug are proportional to $g^{\frac{3}{1+3\delta}}$, taking (6.4.23) with $C_4=0$ leads to an ansatz for U of the form $U = C_3e^{(\frac{2}{3}-\delta)\alpha\theta} + C_5e^{-(\frac{1}{3}+\delta)\alpha\theta}$ and yields a solution

$$g = 2^{\pm i\frac{k_7}{k_8}}\left(\frac{\nu C_3}{k_7}\right)^{\pm i\frac{k_7}{2k_8}} e^{\pm i\theta}\,, \quad U = 2^{-2\mp i\frac{k_7}{2k_8}}\left(\frac{k_7}{k_8}\right)^2 C_3\left(\frac{\nu C_3}{k_7}\right)^{\mp i\frac{k_7}{2k_8}} e^{(\mp i+\frac{2k_8}{k_7})\theta}\,,$$
$$f = C_6\eta^{\mp i\frac{k_8}{k_7}} \quad \text{and} \quad p = C_8\,.$$

Thirdly, trying an ansatz of

$$g = Ae^{\alpha\theta}\,, \quad U = \frac{C_3}{27A\alpha^3}e^{2\alpha\theta} + \frac{1}{A}(C_4\theta + C_5)e^{-\alpha\theta} \quad \text{and} \quad f = C_6\eta^k$$

does not yield any new solutions with all the constants non-zero.

6.6.3 Two conditions on f for a specific relationship between g and U.

It is clear from solutions (6.6.43) and (6.6.44) that with

$$g = Ae^{\pm i\theta} \quad \text{and} \quad U = C_5e^{\mp i\theta}$$

f is not restricted to a single term in η. This arises due to the fact that the exponent in U is the negative of the exponent in g.
So if

$$g = Ae^{\alpha\theta} \quad \text{and} \quad U = C_5e^{-\alpha\theta} \tag{6.6.45}$$

is substituted into (6.2.6a) and (6.2.6b) and integrated, the two expressions for p are

$$p_1 = \frac{(1+\alpha^2)C_5\rho e^{-2\alpha\theta}}{A}\Big(AC_5\int\frac{f'^2}{\eta}d\eta - \alpha\nu\bigg(\int\frac{f'}{\eta^2}d\eta + 3\int\frac{f''}{\eta}d\eta + f''\bigg)\Big), \tag{6.6.46a}$$

$$p_2 = \frac{(1+\alpha^2)C_5\nu\rho e^{-2\alpha\theta}}{2A\alpha}\Big(-\frac{f'}{\eta} + f'' + \eta f'''\Big). \tag{6.6.46b}$$

Comparing (6.6.46a) to (6.6.46b), the first term inside the brackets for p_1 is conspicuously the only term not explicitly multiplied by ν. Thus if I assume that the coefficient of this term is proportional to ν, that is

$$C_5A = \beta\nu, \tag{6.6.47}$$

the two terms inside the brackets can then be equated. Differentiating with respect to η, then either $\alpha^2+1=0$ or

$$\frac{1}{\alpha}\left(\eta^2\frac{d^4f}{d\eta^4}+2(\alpha^2+1)\eta\frac{d^3f}{d\eta^3}+(6\alpha^2-1)\frac{d^2f}{d\eta^2}-2\alpha\beta\Big(\frac{df}{d\eta}\Big)^2+(2\alpha^2+1)\frac{1}{\eta}\frac{df}{d\eta}\right)=0. \tag{6.6.48}$$

Assuming that $\alpha\neq 0$, multiplying (6.6.48) by $\alpha\eta^2$ gives

$$\eta^4\frac{d^4f}{d\eta^4}+2(\alpha^2+1)\eta^3\frac{d^3f}{d\eta^3}+(6\alpha^2-1)\eta^2\frac{d^2f}{d\eta^2}-2\alpha\beta\Big(\eta\frac{df}{d\eta}\Big)^2+(2\alpha^2+1)\eta\frac{df}{d\eta}=0. \tag{6.6.49}$$

With the substitution $\eta=e^z$, (6.6.49) becomes

$$\frac{d^4f}{dz^4}+2(\alpha^2-2)\frac{d^3f}{dz^3}+4\frac{d^2f}{dz^2}-2\alpha\beta\Big(\frac{df}{dz}\Big)^2=0,$$

and with the substitution $Y=\frac{df}{dz}$,

$$\frac{d^3Y}{dz^3}+2(\alpha^2-2)\frac{d^2Y}{dz^2}+4\frac{dY}{dz}-2\alpha\beta Y^2=0. \tag{6.6.50}$$

If I let $\alpha=\gamma+i\delta$, (6.6.50) is split into two differential equations, corresponding to the real part

$$\frac{d^3Y}{dz^3}+\Big(2(\gamma^2-\delta^2)-4\Big)\frac{d^2Y}{dz^2}+4\frac{dY}{dz}-2\gamma\beta Y^2=0 \tag{6.6.51}$$

and the imaginary part

$$\frac{d^2Y}{dz^2}-\frac{\beta}{\gamma}Y^2=0, \tag{6.6.52}$$

if we assume that β is a non-zero real variable. This is a reasonable assumption, because once α is complex, A becomes the amplitude of the sinusoidal term for the boundary layer width g, and similarly C_5 is the amplitude for the sinusoidal term for the speed external to the boundary layer, U. With the viscosity being a measurable real quantity, thus every term in (6.6.47) is real.

Equation (6.6.52) is the Emden-Fowler equation (2.5.24) with $n=0$, has two symmetries and can be reduced to quadrature thus

$$z=\int\frac{dY}{\sqrt{\frac{2\beta}{3\gamma}Y^3-2C_1}}. \tag{6.6.53}$$

Substituting (6.6.53) into (6.6.51) will give the relationship between δ and $\frac{\beta}{\gamma}$. Also, obtaining an expression for Y in terms of z and thus $f(\eta)$ from (6.6.53) would then allow the corresponding expression for $p(\theta, \eta)$ from (6.6.46a) and (6.6.46b) to be found.

So the choice of (6.6.45) for U and g ensures that the PDE becomes an ODE for $f(\eta)$ and so we have a similarity solution of the equations (6.2.6a) and (6.2.6b). A dimensional analysis argument was not used, so this solution is a self-similar solution of the second kind.

6.7 The relationship between the similarity solutions and the corresponding physical solutions

The similarity solutions found in the previous section can be used to construct physical solutions. The complexity of this process will depend upon the Reynolds number of the flow in question. The general idea here is that the similarity solution found is a solution to the 2-D Navier-Stokes equations in the boundary layer. The term *boundary layer* has a physical meaning in that it can be actually observed as the region in a flow close to a boundary. However, in what follows a definition more relevant to the governing differential equations is required. The boundary layer is the region in which the external inviscid fluid flow adjusts to the presence of the boundary in order that the zero velocity (or no-slip) boundary condition be satisfied. I extend this idea to a zero velocity streamline, in that a boundary layer will exist in the vicinity of such a streamline, and the external inviscid flow will adjust across this boundary layer to meet this zero velocity condition. I therefore assert that a solid

object in a 2-D flow with attached vortices can be treated as a solid object whose shape is described by the surfaces of the original object and the zero velocity streamlines that are adjacent to the external fluid flow, provided that these surfaces and streamlines together form a closed loop. Further I assert that this curve will be continuous, but not necessarily smooth.

In the following sub-sections I will consider 2-D flow past a circular cylinder, beginning with low Reynolds number flow. For flow past a 2-D circular cylinder, the width of the boundary layer is now given by

$$g = Ae^{\gamma\theta}e^{i\delta\theta} \tag{6.7.54}$$

and so if the term A is thought of as the amplitude, then the term $Ae^{\gamma\theta}$ can be described as the envelope for the sinusoidal function $e^{i\delta\theta}$.

The separation point θ_{sp} , if it occurs, is determined by the condition

$$\sin\delta\theta = 0 \quad \text{and thus} \quad \theta_{sp} = \frac{\pi}{\delta}\,.$$

The range of values of δ for which this expression is meaningful will be explored in the following sub-sections. The magnitude of δ will have a significant effect on the nature of the flow in the wake of the cylinder.

From this point until the end of the chapter, I will use a nomenclature inspired by the system used by [63] to explain the boundary layer flow before the separation point, because it can logically be extended to describe the flow after the separation point. We can assume that the fluid is inviscid and irrotational before it encounters the cylinder, and I will name this region 1. The curve $g(\theta)$ given by (6.7.54), for $0 \leq \theta \leq \theta_{sp}$ defines a region of viscous rotational fluid flow, and corresponds to the viscous sublayer of the triple deck theory described in Chapter 1. When the fluid that flows through the viscous sublayer (region 2) leaves the region it will enter an inviscid region, just before, to just

after the separation point, however the fluid will retain the vorticity it acquired in the previous region. This is region 3, which corresponds to the main deck in the triple deck theory. Fluid moving past the cylinder that does not travel through region 2 will remain inviscid and irrotational, and thus remains in region 1. This region corresponds to the upper deck in the triple deck theory.

6.7.1 Stokes Flow

Stokes flow, creeping flow of low Reynolds number hydrodynamics refers to the situation where fluid flowing past the 2-D circular cylinder does not separate from the wall until it reaches the rear stagnation point. The boundary layer $g(\theta)$ will not separate iff $\delta < 1$. The triple deck theory referenced in Chapter 1 was devised as a way of matching the external (region 1) flow, which satisfies the boundary condition at infinity with the boundary layer flow, which satisfies the boundary condition at the wall. In this chapter, I have found a solution to the Navier-Stokes equations in the boundary layer which satisfies the boundary conditions at the wall and at the edge of the boundary layer. In this section, I will outline how this solution can be matched to the solution in region 1, and in so doing create a procedure in which physically realizable exact solutions can be constructed. Stokes flow is the simplest situation in which this can be done, and so is a logical place to begin. Fluid flows with a higher Reynolds number, where the flow separates from the cylinder, is a more complicated situation, and I will address these situations in subsequent sections.

The streamlines in region 1 are given by the stream function (2.4.16). The components of the fluid velocity are given by (2.4.17), while the pressure at any point can be determined by (2.4.15). Let $Ai = g_0$ and $C_5 i = U_0$ and

$\alpha = \gamma + i\delta$. Then (6.6.45) becomes

$$g = g_0 e^{\gamma\theta}\sin\delta\theta - ig_0 e^{\gamma\theta}\cos\delta\theta \quad \text{and} \quad U_2 = -U_0 e^{-\gamma\theta}\sin\delta\theta - iU_0 e^{-\gamma\theta}\cos\delta\theta,$$

where the subscript for U_2 denotes the function U from (6.6.45) in region 2. The boundary between region 1 and region 2 is given by $g(\theta)$ for $0 \le \theta \le \frac{\pi}{2\delta}$. Let the two endpoints of this boundary be denoted O at the forward stagnation point ($\theta = 0$) and P, given by

$$\theta = \frac{\pi}{2\delta} \quad \text{and} \quad r = a + g_0 e^{\frac{\gamma\pi}{2\delta}} \quad \text{and} \quad U_2 = -U_0 e^{-\frac{\gamma\pi}{2\delta}}, \tag{6.7.55}$$

where r is given by the radius of the cylinder plus the width of the boundary layer g, and U_2 is the fluid speed on the boundary of the viscous sublayer at P. The next step is to find the fluid speed U_1 at P according to the solution to Euler's equations, for region 1. The subscript for U_1 denotes that this function represents the fluid speed in region 1. Using (2.4.17),

$$U_1^2 = U^2\left(1 - \frac{2a^2}{r^2}\cos 2\theta + \frac{a^4}{r^4}\right),$$

and evaluating U_1^2 at P,

$$U_1^2 = U^2\left(\frac{(a + g_0 e^{\frac{\gamma\pi}{2\delta}})^4 - 2a^2\cos\left(\frac{\pi}{\delta}\right)(a + g_0 e^{\frac{\gamma\pi}{2\delta}})^2 + a^4}{(a + g_0 e^{\frac{\gamma\pi}{2\delta}})^4}\right),$$

while U_2^2 at P is

$$U_2^2 = U_0^2 e^{-\frac{\gamma\pi}{\delta}}.$$

Equating U_1^2 and U_2^2 at P, and letting

$$g_0 = L_T a e^{-\frac{\gamma\pi}{2\delta}} \quad \text{and} \quad U_0 = U_T U e^{\frac{\gamma\pi}{2\delta}} \tag{6.7.56}$$

yields,

$$U_T^2 U^2 a^4 (1 + L_T)^4 = U^2\Bigg(2a^4(1 - \cos\left(\frac{\pi}{\delta}\right)) + 4a^4 L_T(1 - \cos\left(\frac{\pi}{\delta}\right)) + 6a^4 L_T^2(1 - \frac{1}{3}\cos\left(\frac{\pi}{\delta}\right)) + 4a^4 L_T^3 + a^4 L_T^4\Bigg).$$

Canceling the common factor $U^2 a^4$ gives

Proposition 12

$$1 - 2\cos\left(\frac{\pi}{\delta}\right)(1+L_T)^2 + (1-U_T^2)(1+L_T)^4 = 0\,, \tag{6.7.57}$$

the relationship between δ (which will be a function of Re) and L_T and U_T (defined by (2.4.21)*).*

So for Stokes flow past a circular cylinder,

$$\frac{1}{2} < \delta < 1 \quad \text{which leads to} \quad -1 < \cos\left(\frac{\pi}{\delta}\right) < 1\,,$$

because the point P occurs in the range $\frac{\pi}{2} < \theta < \pi$. For $\delta < \frac{1}{2}$, the point P occurs at $\theta > \pi$, which is outside of the domain of the physical flow. This then gives rise to a complication in the matching process described above. If we choose a point P' with $\theta = \pi$ and $\delta < \frac{1}{2}$, then the expressions for g and U_2 at this point are now complex. The real value for U_1^2 is equated to the real part of U_2^2. When the point P occurs at $\theta > \pi$, then a value for $\theta < \frac{\pi}{2\delta}$ must be selected, such as $\frac{\pi}{3\delta}$, $\frac{\pi}{4\delta}$ or $\frac{\pi}{6\delta}$, which give slightly less cumbersome expressions to work with than other values, in the algebra that follows.

Proposition 13 *When $\frac{1}{2} < \delta < 1$, a choice of two expressions for θ in terms of δ will yield an expression for $\frac{\gamma}{\delta}$ in terms of the constants U_T and L_T.*

Consider the point P, with $\theta = \frac{\pi}{2\delta}$ defined above, and another point Q on the boundary between regions 1 and 2, with $\theta = \frac{\pi}{4\delta}$. U_2 is complex at Q, and so we require that U_1^2 is equal to the real part of U_2^2 at this point. This yields

$$1 - 2\cos(2\theta)(1+V\sin(\delta\theta))^2 + (1-W^2\cos(2\delta\theta))(1+V\sin(\delta\theta))^4 = 0\,, \tag{6.7.58}$$

where

$$V = L_T e^{-\frac{\gamma}{2\delta}(\pi - 2\delta\theta)} \quad \text{and} \quad W = U_T e^{\frac{\gamma}{2\delta}(\pi - 2\delta\theta)}\,,$$

for a general value of θ. Evaluating (6.7.58) at Q gives

$$\cos\left(\frac{\pi}{2\delta}\right) = \left(1 + \frac{\sqrt{2}}{2}V_0\right)^2 + \left(1 + \frac{\sqrt{2}}{2}V_0\right)^{-2} \quad \text{where} \quad V_0 = L_T e^{-\frac{\gamma\pi}{4\delta}}\,.$$

Using the double angle formula and substituting for $\cos(\frac{\pi}{2\delta})$ in (6.7.57) and then solving for $\frac{\gamma}{\delta}$ yields

$$\frac{\gamma}{\delta} = -\frac{4}{\pi}\ln\left(\frac{V_1}{L_T}\right) \tag{6.7.59}$$

where

$$V_1 = \sqrt{2}\left(\pm\sqrt[4]{\left(\frac{Y-1}{4}\right)\pm\sqrt{\left(\frac{Y-1}{4}\right)^2-1}}-1\right)$$

where $V_1 > 0$ and the coefficient of the fourth root can also be $\pm i$, and

$$Y = \frac{1+(1-U_T^2)(1+L_T)^4}{2(1+L_T)^2}$$

with $U_T > 0$ and $L_T > 0$.

Theorem 10 *The Reynolds number in the boundary layer, from* (6.6.47)*, is*

$$Re = -\frac{\beta}{\gamma} = -\frac{\beta}{\nu_T}\,.$$

Substituting (6.7.56) into (6.7.55), then at P,

$$U_2 = U_T U \quad \text{and} \quad r = a(1+L_T)\,.$$

Also

$$g_0 U_0 = L_T U_T a U \quad \text{with} \quad Re = \frac{aU}{\nu}$$

and

$$g_0 U_0 = (Ai)(C_5 i) = -AC_5 = -\beta\nu$$

from (6.6.47). Equating these two expressions for g_0U_0, and using (2.4.21) gives the required expression for Re. ■

Equation (6.6.52) now is

$$\frac{d^2Y}{dz^2} + ReY^2 = 0\,,$$

equation (6.6.51) becomes

$$\frac{d^3Y}{dz^3} + \Big(2(\gamma^2 - \delta^2) - 4\Big)\frac{d^2Y}{dz^2} + 4\frac{dY}{dz} + 2\gamma^2 ReY^2 = 0$$

and $\gamma = L_T U_T$. Substituting this expression for γ into (6.7.59), we can solve for δ. Alternatively we can solve for δ from (6.7.57).

In addition to equating the speed at P, the pressure at P, which I will name p_P must also be matched in the following manner. Once f has been calculated, p_{P2} can be calculated from (6.6.46a) and (6.6.46b). The pressure from region 1, p_{P1} is calculated from (2.4.15), by considering the streamline that passes through P, from infinity in front of the cylinder. Hence

$$p_{P1} = p_\infty + \frac{1}{2}\rho U^2(1 - U_T^2)\,. \tag{6.7.60}$$

A plot of the viscous sublayer for an example of a Stokes flow is in Figure 6.1. The flow is symmetrical about the horizontal axis, and separates from the cylinder at the rear stagnation point. The streamline pattern is also symmetrical about the vertical axis.

The appearance of a in the expression for g_0 and U in the expression for U_0 confirms that a is the best choice for the characteristic length and U is the best choice for the characteristic speed for the 2-D Stokes flow past a circular cylinder. Hence these equations can now be made dimensionless with these variables.

Conjecture 1 *The four dimensionless parameters Re, δ and L_T and U_T in conjunction with the solution* (6.6.53)*,* (6.6.45) *and* (6.6.46a) *or* (6.6.46b) *determine all possible behaviour for this system. Any observed behaviour will correspond to a value for each of these four variables.*

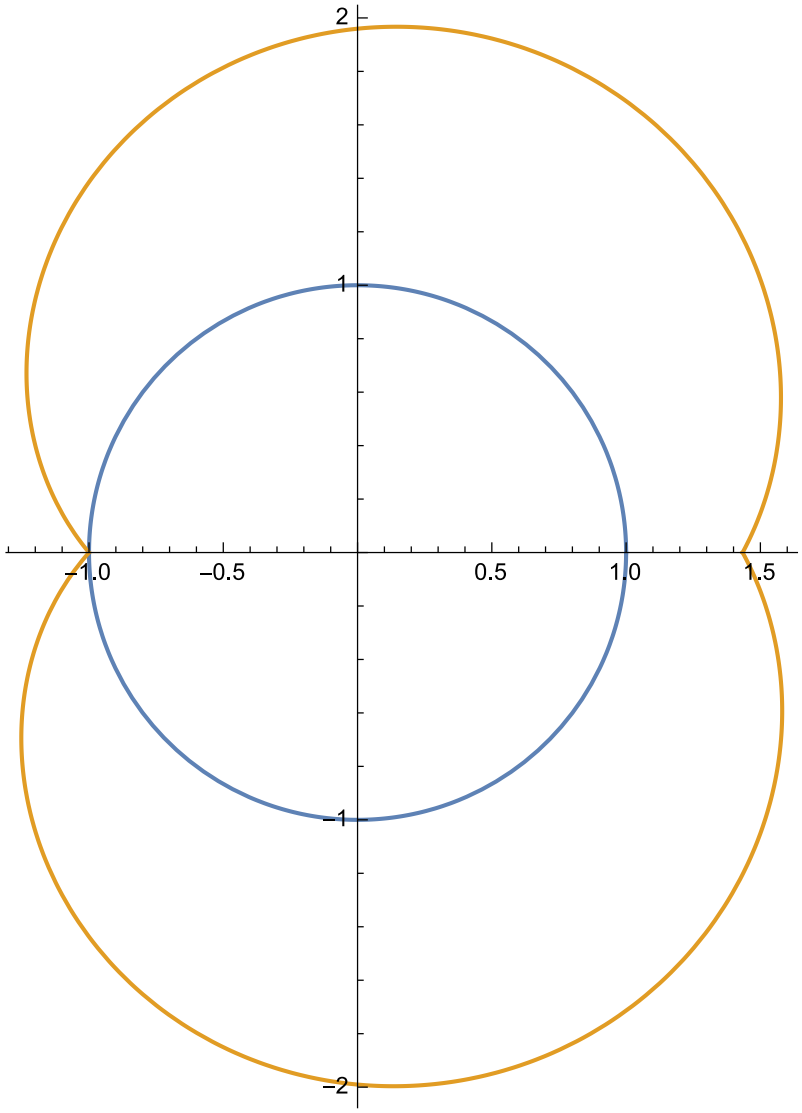

Figure 6.1: A sketch of the 2-D viscous fluid flow past a circular cylinder for a Reynolds number such that there is no separation point, with the direction of fluid flow horizontal from left to right, and the external edge of region 2 in orange.

For each Reynolds number there is a solution from (6.6.53) for the velocity profile $f(\eta)$ in the boundary layer. Substituting this into (6.6.51) gives γ and δ, while substituting into (6.6.46a) and (6.6.46b) will determine U_T from (6.7.60), and thus L_T.

The magnitude of γ determines how large the envelope of the viscous sublayer (region 2) has grown to (for positive values) at the back of the cylinder. The width of the boundary layer is determined by L_T, because L_T is the maximum width of the viscous sublayer, which is carried through to region 3 by the fluid flow, and so L_T is also the width of the main deck. This width will increase as the fluid moves downstream from the cylinder due to diffusion of the vorticity in the boundary layer.

Conjecture 2 *The quantity $U(\theta)g(\theta)$ is a conserved quantity along the entire outer edge of each viscous sublayer and therefore the eddy or turbulent viscosity $\nu_T = L_T U_T$ is a conserved quantity for the solution found in this chapter, and in addition to this I think that it is a conserved quantity for turbulent flows more generally, and so this concept will have a wide range of applications.*

The solution (6.6.45) in this chapter significantly was found when

$$U(\theta)g(\theta) = C_5 A = \nu_T U a \quad \text{or} \quad \bar{U}(\theta)\bar{g}(\theta) = L_T U_T$$

An extension of this idea will be applied to the other versions of the Navier-Stokes equations mentioned in the next sections, that is the 2-D time dependent equations, and the 3-D equations. This system as a whole clearly is not conservative, however, outside of the viscous sub-layers (region 2, and potentially other regions when the flow separates from the cylinder), in some sense the system is conservative. The value of this conserved quantity will in fact be different for each viscous sublayer. The characteristic length L_T will presumably

decrease from one region to the next, due to the viscous dissipation of energy that occurs in the viscous sublayer.

The stream function (6.2.1) now becomes

$$\psi = AC_5 f(\eta), \quad \text{where} \quad \eta = \frac{re^{-\alpha\theta}}{A}\,.$$

The velocity potential ϕ only exists if $\nabla \times \mathbf{u} = \mathbf{0}$. The vorticity in region 2 has a greater effect on fluid closer to the boundary, and it would be useful to quantify the reduction in displacement on each streamline relative to what is expected for the corresponding irrotational flow.

The solution found here may be able to be used to model steady-state low Re vortices more generally. The core of the vortex being a boundary layer, as the speed of the fluid changes from zero at the centre of the vortex to the external speed outside of the vortex.

6.7.2 Steady 2-D Laminar flow

For $\delta > 1$, the flow separates from the cylinder, and as δ increases, θ_{sp} decreases monotonically. This continues until δ reaches a value where the flow becomes unsteady, at $Re \sim 47$ according to [49]. There are two aspects of the flow that need to be determined; the streamlines and the fluid speed at each point on each streamline.

For Stokes flow, the pattern of streamlines is the same as the 2-D irrotational flow (2.4.16), while the fluid speed in region 2 will be determined for a given value of θ by using the solution for the velocity profile f, with the speed at the edge of the boundary layer given by the square root of the real part of $U_2^2(\theta)$. The fluid that flows through region 2 flows into region 3 with the same

speed as the corresponding irrotational flow, but with some vorticity. That is, a small blob of fluid that has moved through region 2 remains on the same streamline as the corresponding irrotational flow, but is not as far along the streamline.

For a steady 2-D laminar flow, the flow separates from the cylinder at θ_{sp}, and thus the pattern of streamlines changes accordingly. As described above, two attached vortices will form at the rear of the cylinder, above and below the axis of symmetry parallel to the direction of fluid flow at infinity. Each vortex is enclosed by a zero velocity streamline, given by the surface of the cylinder, the axis of symmetry joining the rear stagnation point and another point known as the wake stagnation point, and a curve joining this point and the separation point determined by $g(\theta)$. In this manner, the cylinder and the two attached vortices form a closed loop. To find the streamline pattern around this loop, a conformal mapping of a circle of radius a to this closed loop can be calculated, which maps the streamline pattern for the irrotational flow to the required pattern for the 2-D steady laminar flow. The function $g(\theta)$ describes the extent of the viscous sublayer, in that for

$$0 < \theta < \theta_{sp}\,, \quad g(\theta) > 0,$$

and this represents the boundary of region 2 adjacent to regions 1 and 3. If we consider $r = a + g(\theta)$ for $0 < \theta < \theta_{sp}$ then $r = a$ represents the boundary of the cylinder with region 2. For $\theta_{sp} < \theta < \pi$, the curve enclosing the attached vortex is given by

$$r = a + |g(\theta)|, \quad \text{or} \quad r = a - g(\theta)$$

because g is negative for these values of θ. One way to visualize this is to consider the curve $y = g(\theta)$ (Figure 6.2) where the curve $y = 0$ represents

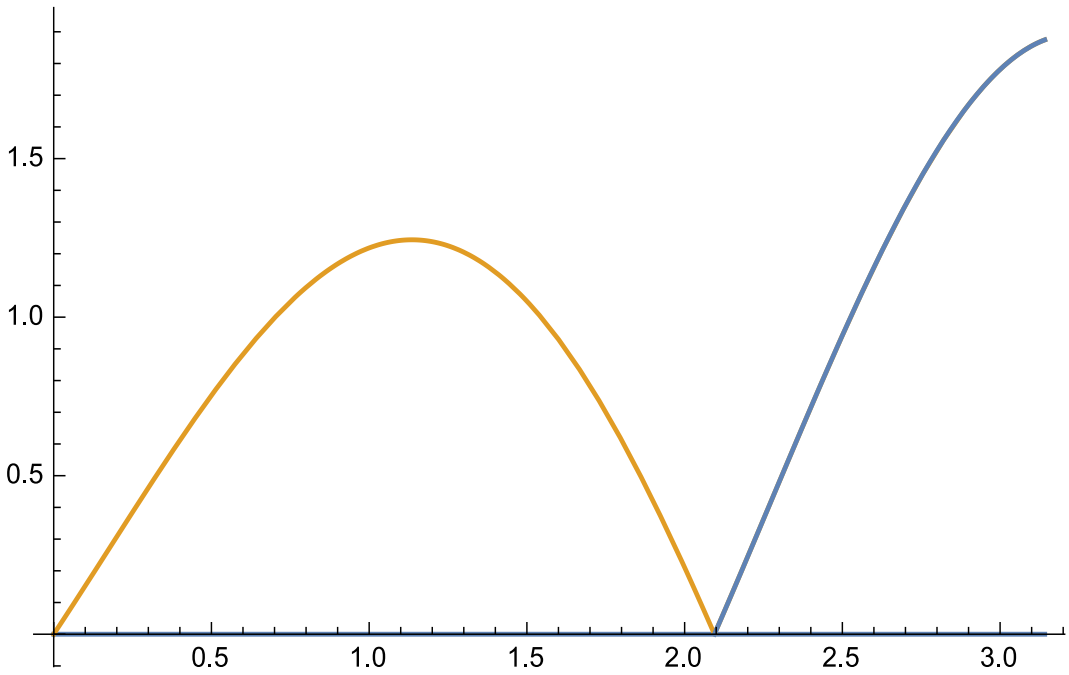

Figure 6.2: The viscous sublayer $g(\theta)$ with separation point $\theta_{sp} = \frac{2\pi}{3}$ shown in Cartesian coordinates. The edge of the viscous sublayer is shown in orange, while the zero velocity streamlines are in blue.

a zero velocity streamline on the surface of the cylinder which separates at $\theta = \theta_{sp}$ and encloses the vortex for $\theta_{sp} < \theta < \pi$. Then $g(\theta)$ will be on the surface of the cylinder for $\theta_{sp} < \theta < \pi$. I will name the enclosed vortex region 4. The streamline pattern and fluid speed need to be determined in this region. It is not clear yet what method is the most suitable to solve this problem, whether the transformation (6.2.1) can be used, or if another transformation is more appropriate.

Once the streamline pattern has been determined outside of the closed loop, the speed on each streamline within region 2 is determined using the same method as described above for the Stokes flow. That is, the inviscid flow around the closed loop determines $U_1(\theta)$, which is matched to $U_2(\theta)$, from the

viscous sublayer. Next, a second boundary layer is created for the vicinity of the zero velocity streamline enclosing region 4. A similar method will be used to determine the region adjacent to this new boundary where the fluid speed is adjusted to meet the zero velocity boundary condition. That is, there will be a second viscous sublayer, which I will name region 5. It is not clear at this stage for which values of δ that this second boundary layer will remain attached to the zero velocity streamline all the way to the axis of symmetry, and for which values of δ it will separate, creating a third (and perhaps more) viscous sublayer.

Figure 6.3 shows a plot of an example of a steady 2-D laminar flow, showing the viscous sublayer and attached vortices at the rear of the cylinder. The flow is divided into three distinct domains: the two attached vortices, and the third domain bounded by the surface of the cylinder, and the sinusoidal shapes with the increasing amplitude envelope which defines the extent of the two vortices. This plot and Figures 6.1 and 6.2 are only qualitative visualizations of the solution, presented here for the reader's benefit. The actual values of Re, δ and L_T and U_T are needed for a more precise representation of what a particular flow will look like.

The boundary of the viscous sublayer (region 1) is given by $g(\theta)$. For Stokes flow, C_D can be determined by integrating over this region. When the flow separates, another one or more viscous sublayers are created. If the function corresponding to $g(\theta)$ can be found for each viscous sublayer, then integration over each region to determine C_D may be possible. Subsequently a determination of how these structures change as Re changes is required to determine the relationship between C_D and Re over a range of values for Re.

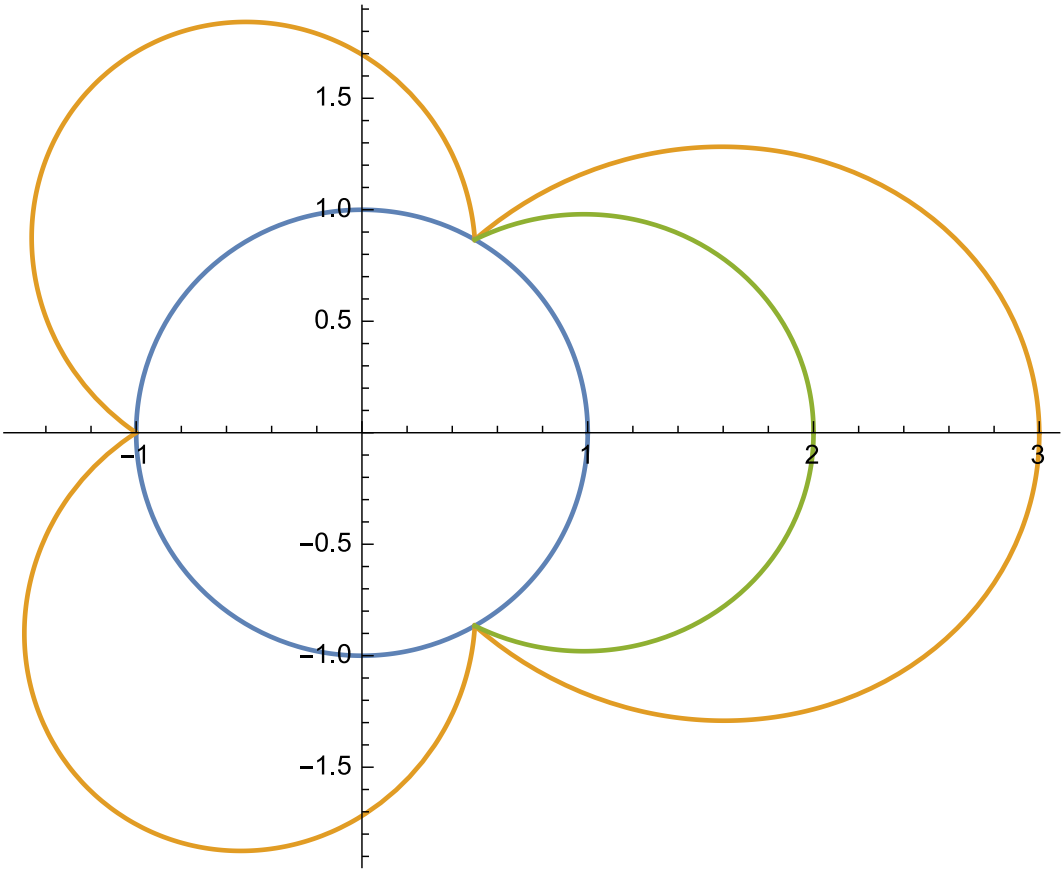

Figure 6.3: A sketch of the 2-D laminar fluid flow past a circular cylinder with the separation point at $\frac{2\pi}{3}$ from the forward stagnation point, with the direction of fluid flow horizontal from left to right, the external edge of region 2 in orange; top left, zero velocity streamlines in green (and from 1 to 2 on the horizontal axis) marking the edge of region 4, the edge of region 5 in orange; top right and the cylinder in blue.

6.7.3 Fluid flows for higher Reynolds numbers

As discussed in Chapter 1, the nature of the flow changes at $Re \sim 47$ to an unsteady 2-D flow, and the solution found in this thesis can no longer be used. However, the method used to find the 2-D steady state similarity solution is likely to be useful in finding the 2-D time dependent similarity solution. The process described in the previous section will need to be adapted to the time dependent situation to find the physically realizable solutions. The Strouhal number now becomes relevant, and it is likely that it will appear as a parameter in the relevant differential equation. C_D will be time dependent, and thus the size, shape and location of the viscous sublayers may all be time dependent. Similarly, this method with appropriate adaptation will be applied to the 3-D case.

The method described in this chapter has been successfully used to find a new similarity solution to the 2-D incompressible steady-state Navier-Stokes equations.

Conjecture 3 *The similarity solutions to the 2-D incompressible steady-state Navier-Stokes equations found in this chapter are the only physically realizable solutions obtainable with the transformation* (6.2.1).

What remains to be done here to prove this conjecture is an investigation of possible solutions with two or more terms for $g(\theta)$. This method (of searching for solutions) could be applied to the Navier-Stokes equations in both 2-D and 3-D, for all the known transformations that admit a similarity solution, to prove that no more solutions exist for each transformation. Also, this method may be able to find new solutions in the 3-D case.

Discussion The shape of the yarn balloon, and thus the orientation of the yarn element to the oncoming air flow presents horizontal cross-sections which are ellipses in a range of orientations. The relationship between C_D and Re will be determined by integrating over each of the viscous sub-layers. If this can be done, then what remains to be done is to determine how C_D changes when mapping from the fluid flow past a circular cylinder to fluid flow past an elliptical cylinder for the range of orientations of the cylinder to the direction of the fluid flow.

Future Work The method created in this chapter has significant potential to find more new similarity solutions to the 2-D or 3-D Navier-Stokes equations, as well as other partial differential equations. The method is not fully algorithmic, but is systematic, and may require some intuition as demonstrated in this chapter. For the 2-D and 3-D boundary layer flows discussed above, the starting point will be to consider the conserved quantity Ug, and generalizing the concept as required.

The relationship between δ and the Reynolds number remains to be found, although it is likely to come from (6.6.51), once the solutions for $f(\eta)$ are found from (6.6.52). This would then lead to an exact expression for the separation point in terms of the Reynolds number for the 2-D steady state range.

Concluding Remarks The solution to the Navier-Stokes equations found in Chapter 6 appears to be a self-similar solution of the second kind. Different versions of the Navier-Stokes equations govern different ranges of values for Re, based upon experimental observations, confirmed by numerical simulations of the appropriate version of the Navier-Stokes equations. These simulations have led to numerical formulae for the relationship between θ_{sp} and Re, valid for a specific range of values for Re [49]. It seems reasonable to expect that for

the same range of values, there will be a relationship between C_D and Re and the exact solution to the relevant version of the Navier-Stokes equations will be pivotal if the exact relationship is to be found. If the relationship between C_D and Re is to be found for any range of values for Re, it will enable a more accurate air drag term for the yarn balloon equations to be found. In addition it will likely lead to new models for air drag in many other applications.

Chapter 7

Conclusion

This thesis brings together three distinct areas of study in mathematics. The first being the mathematical modelling of yarn spinning devices used in the textile manufacturing industry, while the second is the modelling of fluid flow past a circular cylinder, a classical problem in fluid dynamics. The pertinent connection between these two areas is that the drag force created by the fluid flow past the cylinder is a crucial part in the dynamical model of how yarn behaves in these devices. The third area is differential geometry, which is used to express the yarn balloon model in intrinsic coordinates, which is a more suitable coordinate system than has ever been used for this model before.

In all recent modelling of these devices, the coefficient of the drag force term, C_D was assumed to be equal to 1, along the entire length of the yarn balloon, based on experimental data reproduced in [2], [33], [60], [30] etc, which demonstrates that C_D is in fact a function of the Reynolds number, Re, so the assumption that C_D is constant is only valid for large values of Re in typical yarn balloons. According to Batra & Fraser [2], in the yarn spinning processes modelled in this thesis, the highest values of Re typically reached are $O(10^3 - 10^4)$. Given the typical shape of a yarn balloon, found numerically

in [2], [7] etc, it is clear that Re will be small where the yarn passes through the guide-eye, and will increase to its maximum value when the radius of the yarn balloon is maximum. Thus C_D will be larger near the guide-eye than the Padfield model has accounted for. This is one factor that motivates the current efforts described in this thesis to improve the mathematical model for these devices.

Another factor is what effect the shape and smoothness of the yarn itself has on the shape of the yarn balloon. The analysis carried out in Chapter 4, in which the yarn balloon equations are cast in a new frame of reference S', using the method established in Chapter 3, lays the foundation for multi-ply and hairy yarns to be modelled more accurately when a more accurate expression for the air drag term is found.

In Chapter 6, a new similarity solution of the 2-D incompressible steady state Navier-Stokes equations is found for fluid flow past a circular cylinder. This solution is shown to be physically realizable for laminar flows corresponds to Reynolds number in the range $0 < Re \leq 6.29$. For the range $6.29 \leq Re \leq 47$ I have outlined a process in which I believe this similarity solution can be used to find a physically realizable solution. These solutions can then be used to find the relationship between C_D and Re in this range. For $47 < Re < 190$, the flow becomes unsteady, and I expect that the method used in this thesis to find the similarity solution for the 2-D steady state case will also be applicable in finding a similarity solution in the 2-D unsteady state case, with the goal of constructing physically realizable solutions, and then attempting to use this solution to find the corresponding relationship between C_D and Re. The method will also be applied to the 3-D case, for $Re > 190$. If this method is successful in finding a physically realizable solution in the 3-D case,

notwithstanding the many other applications this result could be applied to, I would then be able to find expressions for C_D in terms of Re across the entire range for Re relevant to the yarn balloon problem. On the other hand, if this is not possible with this method, and I am only able to find the relationship between C_D and Re for the 2-D flow ranges, then I could still use the original assumption, $C_D = 1$ for $Re > 190$, and this would be reasonable, and certainly an improvement on the current model because at $Re = 190, 1 < C_D < 2$. With these expressions for C_D, the drag on each infinitesimal section of the yarn balloon can be found by dividing the balloon up into thin horizontal slices, and considering the relevant 2-D flow and corresponding value for C_D on each one. The process described in section 5.5 will translate the expressions found for C_D for flow past a circular cylinder into expressions for the drag force on the infinitesimal yarn element, which is used with the framework found in Chapter 4 to establish new differential equations for the yarn balloon model. These equations will then be solved for the parameter spaces described in [2], with the objective of further optimization of the system.

The fact that the 3-D solution transitions to turbulence in the wake of the cylinder at $Re \sim 1200$, and thus some yarn balloon configurations will generate a turbulent wake will also need to be considered. The yarn spinning devices being modelled in this thesis are operated in large arrays of identical devices, in close proximity to one another, often separated by a vertical panel or guard. How the turbulent air generated by these devices interact with these panels or guards may in fact determine whether the yarn balloon is moving through still or turbulent air, and thus what the drag coefficient C_D is. The first step would be to determine the magnitude of the effect of this phenomenon on the shape of the yarn balloon. Further work in this direction may be from the

perspective of productivity of the overall system. Are there optimal values of the rotational speed of the device, coupled with the design of the device and the region around the device, considering the behaviour of the air around the device, that optimizes the throughput and the quality of the yarn produced.

All the relevant calculations arising from the similarity solution found in this thesis have not yet been done, due to the necessity of the timely submission of this thesis, thus I cannot be categorically certain yet that the solution is a physically realizable solution. However, I am confident that it is, for the following reasons. Firstly, for Stokes flow, I match a solution that satisfies the required boundary conditions on the boundary of the cylinder and at the edge of the boundary layer with a solution that satisfies the boundary conditions at infinity, meaning that I have found a flow that satisfies the relevant differential equation over the whole domain, and satisfies all the boundary conditions of this domain. Secondly, the solution is qualitatively in agreement with the triple deck theory described in [63] for the flow in the vicinity of the separation point. Thirdly, the plots of the solution for a Stokes flow in Figure 6.1 and for a 2-D steady laminar flow in Figure 6.3 are qualitatively similar to the photographs reproduced in Plate 1 of [33], and flow visualization pictures in [65] for 2-D steady flow past a circular cylinder. The procedure devised in section 6.7.1 leading to (6.7.57) provides a relationship between the characteristic length and the characteristic velocity which may be able to be tested experimentally. When all relevant calculations have been carried out, I expect to have exact values for Re_s, the value of the Reynolds number for the onset of flow separation, and the Reynolds number for which the 2-D laminar flow becomes unsteady.

Appendix A

Darboux frame field and connection forms

From the definition (2.2.9) of the Darboux frame, with the expressions for $\mathbf{T}$, $\mathbf{U}$ and $\mathbf{V}$,

$$\begin{aligned}
\mathbf{T} &= ((r'\cos\theta - r\theta'\sin\theta), (r'\sin\theta + r\theta'\cos\theta), z'),\\
\mathbf{U} &= \frac{1}{\sqrt{r'^2 + z'^2}}(-z'\cos\theta, -z'\sin\theta, r'),\\
\mathbf{V} &= \frac{1}{\sqrt{r'^2 + z'^2}}\Big\{(-\sin\theta(r'^2 + z'^2) - rr'\theta'\cos\theta),\\
&\qquad (\cos\theta(r'^2 + z'^2) - rr'\theta'\sin\theta), -r\theta' z')\Big\},
\end{aligned}$$

k, t and g are

$$\begin{aligned}
k &= \frac{(-z'(r'' - r\theta'^2) + r'z'')}{\sqrt{r'^2 + z'^2}},\\
t &= \theta' z' - \frac{r\theta'(r'z'' - r''z')}{(r'^2 + z'^2)},\\
g &= \frac{(-rr'\theta'(r'' - r\theta'^2) + (r'^2 + z'^2)(2r'\theta' + r\theta'') - r\theta' z' z'')}{\sqrt{r'^2 + z'^2}}.
\end{aligned}$$

For the frame field $\mathbf{E}_1 = \mathbf{T}$, $\mathbf{E}_2 = \mathbf{V}$ and $\mathbf{E}_3 = \mathbf{U}$, the connection forms ω_{ij}

are

$$\omega_{11} = (r'^2 r'' + r\theta'^2)dr + r^2\theta'^2\theta''d\theta + z'^2 z''dz,$$

$$\omega_{22} = \omega_{11},$$

$$\omega_{33} = 0,$$

$$\omega_{12} = \left(\theta'\sqrt{r'^2+z'^2} - \frac{rr'^2r''\theta'}{\sqrt{r'^2+z'^2}}\right)dr + \left((r'+r\theta'\theta'')\sqrt{r'^2+z'^2} + \frac{r^2r'\theta'^2}{\sqrt{r'^2+z'^2}}\right)d\theta - \left(\frac{r\theta' z'^2 z''}{\sqrt{r'^2+z'^2}}\right)dz,$$

$$\omega_{21} = -\omega_{12},$$

$$\omega_{13} = \left(-\frac{r'r''z'}{\sqrt{r'^2+z'^2}}\right)dr + \left(\frac{r\theta' z'}{\sqrt{r'^2+z'^2}}\right)d\theta + \left(\frac{r'z'z''}{\sqrt{r'^2+z'^2}}\right)dz,$$

$$\omega_{31} = -\omega_{13},$$

$$\omega_{23} = \left(\frac{rr'r''\theta'z'}{(r'^2+z'^2)}\right)dr + z'd\theta - \left(\frac{rr'\theta'z'z''}{(r'^2+z'^2)}\right)dz,$$

$$\omega_{32} = -\omega_{23}.$$

The dual 1-forms are

$$\theta_1 = r'dr + r^2\theta'd\theta + z'dz,$$

$$\theta_2 = -\left(\frac{rr'\theta'}{\sqrt{r'^2+z'^2}}\right)dr + r\sqrt{r'^2+z'^2}d\theta - \left(\frac{r\theta'z'}{\sqrt{r'^2+z'^2}}\right)dz,$$

$$\theta_3 = -\left(\frac{z'}{\sqrt{r'^2+z'^2}}\right)dr + \left(\frac{r'}{\sqrt{r'^2+z'^2}}\right)dz.$$

Appendix B

Padfield's air drag term in intrinsic coordinates

In this section we represent the air drag term used in the Padfield model (2.3.10) in terms of the Frenet-Serret coordinates.

In dimensionless form, (2.3.11) becomes

$$\mathbf{v} = \mathbf{k} \wedge \mathbf{r} = r\mathbf{e}_\theta \,,$$

and (2.3.12) becomes

$$\mathbf{v_n} = \mathbf{T} \times \Big(r\mathbf{e}_\theta \times \mathbf{T} \Big),$$

which is

$$\mathbf{v_n} = \frac{r}{\kappa}(2r'\theta' + r\theta'')\mathbf{N} + \frac{r}{\kappa}(-r'z'' + r''z' - r\theta'^2 z')\mathbf{B}\,,$$

and so

$$|\mathbf{v_n}| = \frac{r}{\kappa}\sqrt{(2r'\theta' + r\theta'')^2 + (-r'z'' + r''z' - r\theta'^2 z')^2}\,.$$

Therefore the air drag term is given by

$$\mathbf{F} = -\frac{p_0 r^2}{16}\frac{\sqrt{(2r'\theta' + r\theta'')^2 + (-r'z'' + r''z' - r\theta'^2 z')^2}}{((r'' - r\theta'^2)^2 + (2r'\theta' + r\theta'')^2 + z''^2)} \left((2r'\theta' + r\theta'')\mathbf{N} + (-r'z'' + r''z' - r\theta'^2 z')\mathbf{B} \right).$$

Appendix C

$(\mathbf{u} \times \omega) \cdot (\nabla \times \omega)$ in 3-D Cartesian coordinates

In 3-D Cartesian coordinates,

$$\begin{aligned}(\mathbf{u} \times \omega) \cdot (\nabla \times \omega) = &-\mathbf{u} \cdot \nabla\Big(\frac{1}{2}\omega^2\Big) + (\nabla \cdot \mathbf{u})(\omega^2) \\ &+ \omega_x\Big(\frac{\partial u_x}{\partial x}\frac{\partial u_z}{\partial y} - \frac{\partial u_x}{\partial y}\frac{\partial u_z}{\partial x} + \frac{\partial u_x}{\partial z}\frac{\partial u_y}{\partial x} - \frac{\partial u_x}{\partial x}\frac{\partial u_y}{\partial z}\Big) \\ &+ \omega_y\Big(\frac{\partial u_x}{\partial z}\frac{\partial u_y}{\partial y} - \frac{\partial u_y}{\partial z}\frac{\partial u_x}{\partial y} + \frac{\partial u_z}{\partial y}\frac{\partial u_y}{\partial x} - \frac{\partial u_y}{\partial y}\frac{\partial u_z}{\partial x}\Big) \\ &+ \omega_z\Big(\frac{\partial u_y}{\partial x}\frac{\partial u_z}{\partial z} - \frac{\partial u_y}{\partial z}\frac{\partial u_z}{\partial x} + \frac{\partial u_z}{\partial y}\frac{\partial u_x}{\partial z} - \frac{\partial u_x}{\partial y}\frac{\partial u_z}{\partial z}\Big),\end{aligned}$$

where

$$\omega = \omega_x\mathbf{i} + \omega_y\mathbf{j} + \omega_z\mathbf{k}$$

and

$$\mathbf{u} = u_x\mathbf{i} + u_y\mathbf{j} + u_z\mathbf{k}\,.$$

Bibliography

[1] Lawrence, C. A., 2003. *Fundamentals of Spun Yarn Technology*, CRC Press, Boca Raton.

[2] Batra, S.K., Fraser, W.B. 2015. *Engineering Fundamentals of Ring Spinning/Twisting, Over-End Unwinding and Two-For-One Twisting in Textile Processes.* DEStech, Lancaster.

[3] O'Neill, B. 1997. *Elementary Differential Geometry*, Academic Press, San Diego, 2nd edition.

[4] Spivak, M., 1970. *A Comprehensive Introduction to Differential Geometry*, Publish or Perish, Inc., Boston, Mass. Vol 2.

[5] Lipschutz, M.M., 1969. *Schaum's Outline of Theory and Problems of Differential Geometry*, McGraw-Hill, New York.

[6] Lovett, S., 2010. *Differential Geometry of Manifolds*, A K Peters, Ltd., Natick.

[7] Cave, G.E., Fraser, W.B. 2011. The effect of yarn elasticity on the stability of the two-for-one twister balloon, *J. Textile Inst.*, Vol 102, 373-388.

[8] Acheson, D.J. 1990. *Elementary Fluid Dynamics*, Oxford University Press, Oxford.

[9] Hydon, P.E. 2000. *Symmetry Methods for Differential Equations: A beginner's guide*, Cambridge University Press, Cambridge.

[10] Gradshteyn, I.S. and Ryzhik, I.M. 2015. *Table of Integrals, Series, and Products, Eighth Edition*, Academic Press, Waltham.

[11] Seaborn, J.B. 1991. *Hypergeometric Functions and Their Applications*, Springer-Verlag, New York.

[12] Polyanin, A.D., Zaitsev, V.F. 2003. *Handbook of Exact Solutions for Ordinary Differential Equations, Second Edition*, Chapman & Hall/CRC, Boca Raton.

[13] Batchelor, G.K., Moffatt, H.K., Worster, M.G. 2000. *Perspectives in Fluid Dynamics: A Collective Introduction to Current Research*, Cambridge University Press, Cambridge.

[14] Mack, C. 1953 33–Theoretical study of ring and cap spinning balloon curves (with and without air drag). *J. Text. Inst. Trans.*, **44:11**, T483–T498.

[15] Crank, J. 1953 A Theoretical Investigation of Cap and Ring Spinning Systems. *Text. Res. J.* **23**, 266–276.

[16] Hanna, J. A. 2013 Rotating strings. J. *Phys. A: Math. Theor.*, **46:235201**.

[17] Aristoff, J. M., Stone, H. A. 2012 The aerodynamics of jumping rope. *Proc. R. Soc. A*, **468** 720–730.

[18] Chakrabarti, B., Hanna, J.A. 2016 Catenaries in viscous fluid. *Journal of Fluids and Structures* **66** 490–516

[19] Fraser, W.B. 1993a On the theory of ring spinning. *Phil. Trans. R. Soc. Lond.* A **342**, 439–468.

[20] Fraser, W.B., Ghosh, T. K. & Batra, S. K. 1992 On unwinding yarn from a cylindrical package. *Proc. Roy. Soc. Lond.* A **436**, 479–498.

[21] Fraser, W.B. 1993b On the dynamics of the two-for-one twister. *Proc. Roy. Soc. Lond.* A **447**, 409–425.

[22] Mack, C. & Smart, E. J. L. 1954 20–Measurements of the air-drag of textile threads. *J. Text. Inst. Trans.*, **45:4**, T348-T362.

[23] Stump, D.M., & Fraser, W.B. 1995 Dynamic bifurcations of the ring-spinning balloon, *Math. Engng. Ind.* **5**, 161-186.

[24] Clark, J.D., Fraser, W.B., Sharma, R. & Rahn, C.D. 1998 The dynamic response of a ballooning yarn: theory and experiment. *Proc. Roy. Soc. Lond.* A **454**, 2767–2789.

[25] Drazin, P., Riley, N. 2006. *The Navier-Stokes Equations: A Classification of Flows and Exact Solutions*, Cambridge University Press, Cambridge.

[26] Gopalakrishnan, K. March 31, 2017. KTTM sets another record of selling one million spindles of RX 300 machine. The Textile Magazine, `http://www.indiantextilemagazine.in/kttm-sets-another-record-of-\selling-one-million-spindles-of-rx-300-machine/`

[27] Toyota Textile Machinery, Inc. `http://www.toyotatextilemachinery.com/wp-content/uploads/2016/11/RX300$_$E$_$2016.pdf`

[28] Rieter business model document, 2019. `http://www.rieter.com/fileadmin/\user$_$upload/investor-relations/documents/business-model/rieter-business-model-2019.pdf`

[29] Lüdicke, A., 1881. Eine Studie über de Ringspindel, *Dingler's Polytechnisches Journal* **242**, 334–345.

[30] Vogel, S., 1981. *Life in moving fluids : the physical biology of flow*, W. Grant Press, Boston, Mass.

[31] Bishop, R.E.D., Hassan, A.Y. 1964.The lift and drag forces on a circular cylinder in a flowing fluid. *Proc. Roy. Soc. Lond.* A **277**, 32–50.

[32] Ma, P. K. H., Hui, W. H. 1990. Similarity solutions of the two-dimensional unsteady boundary-layer equations, *J. Fluid Mech.* **216**, 537–559.

[33] Batchelor, G.K., 1967. *An Introduction to Fluid Dynamics*, Cambridge University Press, Cambridge.

[34] Goldstein, H. 1981. *Classical Mechanics*, Addison-Wesley Publishing Company, Reading, Mass.

[35] Ibragimov, N. H. 1995. *CRC Handbook of Lie Group Analysis of Differential Equations Volume 2 Applications in Engineering and Physical Sciences*, CRC Press, Boca Raton.

[36] Ince, E. L. 1956. *Ordinary Differential Equations*, Dover Publications, New York.

[37] Olver, P. J. 1993. *Applications of Lie Groups to Differential Equations*, Springer-Verlag, New York.

[38] Bluman, G. W. 1989. *Symmetries and Differential Equations*, Springer-Verlag, New York.

[39] Cantwell, B. J. 2002. *Introduction to Symmetry Analysis*, Cambridge University Press, Cambridge.

[40] Rosenhead, L. (ed.) 1963. *Laminar Boundary Layers*, Oxford University Press, London.

[41] Spiegel, M. R. 1981. *Theory and Problems of Complex Variables: SI(Metric) edition*, McGraw-Hill Book Company, Singapore.

[42] Nugroho, G., Ali, A. M. S., Abdul Karim, Z. A. 2009. Toward a New Simple Analytical Formulation of Navier-Stokes Equations *World Academy of Science, Engineering and Technology International Journal of Mechanical and Mechatronics Engineering* **3**, No:3.

[43] Lenz, M., Hossain, M. , Beitelschmidt, M., Cherif, C., Abdkader, A. 2020. Natural oscillations of yarn balloons in ring spinning, *App. Math. Mod.* **88**, 518-528.

[44] Achenbach, E. 1968. Distribution of local pressure and skin friction around a circular cylinder in cross-flow up to $Re = 5X10^6$. *J. Fluid Mech.* **34**, 625-639.

[45] Papanikolaou, M., Frank, M., Drikakis, D. 2017. Effects of surface roughness on shear viscosity, *Phys. Rev.* E 95, 033108

[46] Dimitriou, I. 2009. Introducing a Geometric Potential Theory for two-dimensional steady flows, *J. Eng. Math.* **63** 1–15

[47] Dimitriou, I. 2017. Planar incompressible Navier-Stokes and Euler equations: A geometric formulation, *Phys. Fluids* **29**, 117101

[48] Kobayashi, M. H. 2008. On the Navier-Stokes equations on manifolds with curvature, *J. Eng. Math.* **60** 55–68.

[49] Jiang, H. 2020. Separation angle for flow past a circular cylinder in the subcritical regime, *Phys. Fluids* **32**, 014106

[50] Kothari, V.K. & Leaf, G.A.V. 1979a The unwinding of yarns from packages Part I: The Theory of Yarn Unwinding. *J. Textile Inst.* **70**, 89–95.

[51] Kim, K-W. Lee J-W. Yoo W-S. 2012. Effect of gravity and tangential air resistance on unwinding cable, *Nonlinear Dyn.* **70**, 67-87.

[52] Fraser, W.B. & Stump, D.M. 1998. Yarn Twist in the Ring-Spinning Balloon, *Proceedings: Mathematical, Physical and Engineering Sciences* **454**, 707-723.

[53] Fraser W.B. & Stump D.M. 1998. Twist in Balanced-ply Structures, *J. Text. Inst.* **89**, 485-497.

[54] Phillips D. G., Tran, C-D. , Fraser W. B. & van der Heijden, G. H.M. 2010. Torsional properties of staple fibre plied yarns, *J. Text. Inst.* **101**, 595-612.

[55] Padfield, D.G. 1958 The motion and tension in an unwinding balloon. *Proc. R. Soc. Lond.* A **245**, 382-407.

[56] Bluman G.W., Cheviakov A.F., Anco S.C. 2010. *Applications of Symmetry Methods to Partial Differential Equations.* Springer, New York.

[57] Barenblatt, G.I., Zel'dovich, Y.B. 1972. Self-similar solutions as intermediate asymptotics. *Ann. Rev. Fluid Mech.* **4**, 285-312.

[58] Ludlow, D.K., Clarkson, P.A., Bassom, A.P. 1999. Nonclassical symmetry reductions of the two-dimensional incompressible Navier-Stokes equations. *Stud. appl. Math.* **103**, 183-240.

[59] Ludlow, D.K., Clarkson, P.A., Bassom, A.P. 2000. New Similarity Solutions of the Unsteady Incompressible Boundary-Layer Equations. *Q. Jl Mech. appl. Math.* **53(2)**, 175-206.

[60] Goldstein, S. (ed.) 1938. *Modern Developments in Fluid Dynamics*, Oxford University Press, Oxford.

[61] Baltz, W.E. 1948. *Kunstseide u. Zellwolle* **26**, 42.

[62] Proudman, I., Pearson J.R.A. 1957. Expansions at small Reynolds numbers for the flow past a sphere and a circular cylinder. *Journal of Fluid Mechanics,* **2 (3)**, 237–262.

[63] Sychev, Vladimir V., Ruban, A.I., Sychev, Victor V., Korolev, G. L. 1998. *Asymptotic theory of separated flows*, Cambridge University Press, Cambridge.

[64] Sen, S., Mittal, S., Biswas, G., 2009. Steady separated flow past a circular cylinder at low Reynolds numbers. *J. Fluid Mech.* **620**, 89-119.

[65] Wu, M. H., Wen, C. Y., Yen, R. H., Weng, M. C., Wang, A. B., 2004. Experimental and numerical study of the separation angle for flow around a circular cylinder at low Reynolds number. *J. Fluid Mech.* **515**, 233–260.

[66] Jiang, H., Cheng, L. 2017. Strouhal–Reynolds number relationship for flow past a circular cylinder. *J. Fluid Mech.* **832**, 170–188.

[67] Waleffe, F. 2009. Exact coherent structures in turbulent shear flows. *Turbulence and Interactions*, Springer, Berlin, Heidelberg, 139-158.

[68] Gray, A. 1918. *A Treatise on Gyrostatics and Rotational Motion*, MacMillan and Co. Ltd., London.

[69] Hanna, J.A., Pendar, H. 2016. A conserved quantity in thin body dynamics. *Physics Letters A* **380**, 707-711.